Universidade de Brasília
Instituto de Geociências
Programa de Pós-graduação em Geologia

GEOMETRIA PROFUNDA DO NÚCLEO ARQUEANO CAMPO GRANDE, PROVÍNCIA BORBOREMA: UMA ABORDAGEM MAGNETOTELÚRICA 3D

Layandra Oliveira Pessanha

Dissertação de Mestrado N° 549

Orientador: Prof. Dr. Elton Luiz Dantas

Brasília, 25/ 03 /2026

Universidade de Brasília
Instituto de Geociências
Programa de Pós-graduação em Geologia

GEOMETRIA PROFUNDA DO NÚCLEO ARQUEANO CAMPO GRANDE, PROVÍNCIA BORBOREMA: UMA ABORDAGEM MAGNETOTELÚRICA 3D

Layandra Oliveira Pessanha

Dissertação apresentada ao Programa de Pós-Graduação em Geologia – Instituto de Geociências – IG da Universidade de Brasília – UnB
como requisito parcial obrigatório para a obtenção do título de Mestre em Geologia.
Área de concentração: Geologia Regional
Orientador: Prof. Dr. Elton Luiz Dantas

Comissão Examinadora:
Prof. Dr.; Luis Gustavo Ferreira Viegas (IG/UnB);
Prof. Dr.; Mauricio de Souza Bologna (IAG/USP).

Ficha catalográfica elaborada automaticamente, com os dados fornecidos pelo(a) autor(a)

PP475g

Pessanha, Layandra
Geometria profunda do Núcleo Arqueano Campo Grande, Província Borborema: Uma abordagem Magnetotelúrica 3D / Layandra Pessanha; orientador Elton Dantas. Brasília, 2026.
92 p.

Dissertação(Mestrado em Geologia) Universidade de Brasília, 2026.

1. Magnetotelúrico. 2. Província Borborema. 3. Modelagem 3D. 4. Núcleo Arqueano. 5. Zona de Cisalhamento Portalegre. I. Dantas, Elton , orient. II. Título.

AGRADECIMENTOS

Sou profundamente grata por ter aprendido que aprender é, por si só, um desafio — e talvez o mais transformador deles. *"não é possível resolver um problema com o mesmo nível de consciência que o criou."*

Agradeço, antes de tudo, aos meus pais, Denise Aparecida Oliveira Pessanha e Walser de Souza Pessanha, que me cercaram de amor e amparo ao longo de toda essa trajetória. Tudo o que sou e tudo o que construí até aqui carrega a marca dessa dedicação. A vocês dedico este mestrado — por sempre acreditarem em mim e me darem forças para não desistir, mesmo quando essa parecia a opção mais sensata. Cada sacrifício, cada palavra de incentivo, cada silêncio compreensivo me trouxe até aqui. Mãe, pai: eu consegui. E essa conquista é tão de vocês quanto minha.

Aos meus amigos Ana Clara Legora, Pedro Borborema, Pedro Manhães e Rennan Cardoso — que, mesmo à distância, me ofereceram o tipo de apoio que não se encontra facilmente. Obrigada pela amizade sincera, pela presença mesmo na ausência, e por me lembrarem de quem eu sou quando eu mesma esquecia.

Ao meu orientador, Prof. Dr. Elton Luiz Dantas, agradeço pela confiança depositada em mim para o desenvolvimento deste projeto e pela generosidade em compartilhar seu conhecimento. Mais do que orientação acadêmica, recebi acolhimento nos dias difíceis, empatia genuína e o exemplo de alguém que se importa verdadeiramente com seus alunos. Foi um privilégio aprender contigo, professor.

Aos professores Dr. Fabiano Mota, Dr. Nilton Silva e Dr. Christiano Magini, agradeço pela paciência imensurável no ensino do método magnetotelúrico e pelo acompanhamento em cada etapa deste trabalho. Ao Prof. Dr. Alanielson Ferreira, agradeço por iluminar as ideias sobre a geologia regional, pelos conselhos valiosos e pelas discussões que ampliaram minha compreensão sobre a área de estudo. Ao Prof. Dr. Reinhardt Fuck, minha gratidão pelas críticas construtivas e sugestões apresentadas, que foram essenciais para o amadurecimento desta dissertação.

Agradeço à Universidade de Brasília (UnB) pelo ambiente acadêmico que tornou esta pesquisa possível, e à Universidade Federal do Ceará (UFC) pela disponibilização dos dados magnetotelúricos utilizados neste estudo. O presente trabalho foi realizado com apoio da Coordenação de Aperfeiçoamento de Pessoal de Nível Superior — Brasil

(CAPES) — Código de Financiamento 001, sendo a autora bolsista Proex/CAPES durante o período do mestrado. Este estudo é também uma contribuição do INCT-Estudos Tectônicos (CNPq 57.3713/2008-1).

"Toda grande mudança é precedida pelo caos." — Deepak Chopra

RESUMO

Fragmentos de crosta arqueana preservados na Província Borborema, NE do Brasil, como pequenos núcleos bordejados por terrenos pré-cambrianos mais jovens, constituem janelas privilegiadas para a compreensão dos processos de crescimento e estabilização continental durante a formação do Gondwana Ocidental. O Bloco Campo Grande, situado na porção central do Domínio Rio Grande do Norte, representa um desses remanescentes, cuja expressão em profundidade permanecia desconhecida até o presente estudo. Este trabalho investigou a estrutura geoelétrica do Bloco Campo Grande e terrenos adjacentes por meio de levantamento magnetotelúrico de banda larga, configurado em perfil E-W de 100 km entre Itaú e Paraú (RN) com 21 estações e espaçamento de 10 km, adensado para 5 km sobre a área do núcleo arqueano. O processamento dos dados envolveu filtragem de ruídos culturais, análise de dimensionalidade por tensor de fase e inversão tridimensional com o algoritmo ModEM, e o modelo resultante foi avaliado criticamente quanto à robustez para fornecer visão coerente da estrutura regional. A inversão revelou significativa heterogeneidade da resistividade elétrica na crosta, com a identificação de três corpos resistivos (R1 a R3) e três condutores principais (C1 a C3), além de dois condutores periféricos (C4 e C5) cuja caracterização é limitada pela cobertura do levantamento. O corpo R1 foi interpretado como correspondente ao Complexo Jaguaretama, composto por ortognaisses e paragnaisses do Neoproterozoico, com contraste de resistividade de aproximadamente 8 km de profundidade. R2 está relacionado a granitos neoproterozoicos com profundidade geoelétrica de 16 km.O domínio R3 apresenta contraste de resistividade que se estende até 17 km de profundidade. Seu núcleo, com resistividade de 10^4 Ω·m concentra-se nos primeiros 5 km e é circundado por zona moderadamente menos resistiva com mergulho para sudoeste. Essa arquitetura é consistente com um padrão de acresção crustal em torno de um núcleo arqueano, e os valores de resistividade observados são compatíveis com ortognaisses migmatíticos arqueano do Complexo Campo Grande no núcleo e ortognaisses paleoproterozoicos nas porções envolventes. O condutor C1 marca a Zona de Cisalhamento Portalegre, com mergulho para oeste até 14 km de profundidade, confirmando seu papel como limite crustal entre os domínios Jaguaribe e Rio Grande do Norte. O modelo 3D de resistividade também evidencia movimentação dextral nos corpos identificados. A geometria alongada e o deslocamento lateral dos blocos resistivos em profundidade indicam cinemática compatível com os esforços transcorrentes na estruturação crustal da região. Os condutores C2 e C3 sugerem, respectivamente, estrutura intracrustal de baixo ângulo e zona de sutura paleoproterozoica que atinge a crosta média. Os resultados obtidos confirmam a complexidade estrutural da Província Borborema e demonstram o potencial da metodologia MT 3D na caracterização de estruturas crustais profundas e na compreensão da evolução tectônica regional, como resultado da amalgamação de terrenos ao longo de ciclos orogênicos pré-cambrianos. A assinatura geoelétrica do Bloco Campo Grande confirma a presença de estrutura em domo gnáissico, sendo típica de litosfera antiga termalmente estabilizada, preservada como inlier do embasamento, posteriormente compartimentada e exumada pela tectônica transcorrente brasiliana. Este estudo mostra que a metodologia aplicada é eficaz para

delimitar extensões de blocos crustais individuais, bem como permitir a visualização integrada da arquitetura do arcabouço tectonico regional. Além disso, pode ser aplicada na identificação e caracterização de zonas de cisalhamento profundas e individualização e compartimentação de unidades litológicas menores, mas com alto contraste de resistividade, como rochas máfico-ultramáficas em complexos gnáissico-migmatíticos e intrusões de granitos ao longo de zonas de cisalhamento. Portanto, é uma metodologia com alto potencial para aplicações em outras áreas, principalmente para revelar configurações crustais em diferentes profundidades. Também concluímos que o método magnetotelúrico 3D, em arranjo de malha adensada, permite discriminar em profundidade domínios crustais de diferentes idades e composições em terrenos polideformados, oferecendo resolução adequada para caracterizar a geometria de núcleos arqueanos e as estruturas que os delimitam.

***Palavras-chave*:** Magnetotelúrico; Província Borborema; Modelagem 3D; Bloco Campo Grande; Núcleo arqueano; Zona de Cisalhamento Portalegre.

ABSTRACT

Fragments of Archean crust preserved in the Borborema Province, NE Brazil, as small nuclei bordered by younger Precambrian terranes, constitute privileged windows for understanding the processes of continental growth and stabilization during the formation of West Gondwana. The Campo Grande Block, situated in the central portion of the Rio Grande do Norte Domain, represents one of these remnants, whose expression at depth remained unknown until the present study. This work investigated the geoelectrical structure of the Campo Grande Block and adjacent terranes through a broadband magnetotelluric survey, configured as a 100 km E-W profile between Itaú and Paraú (RN) with 21 stations and 10 km spacing, densified to 5 km over the Archean core area. Data processing involved cultural noise filtering, dimensionality analysis by phase tensor, and three-dimensional inversion with the ModEM algorithm, and the resulting model was critically evaluated for robustness to provide a coherent view of the regional structure. The inversion revealed significant heterogeneity of electrical resistivity in the crust, with the identification of three resistive bodies (R1 to R3) and three main conductors (C1 to C3), in addition to two peripheral conductors (C4 and C5) whose characterization is limited by the survey coverage. Body R1 was interpreted as corresponding to the Jaguaretama Complex, composed of Neoproterozoic orthogneisses and paragneisses, with a resistivity contrast at approximately 8 km depth. R2 is related to Neoproterozoic granites with a geoelectrical depth of 16 km. The R3 domain presents a resistivity contrast extending to 17 km depth. Its core, with resistivity of 10^4 Ω·m, is concentrated in the first 5 km and is surrounded by a moderately less resistive zone dipping to the southwest. This architecture is consistent with a pattern of crustal accretion around an Archean core, and the observed resistivity values are compatible with Archean migmatitic orthogneisses of the Campo Grande Complex in the core and Paleoproterozoic orthogneisses in the surrounding portions. Conductor C1 marks the Portalegre Shear Zone, dipping westward to 14 km depth, confirming its role as a crustal boundary between the Jaguaribe and Rio Grande do Norte domains. The 3D resistivity model also evidences dextral movement in the identified bodies. The elongated geometry and lateral displacement of the resistive blocks at depth indicate kinematics compatible with the transcurrent stresses in the crustal structuration of the region. Conductors C2 and C3 suggest, respectively, a low-angle intracrustal structure and a Paleoproterozoic suture zone reaching the middle crust. The results obtained confirm the structural complexity of the Borborema Province and demonstrate the potential of the 3D MT methodology in the characterization of deep crustal structures and in the understanding of regional tectonic evolution, as a result of terrane amalgamation along Precambrian orogenic cycles. The geoelectrical signature of the Campo Grande Block confirms the presence of a gneiss dome structure, typical of thermally stabilized ancient lithosphere, preserved as a basement inlier, subsequently compartmentalized and exhumed by Brasiliano transcurrent tectonics. This study shows that the applied methodology is effective in delimiting the extents of individual crustal blocks, as well as enabling the integrated visualization of the regional tectonic framework architecture. Furthermore, it can be applied in the identification and characterization of deep shear zones and in the individualization and compartmentalization of smaller lithological units with high resistivity contrast, such as mafic-ultramafic rocks in gneissic-migmatitic complexes and granite intrusions along shear zones. Therefore, it is a methodology with high potential for applications in other areas, mainly to reveal crustal configurations at different depths. We also conclude that the 3D magnetotelluric method, in a densified grid array, allows the discrimination at depth of crustal domains of different

ages and compositions in polydeformed terranes, offering adequate resolution to characterize the geometry of Archean nuclei and the structures that delimit them.

Keywords**:** Magnetotelluric; Borborema Province; 3D modeling; Campo Grande Block; Archean nucleus; Portalegre Shear Zone.

LISTA DE ABREVIATURAS

1D — Unidimensional

2D — Bidimensional

3D — Tridimensional

BBMT — Broadband Magnetotelluric (Magnetotelúrico de banda larga)

BCG — Bloco Campo Grande

CAOB — Central Asian Orogenic Belt (Cinturão Orogênico da Ásia Central)

DCC — Domínio Ceará Central

DRGN — Domínio Rio Grande do Norte

E — Campo elétrico (V/m)

EDI — Electrical Data Interchange (formato de dados MT)

EM — Eletromagnético

Ex, Ey — Componentes horizontais do campo elétrico (direções NS e EW)

FIR — Finite Impulse Response (Filtro de resposta ao impulso finita)

H — Campo magnético (A/m)

Hx, Hy — Componentes horizontais do campo magnético (direções NS e EW)

Hz — Componente vertical do campo magnético

INCT — Instituto Nacional de Ciência e Tecnologia

MPI — Message Passing Interface (interface de computação paralela)

MT — Magnetotelúrico / Magnetotelúrica

MTpy — Pacote Python para análise de dados magnetotelúricos

ModEM — Modular Electromagnetic Inversion

NLCG — Non-Linear Conjugate Gradient (Gradiente Conjugado Não-Linear)

nRMS — Normalized Root Mean Square (RMS normalizado)

PB — Província Borborema

RMS — Root Mean Square (Raiz do erro quadrático médio)

SAMTEX — Southern African Magnetotelluric Experiment

Sm-Nd — Sistema geocronológico Samário-Neodímio

TE — Transverse Electric (modo elétrico transversal)

TM — Transverse Magnetic (modo magnético transversal)

TSMP — Time Series Manipulation Process

U-Pb — Sistema geocronológico Urânio-Chumbo

VMS — Volcanogenic Massive Sulfide (Sulfeto maciço vulcanogênico)

Z — Tensor de impedância

Zxx, Zxy, Zyx, Zyy — Elementos do tensor de impedância

ZCFG — Zona de Cisalhamento Frutuoso Gomes

ZCP — Zona de Cisalhamento Portalegre

ZCPa — Zona de Cisalhamento Patos

β — Ângulo de skew normalizado (parâmetro de dimensionalidade)

δ — Skin-depth (profundidade de penetração)

Φ — Tensor de fase

Φmax, Φmin — Eixos principais do tensor de fase

μ_0 — Permeabilidade magnética do vácuo

ω — Frequência angular (rad/s)

ρ_a — Resistividade aparente ($\Omega \cdot m$)

τ — Parâmetro de regularização

$\Omega \cdot m$ — Ohm-metro (unidade de resistividade)

LISTA DE FIGURAS

SUMÁRIO

CAPÍTULO 1

INTRODUÇÃO

1. INTRODUÇÃO

Reconstruir a evolução tectônica de orógenos pré-cambrianos é um desafio corrente em estudos geológicos, principalmente devido à ausência de dados morfológicos e composicionais das feições tectônicas acrescionárias em profundidade. Ao contrário dos cinturões fanerozoicos, cujo registro estratigráfico e paleontológico oferece continuidade razoável, os orógenos pre-cambrianos têm suas histórias sobrepostas por ciclos deformacionais sucessivos e modificados ao longo de bilhões de anos. Por essa razão, a integração entre observações geológicas de superfície e dados geofísicos profundos é imprescindível para resolver a geometria e as relações entre os blocos crustais que compõem terrenos polideformados. Nesse sentido, a aplicação do método magnetotelúrico tem-se mostrado eficiente em investigações em estruturas tectônicas profundas, zonas de sutura, limites de terrenos e anomalias condutivas associadas a fluidos e fusão parcial (e.g., Correa *et al.*, 2023; Meqbel *et al.*, 2014; Padilha *et al.*, 2013, 2019; Yang *et al.*, 2015; Silva *et al.*, 2026).

A aplicação do método magnetotelúrico na caracterização subsuperficial em diferentes contextos geodinâmicos evidencia sua versatilidade e resolução espacial. Estudos conduzidos em crátons arqueanos ao redor do mundo demonstraram que essas unidades preservam assinaturas geoelétricas distintivas, caracterizadas por elevada resistividade associada a litosfera termalmente estabilizada e quimicamente depletada, e demonstram a capacidade do método em discriminar domínios litológicos de diferentes composições e idades. Levantamentos MT com espaçamento adensado de estações, integrados a dados sísmicos e geológicos, permitem identificar condutores crustais atribuídos a sulfetos interconectados e elevado teor de ferro em silicatos portadores de Fe/Mg, além de caracterizar as estruturas internas de sequências do tipo *greenstone belt* (Ma *et al.*, 2021). Núcleos arqueanos mostram assinaturas resistivas profundas nos crátons Kaapvaal e Congo, e são delimitados por anomalias condutoras em escala litosférica, comumente associadas a zonas de sutura e processos metassomáticos (Jones *et al.*, 2009; Moorkamp *et al.*, 2022). Complexos e domos gnáissicos pré-cambrianos e jovens oferecem um campo de aplicação ainda pouco explorado para o método MT e ilustram como a assinatura geoelétrica de domos gnáissicos é controlada não apenas pela composição litológica, mas também pelo contexto geodinâmico e pelo estado termal da litosfera. Zona moderadamente resistiva em profundidades de 30 a 40 km truncam lateralmente condutores interpretados como fundidos ricos em água e fluidos liberados durante a

subducção da placa Indiana sob a Asiática (Sheng *et al.*, 2023), bem como valores condutivos podem ser associados ao transporte ascendente de material parcialmente fundido em domos gnaíssicos (Chen *et al.*, 1996). Em contrastes, valores resistivos também são registrados em domos em cinturões orogênicos colisionais (Yi *et al.*, 2022), quando se utiliza malha adensada de estações a cada 10 km e 5 km de distância. O imageamento de condutores mergulhando em determinada direção, são interpretados como vestígios de crosta oceânica subductada, demonstrando o potencial do método para caracterizar suturas profundas preservadas em orógenos antigos.

A Província Borborema, no nordeste brasileiro, reúne as condições adequadas para aplicação dessas abordagens geofísicas. Sua arquitetura crustal resulta da amalgamação diacrônica de múltiplos terrenos durante os ciclos orogênicos que culminaram na formação do Gondwana Ocidental no Neoproterozoico (Brito Neves *et al.*, 2000; Van Schmus *et al.*, 2008). O registro geológico expõe um mosaico de blocos paleoproterozóicos e arqueanos, parcialmente recobertos por sequências metavulcanossedimentares, intensamente retrabalhados durante a Orogenia Brasiliana e seccionados por uma rede de zonas de cisalhamento transcorrentes de escala continental (Arthaud *et al.*, 2008; Brito Neves & Fuck, 2014).

Os levantamentos magnetotelúricos conduzidos na Província Borborema ao longo das últimas décadas forneceram panorama regional da distribuição de resistividade elétrica, que identifica blocos resistivos delimitados por condutores associados a grandes lineamentos transcorrentes (Padilha *et al.*,2014, 2017), e caracterizaram a estrutura litosférica de diferentes domínios tectônicos. O arcabouço tectônico da Província Borborema mostra arquitetura heterogênea com condutores crustais coincidentes com zonas de cisalhamento interpretadas como extensões em profundidade dessas estruturas (Garcia *et al.*, 2019). A profundidade de corpos condutores atinge 10 a 20 km, associados a estruturas horizontalizadas (Santos Matos *et al.*, 2019). Mais recentemente, Padilha *et al.* (2021) e Benevides *et al.* (2026) identificaram estrutura resistiva no complexo arqueano São José do Campestre, e feições dômicas sob o Maciço Tróia-Tauá, também de idade arqueana. Essas contribuições, entretanto, adotaram dominantemente estratégias de aquisição em escala regional, com espaçamentos entre estações da ordem de 50 a 70 km, adequados para caracterizar feições de primeira ordem, porém insuficientes para resolver heterogeneidades de menor dimensão ou investigar com detalhe a estrutura interna de blocos específicos.

Na porção central do Domínio Rio Grande do Norte, onde se situa o Bloco Campo Grande (BCG), a estrutura crustal profunda permanece não investigada por métodos eletromagnéticos. Este fragmento crustal, com aproximadamente 1.500 km² e geometria dômica de eixo SSW-NNE, preserva um dos raros registros de crosta arqueana na Província Borborema (Ferreira *et al.*, 2020a, 2020b). O núcleo do bloco é constituído por complexo migmatítico de composição tonalítica a granítica, com idades de cristalização entre 2,98 e 2,66 Ga, que hospeda lentes de rochas máfico-ultramáficas interpretadas como retroeclogitos — uma assembleia singular que representa cenário distinto de todos os retroeclogitos previamente descritos em sequências supracrustais neoproterozoicas no Gondwana Ocidental (Ferreira *et al.*, 2020a, 2021). Este núcleo arqueano encontra-se envolto por ortognaisses alcalinos paleoproterozoicos do Complexo Caicó e, externamente, por intrusões graníticas neoproterozoicas de alto K, configurando arranjo concêntrico que sugere crescimento crustal progressivo ao longo de quase três bilhões de anos. A oeste do BCG, a Zona de Cisalhamento Portalegre — estrutura de centenas de quilômetros de extensão e direção NNE-SSW — delimita o bloco e corresponde ao limite reconhecido entre os domínios Jaguaribe e Rio Grande do Norte (Cavalcante *et al.*, 1998; Archanjo *et al.*, 1998).

A despeito de sua relevância para a compreensão da evolução crustal da província, a geometria profunda do Bloco Campo Grande permanecia desconhecida. Questões fundamentais aguardavam investigação: qual a extensão vertical do núcleo arqueano? Como se articulam em profundidade as diferentes unidades que compõem o bloco? Qual a expressão geoelétrica da Zona de Cisalhamento Portalegre e até que profundidade esta estrutura penetra na crosta? É possível distinguir, por meio da assinatura magnetotelúrica, o núcleo arqueano de seu envelope paleoproterozóico? Estas perguntas não poderiam ser respondidas pelos levantamentos MT regionais preexistentes, cujo espaçamento não permitia resolução adequada para estruturas dessa escala.

O presente trabalho foi concebido para preencher esta lacuna. Implementou-se, pela primeira vez na região, um levantamento magnetotelúrico de banda larga com arranjo adensado, compreendendo um transecto E-W de 100 km com espaçamento de 10 km, complementado por arranjo em grade com espaçamento de 5 km sobre o Bloco Campo Grande.

O objetivo central desta dissertação é caracterizar a estrutura geoelétrica tridimensional do Bloco Campo Grande e terrenos adjacentes, contribuindo para o entendimento da

arquitetura crustal e da evolução tectônica da porção central do Domínio Rio Grande do Norte. Especificamente, busca-se: (i) definir a geometria e a extensão em profundidade dos principais domínios resistivos, correlacionando-os com as unidades geológicas mapeadas em superfície; (ii) caracterizar as zonas condutoras que delimitam esses domínios, investigando sua associação com estruturas tectônicas regionais, particularmente a Zona de Cisalhamento Portalegre; (iii) avaliar a capacidade do método MT de banda larga, em arranjo de malha adensada, para discriminar núcleos arqueanos preservados em terrenos polideformados; e (iv) estabelecer comparações com assinaturas geoelétricas documentadas em terrenos arqueanos de outras localidades, contribuindo para o entendimento dos fatores que controlam a resposta magnetotelúrica de domos gnáissicos pré-cambrianos.

Esta dissertação está organizada em quatro capítulos. O primeiro capítulo apresenta o contexto geotectônico da Província Borborema, com ênfase no Domínio Rio Grande do Norte e no Bloco Campo Grande, além de revisar os estudos magnetotelúricos prévios na região e em terrenos arqueanos análogos. O segundo capítulo aborda os fundamentos teóricos do método magnetotelúrico relevantes para a compreensão do trabalho. O terceiro capítulo corresponde ao artigo científico elaborado para submissão a periódico, contendo a descrição detalhada da aquisição, processamento, inversão e interpretação dos dados. O quarto capítulo reúne as conclusões e considerações finais. Os dados utilizados neste estudo foram adquiridos no âmbito do programa INCT-Estudos Tectônicos, em parceria com o Laboratório de Geofísica da Universidade Federal do Ceará, e compreendem 21 estações magnetotelúricas de banda larga distribuídas entre os municípios de Itaú e Paraú, no Rio Grande do Norte.

CAPÍTULO 2

MÉTODO MAGNETOTELÚRICO

2. MÉTODO MAGNETOTELÚRICO

2.1. Princípios do MT

O método magnetotelúrico (MT) é uma técnica geofísica passiva de exploração eletromagnética que mensura, na superfície terrestre, as variações temporais simultâneas das componentes dos campos elétrico (E) e magnético (H). As fontes do campo eletromagnético natural variam conforme a frequência. Para sinais de baixa frequência (<1 Hz), as variações originam-se da interação entre o vento solar e a magnetosfera terrestre, gerando correntes ionosféricas e pulsações geomagnéticas. Já as fontes de alta frequência (>1Hz) estão associadas à atividade meteorológica global, como tempestades elétricas, que geram pulsos que se propagam no guia de ondas Terra-ionosfera (Chave & Jones, 2012; Simpson & Bahr, 2005)

O objetivo é determinar a distribuição da condutividade elétrica em subsuperfície, partindo da premissa de que as variações de condutividade estão associadas a contrastes litológicos, presença de fluidos, fusão parcial ou variações de temperatura e porosidade. A base teórica que correlaciona os campos naturais ortogonais foi proposta por Tikhonov (1950) e posteriormente aprofundada por Cagniard (1953), permitindo a estimativa de estruturas geoelétricas desde dezenas de metros até centenas de quilômetros de profundidade (Chave & Jones, 2012; Simpson & Bahr, 2005).

O comportamento dos campos eletromagnéticos no método MT é governado pelas equações de Maxwell. No sistema internacional essas equações descrevem as relações fundamentais entre os campos elétrico e magnético e suas fontes. Os fundamentos e as fórmulas encontram-se bem descritas por Simpson & Bahr, (2005):

$$\text{i) } \nabla \cdot B = 0 \tag{1}$$

$$\text{ii) } \nabla \cdot D = \rho \tag{2}$$

$$\text{iii) } \nabla \times E = -\frac{\partial B}{\partial t} \tag{3}$$

$$\text{iv) } \nabla \times H = J_f + \frac{\partial D}{\partial t} \tag{4}$$

em que E representa a intensidade do campo elétrico (V/m), H é a intensidade do campo magnético (A/m), B a indução magnética (T), D é o deslocamento elétrico (C/m²), J é

densidade de corrente elétrica (A/m²), ρ é a densidade volumétrica de carga elétrica (C/m³).

A equação de Gauss (i) indica a inexistência de monopólios magnéticos. A equação de Gauss (ii) relaciona o deslocamento elétrico à densidade de carga elétrica. A lei de Faraday (iii) descreve a indução eletromagnética, fundamental para o método MT, em que um campo magnético variável induz um campo elétrico. Por fim, a lei de Ampère-Maxwell (iv) relaciona o campo magnético à densidade de corrente e à variação temporal do deslocamento elétrico (Halliday *et al.*, 1996; Young & Freedman, 2009).

O conjunto dessas equações estabelece que a variação temporal do campo magnético induz um campo elétrico rotacional, cuja circulação gera correntes que dependem da condutividade do meio atravessado.

A profundidade de investigação, ou *skin-depth* (δ), é definida como a profundidade na qual a amplitude dos campos eletromagnéticos atenua-se para 1/e (aproximadamente 37%) de seu valor na superfície (Telford *et al.*, 1990; McNeill, 1990). Para um semiespaço homogêneo de resistividade ρ (Ω.m), o *skin-depth* é aproximada por:

$$\delta \approx 500\sqrt{\rho_\alpha T} \tag{5}$$

em que δ é a profundidade em metros, T representa o período em segundos e ρ_α é a resistividade aparente do meio em Ω.m. Esta relação demonstra que períodos mais longos (baixas frequências) permitem investigações a maiores profundidades, enquanto períodos curtos (alta frequência) amostram níveis crustais mais rasos.

2.2. Tensor de impedância Magnetotelúrica

No domínio da frequência a relação entre as variações das componentes horizontais dos campos elétrico (E) e magnético (H) ortogonais medidos à superfície é descrita matematicamente por uma função de transferência complexa denominada Tensor de Impedância (Z), expressa pela equação fundamental $E = Z \cdot H$ (Chave & Jones, 2012; Simpson & Bahr, 2005). Matricialmente, essa relação é dada por:

$$\begin{pmatrix} E_x \\ E_y \end{pmatrix} = \begin{pmatrix} Z_{xx} & Z_{XY} \\ Z_{yx} & Z_{yy} \end{pmatrix} \begin{pmatrix} H_x \\ H_y \end{pmatrix} \tag{6}$$

em que E_x, E_y representam as componentes do campo elétrico nas direções NS e EW, respectivamente; enquanto H_x, H_y são as componentes do campo magnético correspondentes. Os termos Z_{ij} constituem os elementos complexos do tensor de impedância, medidos em Ohm (Ω) ou mV/Km/nT (unidade de campo).

Dada a natureza complexa do tensor Z, a interpretação direta é pouco intuitiva. Por essa razão, converte-se a impedância em dois parâmetros físicos fundamentais: a resistividade aparente (ρ_α) e a fase (Φ) para cada par de componentes (ij), conforme Simpson & Bahr (2005):

$$\rho_{ij} = \frac{1}{\omega\mu}|Z_{ij}|^2 \tag{7}$$

$$\Phi = arctan\left(\frac{Im(Z_{ij})}{Re(Z_{ij})}\right) \tag{8}$$

em que ω é a frequência angular (rad/s) e μ é a permeabilidade magnética.

2.3. Dimensionalidade Geoelétrica e efeitos 3D

A análise dos elementos do tensor de impedância permite inferir a dimensionalidade da estrutura geoelétrica investigada (1D, 2D ou 3D), o que é determinante para a escolha adequada das estratégias de modelagem e inversão dos dados magnetotelúricos (Simpson & Bahr, 2005).

Em meios unidimensionais (1D), a condutividade elétrica varia exclusivamente com a profundidade, sem variações laterais. Nesse meio, os elementos da diagonal principal do tensor de impedância são nulos (Zxx = Zyy = 0) e os elementos fora da diagonal são iguais em magnitude, porém com sinais opostos (Zxy= - Zyx). Devido à simetria do problema, a impedância do meio não depende da orientação das medidas no plano horizontal, de modo que a resposta MT é a mesma em qualquer azimute de aquisição (Simpson & Bahr, 2005).

Em meios bidimensionais (2D), a condutividade varia verticalmente e em uma direção horizontal, mas permanece constante ao longo de uma direção preferencial denominada *strike* geoelétrico. Os elementos da diagonal principal do tensor de impedância se anulam (Zxx=Zyy=0) quando o sistema de coordenadas de medição está alinhado com o *strike*.

Os elementos fora da diagonal deixam de ser simétricos em módulo (Zxy ≠Zyx), refletindo a anisotropia lateral da estrutura. Nessas condições as equações de Maxwell se desacoplam em dois modos independentes de polarização: o modo TE (Transverse Eletric), no qual o campo elétrico é paralelo ao *strike* e as correntes fluem nessa mesma direção, e o modo TM (Transverse Magnetic), onde o campo magnético é paralelo ao *strike* e as correntes que fluem perpendicular a ele. O modo TE é mais sensível a estruturas profundas e a estratigrafia elétrica regional, enquanto o modo TM responde preferencialmente a descontinuidades laterais rasas, como falhas e contatos geológicos (Simpson & Bahr, 2005; Santos, 2012)

Em ambientes tridimensionais (3D), a condutividade varia nas três direções espaciais (x,y,z) e nenhum dos elementos do tensor de impedância se anula, impossibilitando o desacoplamento dos campos EM em modos independentes. Essa disposição é típica de ambientes geológicos complexos, como zonas de cisalhamento oblíquas, corpos intrusivos irregulares ou bacias com geometrias não cilíndricas (Simpson & Bahr, 2005). Na prática as aproximações 1D e 2D são viáveis quando a variação da condutividade é dominante em uma ou duas direções e desprezível nas demais; contudo, estruturas geológicas reais frequentemente apresentam comportamento tridimensional que exige abordagens de inversão 3D para representação adequada da subsuperfície:

$$Z_{1D} = \begin{pmatrix} 0 & Z_{xy} \\ -Z_{xy} & 0 \end{pmatrix} \tag{9}$$

$$Z_{2D} = \begin{pmatrix} 0 & Z_{xy} \\ Z_{yx} & 0 \end{pmatrix} \tag{10}$$

$$Z_{3D} = \begin{pmatrix} Z_{xx} & Z_{xy} \\ Z_{yx} & Z_{yy} \end{pmatrix} \tag{11}$$

2.4. Função de Transferência Vertical - *Tipper*

Além do tensor de impedância, que relaciona as componentes horizontais dos campos elétrico e magnético, o método magnetotelúrico viabiliza a estimativa de uma segunda função de transferência fundamental: a função de transferência magnética vertical, comumente denominada *tipper* (Vozoff, 1991; Simpson e Bahr, 2005). Essa grandeza expressa a relação entre a componente vertical do campo magnético (Hz) e as componentes horizontais (Hx e Hy), sendo descrita por um vetor complexo com duas componentes, Tx e Ty, para cada frequência (Chave & Jones, 2012).

A representação gráfica da função de transferência vertical é frequentemente realizada por meio das chamadas setas de indução, decompostas em componentes real e imaginária. Na convenção de Parkinson (1959), amplamente adotada na literatura, a componente real das setas de indução aponta na direção de estruturas eletricamente mais condutoras, fornecendo indicação qualitativa e espacialmente intuitiva da localização de anomalias condutivas em relação às estações de medição.

No presente trabalho a componente vertical do campo magnético não foi registrada durante a aquisição dos dados, em razão das dificuldades logísticas associadas ao transporte, instalação e nivelamento do sensor de campo magnético vertical (bobina Hz) nas condições de campo da área de estudo. Dessa forma, a inversão 3D foi conduzida exclusivamente com base no tensor de impedância completo. Embora a ausência do *tipper* represente uma limitação na sensibilidade lateral do modelo obtido, diversos autores têm demonstrado que inversões 3D baseadas apenas no tensor de impedância são capazes de recuperar as feições de resistividade em primeira ordem, desde que o levantamento possua cobertura espacial adequada e que os dados apresentem boa qualidade (Miensopust, 2017; Tietze & Ritter, 2013).

2.5. Aquisição de Dados

O levantamento magnetotelúrico de banda larga (BBMT) foi executado no âmbito do programa INCT-Estudos Tectônicos, em parceria com a Universidade Federal do Ceará (UFC). A área de estudo abrange a porção central do Domínio Rio Grande do Norte, entre os municípios de Itaú e Paraú, no estado do Rio Grande do Norte, região na qual o Bloco Campo Grande — um dos remanescentes arqueanos reconhecidos na Província Borborema — encontra-se inserido em embasamento paleoproterozoico do Complexo

Caicó e delimitado pelas zonas de cisalhamento Portalegre e Paraú (Ferreira *et al.*, 2020a,b).

Foram instaladas 21 estações distribuídas em duas configurações complementares: (i) um transecto regional de direção E-W (perfil A-A'), com 100 km de extensão e espaçamento médio de 10 km entre as estações, orientado perpendicularmente às principais estruturas e unidades geológicas do domínio; e (ii) um arranjo em grade 3×4 posicionado sobre o Bloco Campo Grande, com espaçamento de aproximadamente 5 km.

A instrumentação consistiu em unidade central ADU-07e (Metronix) operando em modo autônomo, sem estação de referência remota. A disposição de sensores compreendeu duas bobinas de indução para registro das componentes horizontais do campo magnético (Hx e Hy) e quatro eletrodos não polarizáveis de $PbCl_2$ dispostos em arranjo ortogonal para aquisição das componentes do campo elétrico (Ex e Ey), conforme procedimento descrito por Simpson & Bahr (2005). O sistema foi alimentado por baterias estacionárias de 60 Ah.

Os dados foram registrados em bandas de amostragem que cobrem períodos desde $\sim 10^{-5}$ s até $\sim 10^{-2}$ s, totalizando aproximadamente 20 horas de aquisição contínua por estação. Contudo, a elevada demanda computacional associada à inversão 3D e a baixa razão sinal-ruído característica dos períodos mais curtos motivaram a seleção de um subconjunto na faixa de $\sim 2{,}5 \times 10^{-4}$ s a $\sim 7{,}8 \times 10^{-3}$ s para as etapas subsequentes de processamento e modelagem. Após o processamento, as funções de transferência obtidas apresentam cobertura média na faixa de período de aproximadamente 10^{-3} s a 10^{2} s, embora estações individuais alcancem períodos de até 10^{4} s, o que amplia a profundidade de investigação até níveis crustais inferiores a mantélicos. A variabilidade na extensão da banda útil entre estações reflete diferenças na qualidade do sinal, no tempo efetivo de registro e na intensidade do ruído cultural em cada sítio de aquisição

2.6. Processamento de dados

O processamento teve como objetivo obter funções de transferência robustas e minimizar a influência de ruídos nas estimativas de impedância. As séries temporais brutas foram convertidas para o domínio da frequência mediante transformada de Fourier com janelamento, e a remoção de ruídos de origem antrópica, cultural e meteorológica foi conduzida por meio do algoritmo TSMP (*Time Series Manipulation Process*), que torna

possível a identificação e filtragem de interferências em segmentos específicos da série temporal (Borah *et al.*, 2015).

A principal fonte de ruído cultural identificada corresponde à rede elétrica de 60 Hz e seus harmônicos pares e ímpares, reconhecidos na análise espectral executada no *software* TSPlotter. Para supressão desses sinais, foram aplicados filtros FIR (*Finite Impulse Response*) gerados manualmente para cada canal de aquisição (Ex, Ey, Hx, Hy) nas respectivas frequências de amostragem. A banda morta MT, caracterizada por baixa amplitude do sinal natural na faixa de 1 s a 10 s, representa limitação inerente ao método e foi tratada mediante seleção criteriosa de janelas temporais com melhor razão sinal-ruído (Simpson & Bahr, 2005).

O cálculo das funções de transferência foi executado com o *software* ProcMT, que implementa estimadores robustos baseados em estatística de mínimos quadrados ponderados. A qualidade dos dados foi avaliada por meio de curvas de resistividade aparente e fase em função do período, verificando-se a suavidade e a consistência entre as componentes Zxy, Zyx, Zyy, Zxx. Estações com dados de baixa qualidade em determinadas bandas de frequência foram identificadas e os respectivos períodos excluídos da inversão. A ausência de estação de referência remota pode ter comprometido as estimativas de impedância em períodos longos, em que o ruído magnetosférico coerente é mais significativo (Chave & Jones, 2012). A construção do modelo de entrada para a inversão 3D foi realizada com o *software* 3D Grid Academic.

2.7. Análise de dimensionalidade

A determinação da dimensionalidade geoelétrica é etapa prévia indispensável à modelagem magnetotelúrica, pois orienta a escolha da estratégia de inversão e viabiliza avaliar em que medida aproximações bidimensionais são adequadas ou se a complexidade estrutural exige tratamento tridimensional (Groom & Bailey, 1989; Smith, 1995; McNeice & Jones, 2001). Neste trabalho a análise foi conduzida por meio do tensor de fase (*Phase Tensor*), conforme proposto por Caldwell *et al.* (2004). O tensor de fase (Φ), apresenta a propriedade fundamental de ser invariante sob distorções galvânicas causadas por heterogeneidades superficiais. Essa característica torna a análise independente de artefatos superficiais que comprometem métodos convencionais de decomposição, como os de Bahr (1988) e Groom & Bailey (1989), os quais pressupõem estrutura regional 1D

ou 2D. O cálculo foi executado com o pacote de código aberto MTpy (Krieger & Peacock, 2014; Kirkby *et al.*, 2019).

O parâmetro diagnóstico utilizado para discriminar a dimensionalidade é o ângulo de *skew* normalizado (β), que quantifica a assimetria da resposta magnetotelúrica regional (Caldwell *et al.*, 2004). Quando a distribuição de condutividade regional é tridimensional, β assume valores diferentes de zero (±3°), refletindo a assimetria no fluxo das correntes de indução. Graficamente, o tensor de fase é representado por elipse cujos eixos maior e menor correspondem aos eixos principais Φmax e Φmin; em estruturas 1D, a elipse degenera em círculo, ao passo que a elipticidade crescente e a variação angular dos eixos indicam influência de estruturas lateralmente heterogêneas (Caldwell *et al.*, 2004).

A análise integrada das elipses do tensor de fase para ambos os conjuntos de estações torna visível que a distribuição de condutividade crustal na área de estudo é inerentemente tridimensional em todas as escalas de profundidade amostradas (**Figura 1**). As orientações das elipses e os valores do ângulo *skew* (β) variam drasticamente entre as estações, indicando ausência de *strike* regional consistente e refletindo geologia complexa, satisfazendo o critério de Caldwell *et al.* (2004) para identificação de estruturas 3D. Conforme ressaltado por esses autores, a variação espacial rápida na direção dos eixos principais representa indicador mais confiável de tridimensionalidade.

Os resultados da análise por tensor de fase não deixam margem para aproximações bidimensionais. Uma inversão 2D introduziria artefatos nos trechos de maior contraste lateral de condutividade, distorcendo a interpretação geológica. A inversão 3D, além de respeitar a complexidade indicada pelos valores de β, é a abordagem compatível com a geometria em grade das estações sobre o BCG. Além disso, a distribuição das estações posicionadas no BCG é uniforme, em forma de grade 4x3, concordante para uma inversão 3D.

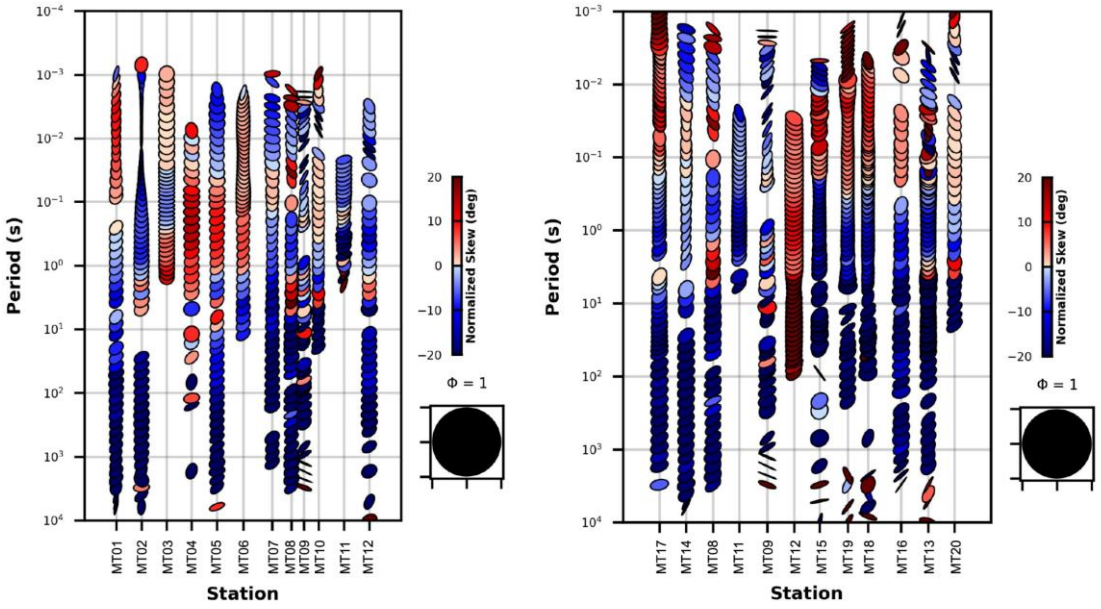

Figura 1 - Análise de dimensionalidade do tensor de fase em função do período para as estações ao longo do perfil E–W (esquerda) e do cluster BCG (direita). As elipses são coloridas pelo ângulo de *skew* normalizado (β): valores próximos de zero (tons claros) indicam estrutura elétrica uni- ou bidimensional, enquanto valores absolutos elevados (azul escuro e vermelho escuro) refletem caráter tridimensional significativo. Um círculo de referência com Φ = 1 é mostrado como escala. Elipses alongadas denotam contrastes laterais de resistividade, e a orientação do eixo maior indica a direção do *strike* geoelétrico em cada período.

2.8. Modelagem Tridimensional

A inversão tridimensional foi conduzida com o código ModEM (*Modular Electromagnetic Inversion*), desenvolvido por Egbert e Kelbert (2012) e detalhado por Kelbert *et al.* (2014). O algoritmo emprega o método *Non-Linear Conjugate Gradient* (NLCG) para minimizar iterativamente a função objetivo, que combina o desajuste entre dados observados e calculados (Φd) com um termo de regularização (Φm) que penaliza variações abruptas de resistividade, ponderados pelo parâmetro de regularização τ. O processamento foi realizado em arquitetura de computação paralela (MPI) no *cluster* da Universidade de Lisboa.

Foram invertidas as quatro componentes do tensor de impedância (Zxx, Zxy, Zyx, Zyy) não rotacionadas. A inclusão das componentes diagonais (Zxx e Zyy), embora teoricamente nulas para estruturas unidimensionais e bidimensionais, incorpora informações sobre heterogeneidades tridimensionais e efeitos de distorção galvânica (Kelbert *et al.*, 2014). A análise de dimensionalidade por tensor de fase, realizada previamente, justifica a abordagem 3D adotada, uma vez que várias estações

apresentaram valores de *skew* $|\beta| > \pm 3°$ em períodos intermediários, indicativos de estrutura tridimensional (Caldwell *et al.*, 2004).

O modelo do transecto E-W utilizou 12 estações com *error floor* de 5% para todas as componentes, valor que previne que dados de alta qualidade dominem excessivamente a inversão sem comprometer a sensibilidade às estruturas de interesse (Miensopust, 2017). A malha computacional foi construída com 30 células na direção N-S, 78 células na direção E-W e 52 camadas verticais, com 10 células de *padding* em cada direção horizontal. O espaçamento horizontal entre as estações foi discretizado em células de 2 km, garantindo ao menos quatro células de separação entre estações adjacentes — condição recomendada para evitar artefatos numéricos na solução do problema direto (Miensopust, 2017). A espessura das camadas verticais inicia em 50m e expande sucessivamente por fator de 1,2, enquanto as células horizontais de *padding* expandem por fator de 1,3. O modelo inicial consiste em semi-espaço homogêneo de 100 Ω·m.

O modelo do Bloco Campo Grande (BCG) empregou malha mais refinada, com 124 células na direção N-S, 124 células na direção E-W e 157 camadas verticais, com espaçamento horizontal de 1 km e ao menos cinco células entre estações adjacentes. A espessura inicial das camadas verticais foi reduzida para 25 m, com fator de expansão em profundidade de 1,2 e fator de expansão horizontal nas células de *padding* de 1,3. O *error floor* foi estabelecido em 10%. O semi-espaço inicial adotado corresponde a 500 Ω·m. A topografia foi incorporada ao modelo por meio do *software* 3D Grid Academic, procedimento que permite representar adequadamente as variações de altitude ao longo da área de estudo e minimizar distorções associadas à interface ar-terra (Kelbert *et al.*, 2014). A correção batimétrica não foi incorporada ao modelo, uma vez que a extensão lateral da malha de inversão restringe-se à porção continental, não abrangendo regiões oceânicas.

2.9. Resolução

Uma estratégia amplamente adotada para avaliar a resolução dos modelos consiste em executar múltiplas inversões, variando-se parâmetros de regularização e suavização, subconjuntos de dados — em termos de estações incluídas, componentes do tensor de impedância e bandas de período — e modelos iniciais, desde semiespaços homogêneos e modelos 1-D estratificados até modelos que incorporam informação *a priori* (Yang *et al.*, 2015; Miensopust, 2017).

Complementarmente, estimativas da profundidade de penetração (*skin depth*) (**Figura 2**) no período mais curto fornecem um indicativo do limite de resolução vertical em profundidades rasas, enquanto o *skin depth* no período mais longo sinaliza a profundidade máxima até a qual a informação de resistividade pode ser considerada confiável (Niblett & Sayn-Wittgenstein, 1960; Miensopust, 2017). Cabe ressaltar, contudo, que aproximações unidimensionais de profundidade de investigação, como o *skin depth* (Niblett & Sayn-Wittgenstein, 1960; Bostick, 1977), não são necessariamente representativas em contextos tridimensionais, uma vez que as correntes induzidas podem contornar corpos resistivos, alterando significativamente os caminhos de circulação e, consequentemente, a profundidade efetiva de amostragem (Miensopust, 2017). Trata-se, portanto, de estimativas rudimentares que podem indicar profundidades de investigação distintas para cada componente do tensor de impedância. Ainda assim, alguma forma de aproximação de profundidade deve ser considerada para avaliar a cobertura espacial dos dados e orientar a interpretação dos limites de confiabilidade do modelo invertido (Miensopust, 2017). Com base nessa premissa, foi elaborado neste trabalho um diagrama de *skin depth* calculado para os períodos mais longos registrados em cada estação, de modo a fornecer estimativa teórica da profundidade máxima de investigação ao longo do perfil e, assim, balizar a interpretação das feições condutivas e resistivas imageadas nas porções mais profundas do modelo.

Portanto, previamente à definição dos modelos finais, diversas configurações foram sistematicamente avaliadas. Foram testados semiespaços homogêneos de 5000, 3000, 1000, 500 e 100 Ω·m associados a diferentes geometrias de malha, bem como valores de *error floor* de 10%, 15% e 20%. O valor médio de resistividade aparente dos sítios em alta frequência é de aproximadamente 5000 Ω·m na transecta EW e 3000 Ω·m no *cluster* BCG, sugerindo *a priori* que semi-espaços de alta resistividade seriam os mais apropriados. Compatível com o documentado por Miensopust (2017), em considerar impedâncias "médias" para restringir a faixa de modelos iniciais adequados. Entretanto, essas configurações apresentaram dificuldade de convergência, imprimindo valores elevados de RMS nos modelos finais. Os melhores ajustes foram obtidos com semiespaço de 100 Ω·m para o transecto E-W e 500 Ω·m para o BCG (Figura 3 e Figura 4).

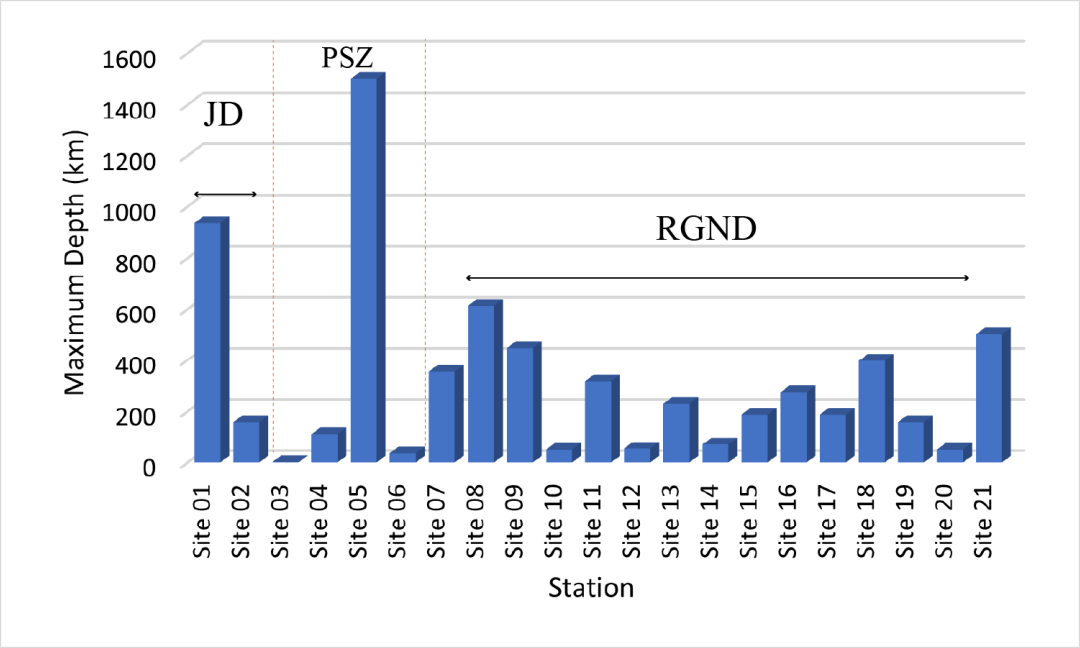

Figura 2 - Gráfico de profundidade máxima de penetração (*skin depth*) para cada estação MT, subdividido de acordo com os domínios geológicos. Variações na altura das barras revelam domínios elétricos distintos, desde zonas resistivas (barras altas) até áreas de atenuação do sinal sobre estruturas condutoras (barras baixas). Legenda: JD – Domínio Jaguaribe; PSZ – Zona de Cisalhamento Portalegre; RGND – Domínio Rio Grande do Norte.

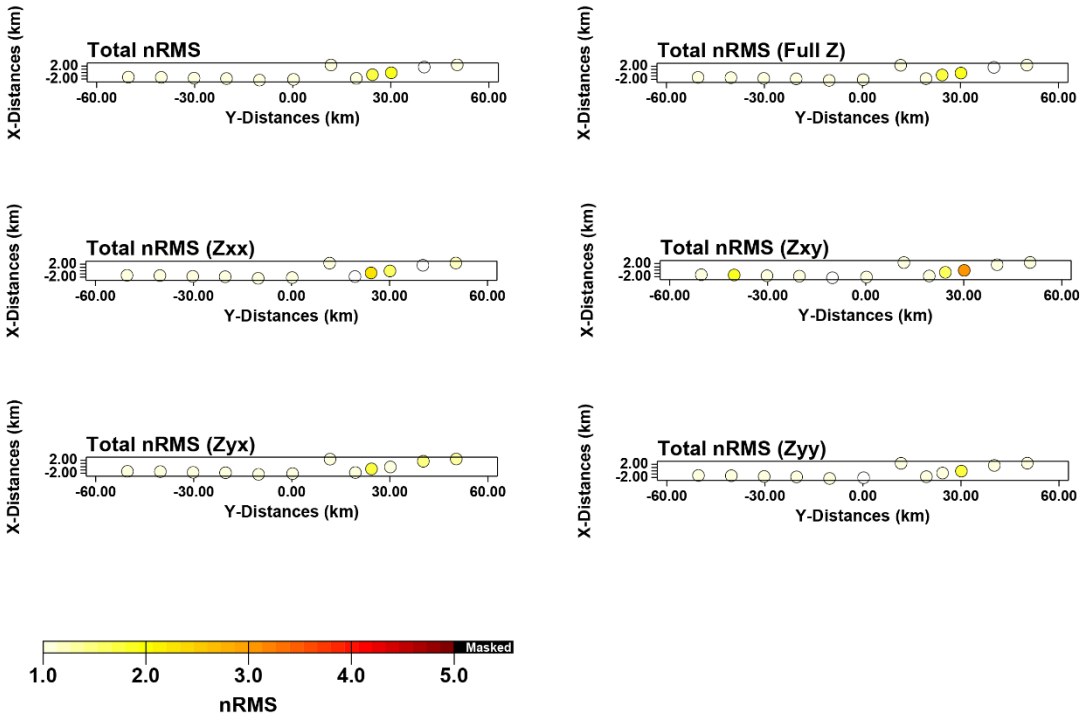

Figura 3 - Distribuição espacial do desajuste nRMS (normalized root-mean-square) da inversão 3D MT para as estações ao longo do perfil E–W. Os mapas apresentam o nRMS total (superior esquerdo), o tensor de impedância completo Z (superior direito) e as componentes individuais Zxx, Zxy, Zyx e Zyy. Cada

círculo representa uma estação MT, colorido de acordo com o valor de nRMS. As 12 estações selecionadas para a inversão ao longo deste transecto estão destacadas.

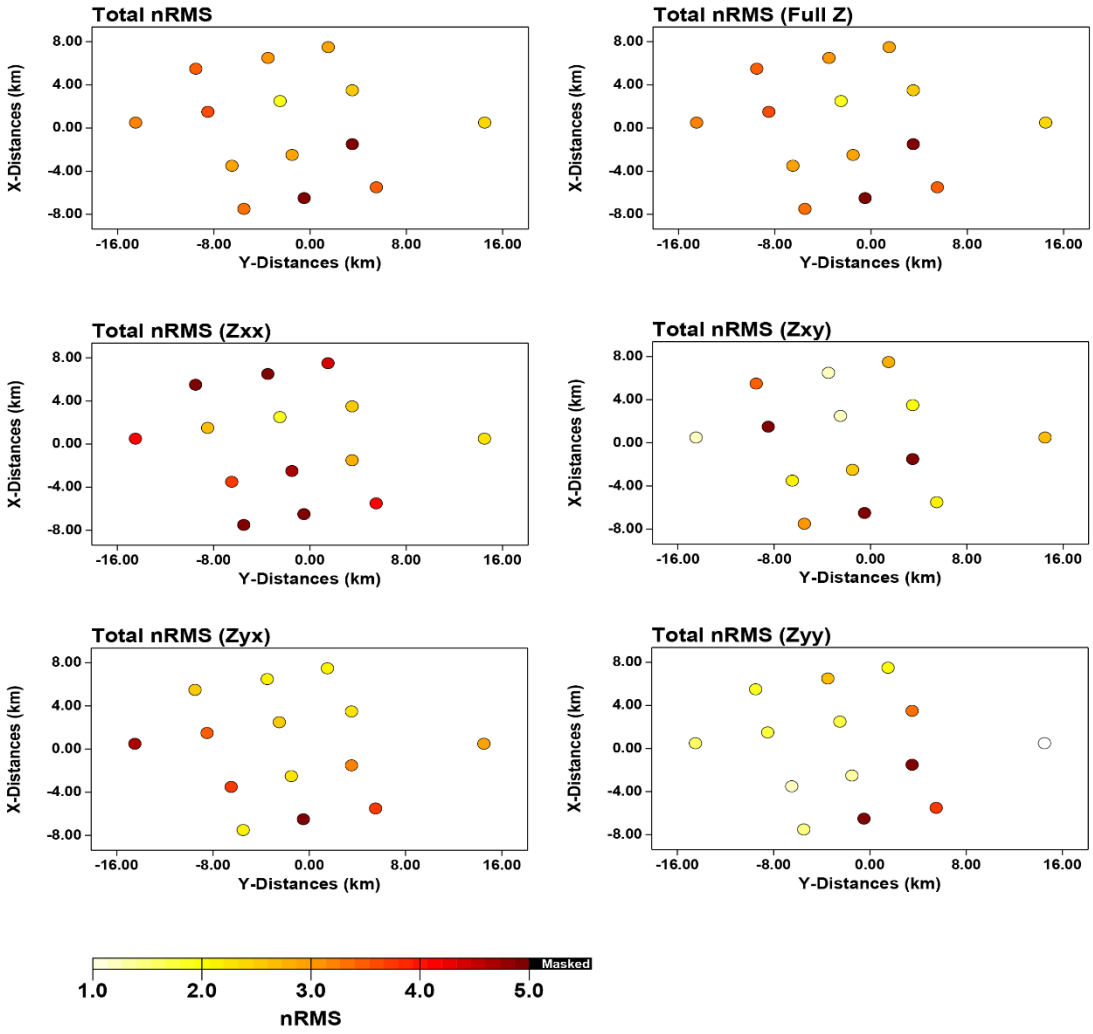

Figura 4 - Distribuição espacial do desajuste nRMS (normalized root-mean-square) da inversão 3D MT para as estações do cluster BCG. Os mapas apresentam o nRMS total (superior esquerdo), o tensor de impedância completo Z (superior direito) e as componentes individuais Zxx, Zxy, Zyx e Zyy. Cada círculo representa uma estação MT, colorido de acordo com o valor de nRMS.

O nRMS mais elevado obtido para o modelo do Bloco Campo Grande em relação ao perfil E-W reflete a maior complexidade tridimensional das estruturas imageadas na configuração em grade, onde o núcleo arqueano resistivo circundado por condutores com geometrias irregulares em todas as direções impõe ao algoritmo de inversão um espaço de parâmetros significativamente mais amplo e com maior trade-off entre ajuste e regularização (Miensopust, 2017). Adicionalmente, a heterogeneidade na cobertura de

banda entre as estações da grade — com algumas estações apresentando períodos máximos limitados a 1–10 s — restringe a capacidade do modelo de reproduzir simultaneamente as respostas de todas as estações em toda a faixa de períodos, contribuindo para o incremento do *misfit* global. Valores de nRMS entre 3 e 5 são frequentemente reportados em inversões 3D de arranjos densos sobre estruturas geologicamente complexas (e.g., Khoza *et al.*, 2013; Burd *et al.*, 2014), sendo considerados aceitáveis quando os principais corpos anômalos mantêm consistência posicional entre os diferentes testes realizados.

Cabe ressaltar que, independentemente das diferenças de nRMS entre os modelos testados, os principais corpos anômalos — domínios resistivos e zonas condutoras — mantiveram posições espaciais concordantes em todos os testes realizados, com variações restritas às estimativas de profundidade e aos efeitos de borda. A persistência das feições frente a diferentes parametrizações funciona como critério de robustez amplamente utilizado na literatura MT (e.g., Burd et al., 2014; Moorkamp *et al.*, 2022; Padilha *et al.*, 2016).

2.10. Testes de sensibilidade

A robustez das anomalias condutivas identificadas nos modelos finais foi avaliada por meio de testes de sensibilidade, procedimento amplamente empregado em estudos magnetotelúricos 3D para verificar se determinada feição é requerida pelos dados observados ou se é um artefato do processo de inversão. O teste consiste em substituir as anomalias condutivas por valores resistivos no modelo final convergido e utilizar o modelo perturbado como ponto de partida para nova inversão, mantendo inalterados todos os demais parâmetros. Se o algoritmo recuperar as feições condutivas nas mesmas posições, demonstra-se que estas são exigidas pelos dados; caso contrário, a anomalia é considerada artefato (Egbert & Kelbert, 2012; Miensopust, 2017; Schwalenberg *et al.*, 2002).

Nos testes realizados todos os corpos condutores identificados foram substituídos simultaneamente por valor resistivo de 1000 Ω·m, mantendo-se inalterados os domínios resistivos, a malha computacional e o conjunto de dados observados. O *error floor* empregado foi de 5% para o transecto E-W e 10% para o BCG, valores idênticos aos das inversões originais. Os modelos perturbados foram submetidos a novos ciclos de inversão com o código ModEM (Kelbert *et al.*, 2014).

No perfil E-W os cinco condutores (C1, C2, C3, C4 e C5) foram forçados a 1000 Ω·m. Após 35 iterações, o algoritmo recuperou as cinco anomalias condutivas nas mesmas profundidades e posições laterais do modelo original, incluindo os condutores C4 e C5, cujas posições situam-se nas porções marginais da cobertura de investigação. A recuperação desses condutores mesmo em regiões com menor densidade de estações reforça que os dados observados exigem a presença dessas anomalias para ser satisfatoriamente ajustados.

No modelo tridimensional do Bloco Campo Grande, o domínio espacial não abrange a Zona de Cisalhamento Portalegre, de modo que o condutor C1 não integra o conjunto de feições testadas. Os condutores C2, C3, C4 e C5, que circundam o núcleo resistivo arqueano nas bordas oeste, leste, sul e norte, respectivamente, foram substituídos por 1000 Ω·m e o modelo perturbado re-invertido sob condições idênticas às da modelagem original.

Após 72 iterações, os quatro condutores aparecem no modelo re-invertido, com geometria e posições próximas às do modelo original, embora apresentem configurações geométricas parcialmente distintas. As variações observadas refletem a não unicidade inerente ao problema inverso em magnetotelúrica, na qual distintos modelos de resistividade podem reproduzir satisfatoriamente o mesmo conjunto de dados (Chave & Jones, 2012). Contudo, a consistência posicional das anomalias indica que a existência desses corpos condutores é uma exigência dos dados, enquanto os detalhes geométricos possuem maior grau de liberdade.

CAPÍTULO 3

ARTIGO

DEEP GEOMETRY OF CAMPO GRANDE ARCHEAN NUCLEUS, BORBOREMA PROVINCE: A 3D MAGNETOTELLURIC APPROACH

Pessanha, L.O.[1]; Dantas, E.L.[1]; Silva, F.M.[2]; Magini, C.[3]; Fuck, R.A.[1]; Ferreira, A.C.D.[1]; Silva, N.C.V. [3]

[1][Universidade de Brasília]; [2][Universidade Federal de Uberlândia]; [3][Universidade Federal do Ceará].

Abstract

Archean crustal fragments preserved in the Borborema Province, NE Brazil, as small nuclei bordered by younger Precambrian terranes, constitute privileged windows into the processes of continental growth and stabilization during the assembly of West Gondwana. The Campo Grande Block, located in the central portion of the Rio Grande do Norte Domain, represents one such remnant, whose expression at depth remained unknown until the present study. This work investigated the geoelectrical structure of the Campo Grande Block and adjacent terrains through a broadband magnetotelluric survey, configured as an E–W profile of 100 km with 21 stations and 10 km spacing, infilled to 5 km over the Archean nucleus area. Data processing involved cultural noise filtering, dimensionality analysis using the phase tensor, and three-dimensional inversion with the ModEM algorithm, and the resulting model was critically assessed for robustness to provide a coherent view of the regional structure. The inversion revealed significant electrical resistivity heterogeneity in the crust, with the identification of three resistive bodies (R1 to R3) and three main conductors (C1 to C3), in addition to two peripheral conductors (C4 and C5) whose characterization is limited by survey coverage. Body R1 was interpreted as corresponding to the Jaguaretama Complex, composed of Neoproterozoic orthogneisses and paragneisses, with a resistivity contrast at approximately 8 km depth, while R2 is related to Neoproterozoic granites with a geoelectrical depth of 16 km. Finally, R3 reaches a resistivity contrast at 17 km depth and was interpreted as belonging to Paleoproterozoic orthogneisses and Archean migmatitic orthogneisses of the Campo Grande Complex. The R3 domain exhibits a domal geometry with a core resistivity exceeding 10,000 Ω·m down to 5 km, enveloped by less resistive material dipping to the southwest down to 17 km depth, a configuration consistent with progressive accretion around an Archean nucleus. Conductor C1 marks the Portalegre Shear Zone with a westward dip to 14 km depth, confirming its role as a crustal boundary between the Jaguaribe and Rio Grande do Norte domains. The 3D resistivity model also reveals dextral displacement within the identified bodies. The elongated geometry and lateral offset of the resistive blocks at depth indicate kinematics consistent with transcurrent stresses in the crustal framework of the region. Conductors C2 and C3 suggest, respectively, a low angle intracrustal structure and a Paleoproterozoic suture

zone reaching the middle crust. The results corroborate the structural complexity of the Borborema Province and demonstrate the potential of 3D MT methodology in characterizing deep crustal structures and in understanding regional tectonic evolution as a result of terrain amalgamation throughout Precambrian orogenic orogenies. Lastly conclude that the 3D magnetotelluric method, in an infilled grid array, allows discrimination at depth of crustal domains of different ages and compositions in polydeformed terrains, offering adequate resolution to characterize the geometry of Archean nuclei and the structures that bound them.

***Keywords*:** Magnetotelluric; Borborema Province; 3D modeling; Campo Grande Block; Archean nucleus; Portalegre Shear Zone.

3.1. Introduction

The application of the magnetotelluric method in subsurface characterization across different geodynamic settings highlights its versatility and spatial resolution (e.g., Yi *et al.*, 2022; Khoza *et al.*, 2013; Meqbel *et al.*, 2014) This magnetotelluric method has proven effective in investigations of deep tectonic structures, suture zones, terrane boundaries, and conductive anomalies associated with fluids and partial melting (e.g., Correa *et al.*, 2023; Meqbel *et al.*, 2014; Padilha *et al.*, 2013, 2019; Yang *et al.*, 2015; Silva *et al.*, 2026).

Specifically, studies conducted in Archean cratons worldwide have demonstrated that these units preserve distinctive geoelectrical signatures, characterized by high resistivity associated with a thermally stabilized and chemically depleted lithosphere, and demonstrate the method's capability to discriminate lithological domains of different compositions and ages (e.g., Evans *et al.*, 2011; Jones *et al.*, 2009; Hill *et al.*, 2021; Ma *et al.*, 2021). MT surveys with densified station spacing, integrated with seismic and geological data, allow the identification of crustal conductors attributed to interconnected sulfides and high iron content in Fe/Mg-bearing silicates, and can characterize the internal structures of greenstone belt sequences (Ma *et al.*, 2021). Archean nuclei exhibit deep resistive signatures in the Kaapvaal and Congo cratons and are bounded by lithospheric-scale conductive anomalies commonly associated with suture zones and metasomatic processes (Jones *et al.*, 2009; Moorkamp *et al.*, 2022). Precambrian and Phanerozoic gneissic complexes and domes offer a still underexplored field of application for the MT method and illustrate how the geoelectrical signature of gneiss domes is controlled not

only by lithological composition but also by the geodynamic setting and the thermal state of the lithosphere (e.g., Kaufl *et al.*, 2020; Roots *et al.*, 2022). Moderately resistive zones at depths of 30 to 40 km laterally truncate conductors interpreted as water-rich melts and fluids released during subduction of the Indian plate beneath the Asian plate (Sheng *et al.*, 2023), while conductive values can be associated with the upward transport of partially molten material in gneiss domes (Chen *et al.*, 1996). In contrast, resistive values are also recorded in domes within collisional orogenic belts (Yi *et al.*, 2022), when using a densified station array at 10 km and 5 km spacing. Thus, the imaging of conductors dipping in a given direction are interpreted as remnants of subducted oceanic crust, demonstrating that the MT method has the potential to characterize deep sutures preserved in ancient orogens.

Conductors situated in Precambrian orogenic settings are generally attributed to interconnected networks of graphite films along grain boundaries, saline aqueous fluids trapped in fracture porosity, conductive opaque minerals such as sulfides and oxides in interconnected arrangements, grain-size reduction zones associated with mylonitization, or combinations of these factors (Jones, 1993; Selway, 2014; Weckmann, 2012). The effective resistivity of the medium depends not only on the presence of these conductive phases but primarily on their interconnectivity, which is controlled by deformational, metamorphic, and hydrothermal processes that affected the crust throughout its evolution (ten Grotenhuis et al., 2004; Kawano et al., 2012). Crustal shear zones constitute preferential sites for the development and preservation of such conditions, as these structures concentrate deformation, channel fluids, and promote the accumulation of conductive mineral phases over extended geological timescale (Abdul Azeez *et al.*, 2017; Yin *et al.*, 2014). Magnetotelluric studies across suture zones and terrane boundaries demonstrate that crustal conductors associated with collisional processes constitute long-lived geoelectrical signatures that preserve the record of past tectonic interactions, even after thermal and mechanical stabilization of the crust (Jones, 1993; Boerner *et al.*, 1996; Unsworth, 2010; Weckmann, 2012; Bologna *et al.*, 2017; Padilha *et al.*, 2019).

The Borborema Province, in northeastern Brazil, presents suitable conditions for the application of these geophysical approaches. Its crustal architecture results from the diachronous amalgamation of multiple terranes during the orogenic cycles that culminated in the formation of West Gondwana in the Neoproterozoic (Brito Neves *et al.*, 2000; Van Schmus *et al.*, 2008). The geological record exposes a mosaic of

Paleoproterozoic and Archean blocks, partially covered by metavolcanosedimentary sequences, intensely reworked during the Brasiliano Orogeny and crosscut by a network of continental-scale transcurrent shear zones (Arthaud *et al.*, 2008; Brito Neves & Fuck, 2014).

Magnetotelluric surveys conducted in the Borborema Province over the past decades have provided a regional overview of electrical resistivity distribution, identifying resistive blocks bounded by conductors associated with major transcurrent lineaments (Padilha *et al.*, 2014, 2017), and characterized the lithospheric structure of different tectonic domains. The tectonic framework of the Borborema Province reveals a heterogeneous architecture with crustal conductors coincident with shear zones interpreted as depth extensions of these structures (Garcia *et al.*, 2019). The depth of conductive bodies reaches 10 to 20 km, associated with sub horizontal structures (Santos Matos *et al.*, 2019). More recently, Padilha *et al.* (2021) and Benevides *et al.* (2026) identified a resistive structure in the Archean São José do Campestre complex, and domal features beneath the Tróia-Tauá Massif, also of Archean age. These contributions, however, dominantly adopted regional-scale acquisition strategies, with station spacings on the order of 50 to 70 km, suitable for characterizing first-order features but insufficient to resolve smaller-scale heterogeneities or to investigate in detail the internal structure of specific blocks.

The present work, therefore, introduces an unprecedented investigative approach for the central portion of the Rio Grande do Norte Domain (RGND), in the Campo Grande Block (CGB). The deep crustal structure of the CGB remains uninvestigated by electromagnetic methods. Seeking to fill this gap, a broadband magnetotelluric survey with a densified array was implemented for the first time in the region, comprising a 100 km E-W transect with 10 km station spacing, complemented by a grid array with 5 km spacing over the Campo Grande Block. This crustal fragment, with approximately 1,500 km² and a domal geometry with a SSW-NNE axis, preserves one of the rare records of Archean crust in the Borborema Province (Ferreira *et al.*, 2020a, 2020b).

3.2. Regional Geology

The Borborema Province comprises a Precambrian shield situated in the north-northeastern portion of the South American continent (Almeida *et al.*, 1981). It consists of Paleoproterozoic to Archean blocks and domains reworked during Paleo- and Neoproterozoic collisional orogenies (e.g., Dantas *et al.*, 2004, 2013; Ferreira *et al.*,

2020). The final configuration of the Borborema Province resulted from the diachronous convergence of the West African–São Luís and São Francisco–Congo cratons during the Neoproterozoic Brasiliano/Pan-African Orogeny (Arthaud *et al.*, 2008; Van Schmus *et al.*, 2008; Brito Neves & Fuck, 2014; Ganade *et al.*, 2016). This multiphase tectonothermal event was responsible for imposing low- to high-grade metamorphism, enabling the intrusion of a large number of granitic plutons and, crucially, developing a complex network of steeply dipping, continental-scale transcurrent shear zones with dominant NE-SW orientations (Brito Neves *et al.*, 2000). This complex system of crustal-scale, high- to low-temperature shear zones separates variably deformed massifs and domains composed of meta-supracrustal sequences and Neoproterozoic granitic intrusions (e.g., Caby *et al.*, 1991; Jardim de Sá, 1994; Brito Neves *et al.*, 2000; Van Schmus *et al.*, 2008; Brito Neves & Fuck, 2014).

The characterization and subdivision of the Borborema Province into distinct sub provinces and geotectonic domains dates back to the pioneering works of Almeida *et al.* (1977, 1981), having been subsequently detailed and refined by several authors (Santos *et al.*, 1984; Brito Neves *et al.*, 1995, 2000; 2021; 2022; Van Schmus *et al.*, 1995; Santos, 1996, 1999; Santos & Medeiros, 1999; Medeiros *et al.*, 2011). From west to east, the northern sub province is divided into three domains separated by the Senador Pompeu and Portalegre ductile shear zones: the Ceará Central, Jaguaribe, and Rio Grande do Norte domains (Arthaud *et al.*, 2008; Brito Neves *et al.*, 2000; 2021; 2022) (**Figure 5**).

The Jaguaribe Domain is bounded by the Senador Pompeu and Portalegre shear zones, separating it from the Ceará Central and Rio Grande do Norte domains, respectively. Paleoproterozoic gneiss and migmatite complexes dominate, along with late Paleoproterozoic volcanosedimentary sequences (1.7–1.8 Ga) and associated intrusive granites (ca. 1.69 Ga) (Sá *et al.*, 1995; Parente & Arthaud, 1995), intensely deformed and recrystallized by Brasiliano deformation. This domain is characterized by high electrical conductivity anomalies, associated with interconnected highly conductive solid phases precipitated from carbon-rich volatiles during late Paleoproterozoic magmatic intrusion, intensified by subsequent compressional events (Padilha *et al.*, 2014).

The Rio Grande do Norte Domain, in the northeastern portion of the Borborema Province, is bounded to the west by the Portalegre Shear Zone, with a NE trend and dextral transcurrent kinematics, and to the south by the Patos-Adamaoua Shear Zone, with an E-W trend (e.g., Jardim de Sá *et al.*, 1994; Brito Neves *et al.*, 2011). Several shear zones

represent local adjustments within each domain, dividing the Rio Grande do Norte Domain into four high-grade migmatitic-gneissic blocks (Caicó, Lajes, Antônio Martins, and Campo Grande–Itajá) (Brito Neves *et al.*, 2000; Van Schmus *et al.*, 2008; Ferreira *et al.*, 2020). U-Pb ages indicate that Rhyacian (2.25 to 2.15 Ga) high-K calc-alkaline metamorphic-magmatic rocks (Hollanda *et al.*, 2011) and Siderian (2.3 Ga) supracrustal rocks form the basement of the Neoproterozoic Seridó Group (Brito Neves & Fuck, 2014; Hackspacher *et al.*, 1990; Alvim *et al.*, 2026). To the east of the Campo Grande Block, the Paraú Lineament develops, defining the boundary with the Itajá Block (Ferreira *et al.*, 2020).

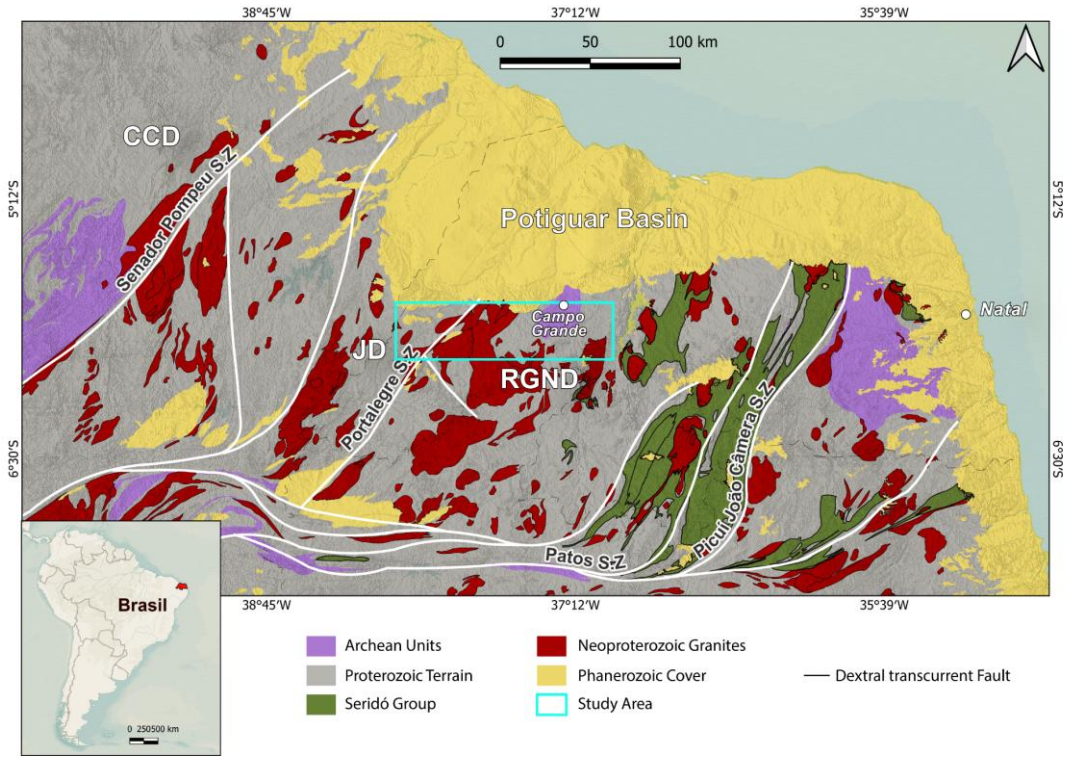

Figure 5 - Simplified map of Rio Grande do Norte state with the study area outlined by the blue rectangle. Legend: CCD- Ceará Central Domain; JD-Jaguaribe Domain; RGND- Rio Grande do Norte Domain.

3.3. Architecture and Compartmentalization of the Campo Grande Block

The Campo Grande Block (CGB) represents a crustal fragment of approximately 1,500 km² with ellipsoidal to domal geometry and a SSW-NNE principal axis (Ferreira *et al.*, 2020a, 2020b). It exhibits a distinctive concentric architecture, with a heterogeneous core built by a migmatitic complex of tonalitic to granitic composition, associated with mafic-ultramafic rocks of Archean age. This central domain is surrounded by a 10 to 20 km ring of coarse-grained biotite and K-feldspar orthogneisses of alkaline affinity and

Paleoproterozoic age. The outer ring comprises Neoproterozoic granitic intrusions enriched in K-feldspar, exemplified by the Caraúbas Granite (Ferreira *et al.*, 2020a,b). The gamma-spectrometric signature reflects this compartmentalization: the central migmatites exhibit elevated Th and K concentrations, which decrease abruptly in the orthogneisses of the intermediate ring and rise again in the outer granites, delineating distinct geological compartments from west to east (Ferreira *et al.*, 2020a,b). The Campo Grande migmatitic complex represents the only 2.9 Ga tonalitic crustal block preserved in the central portion of West Gondwana, despite the intense reworking experienced during the Paleoproterozoic and Neoproterozoic orogenies (Ferreira *et al.*, 2020a,b), exhibiting intense polyphase deformation, including coaxial refolding, pervasive foliation, and NNE-trending shear zone systems, with intensification of reworking processes at the margins of the Archean dome relative to the core (Ferreira *et al.*, 2020a,b).

The oldest record of the CGB corresponds to the formation of tonalitic to granodioritic crust in the Mesoarchean, between 2.92 and 2.89 Ga, which built the substrate upon which subsequent events developed (Ferreira *et al.*, 2020a,b). The domal geometry observed at the center of the core involves migmatites forming an architecture with circular geometry and low-angle dipping foliations.

Magmatic and deformational events dated in the Paleoproterozoic between 2.25 and 2.18 Ga are characterized by high-K calc-alkaline magmatism and represent a zone of thermal weakening that favored both reworking and the addition of juvenile mantle-derived material (Ferreira *et al.*, 2020a,b). In the Borborema Province, this Paleoproterozoic magmatic arc magmatism corresponds to one of the most significant periods of crustal growth in the South American continent. During the Paleoproterozoic orogeny, the Archean magmatic protoliths were tectonically imbricated with the Mesoarchean tonalitic to granodioritic crust (Ferreira *et al.*, 2020a).

Three stages in the Neoproterozoic evolution were recognized by Ferreira *et al.* (2025) and Gordilho-Barbosa *et al.* (2025) in the Campo Grande Block, as follows: (i) crustal thickening and eclogite-facies metamorphism between ca. 624 and 590 Ma; (ii) decompression and exhumation of the CGB initiated between ca. 575 and 563 Ma, an interval constrained by U-Pb ages on deformed titanites aligned with the foliation and shear zones (574.7 to 562.8 Ma), temporally coincident with the development of the main transcurrent structures of the Borborema Province (Ferreira *et al.*, 2025); (iii) cooling and

stabilization at shallow crustal levels between ca. 559 and 523 Ma (Ferreira *et al.*, 2025). This evolution, spanning ca. 100 Ma from eclogite-facies conditions to final cooling, is comparable in timescale to processes documented in Phanerozoic collisional orogens such as the Himalayas (Ferreira *et al.*, 2025).

3.4. Neoproterozoic Granite Magmatism and Strike-Slip Shear Zone System

The Neoproterozoic orogenic system was accompanied by extensive granitic magmatism, represented by different suites well characterized in the region (Galindo, 1993; Galindo *et al.*, 1995; Magini & Hackspacher, 2008; Galindo *et al.*, 2012; Nascimento *et al.*, 2008, 2015).

The Itaporanga-type granites represent one of the most characteristic magmatic suites of Ediacaran plutonism in the Borborema Province. Nascimento et al. (2000, 2008, 2015) and Angelim *et al.* (2006) reorganized the various Ediacaran plutons of the Rio Grande do Norte Domain.

The Tourão-Caraúbas granitic complex crops out northeast of the Umarizal Pluton. It occurs as stocks or dikes and is classified as belonging to the High-K Calc-Alkaline Porphyritic Suite (Nascimento *et al.*, 2000, 2008, 2015; Trindade *et al.*, 1999; Galindo, 1993), with U-Pb zircon ages of 589.3 ± 4.4 Ma (Valcácio *et al.*, 2022) and U-Pb titanite ages of 580 ± 4 Ma (Trindade *et al.*, 1999). Rb-Sr whole-rock isochrons yielded ages of 630–600 Ma for the porphyritic granites of the region (Archanjo *et al.*, 1998).

The Umarizal Pluton has an approximate area of 300–350 km² and dominantly quartz-syenitic and potassic monzogranitic composition, exhibits a dominantly alkaline character and displays A-type and within-plate granite characteristics (Galindo *et al.*, 1995; Archanjo *et al.*, 1998), being classified as representative of the Alkaline Charnockitic Suite of the RGND, dated between 580 and 540 Ma (Nascimento *et al.*, 2000, 2008, 2015; Angelim *et al.*, 2006). The exhumation of the Campo Grande Block is intimately related to the syntectonic emplacement of granitic bodies along the shear zones between 560 and 530 Ma, considering that the transcurrent shear zones bounding the CGB functioned as preferential conduits for the ascent of the block from eclogite-facies depths to shallower crustal levels.

The Portalegre Shear Zone (PSZ) is a NNE-SSW-trending transcurrent fault with an extension of approximately 120 km (Archanjo *et al.*, 1998; Valcácio *et al.*, 2022),

recognized as an important marker in the division between the Rio Grande do Norte Domain, to the east, and the Jaguaribe Domain, to the west (Arthaud *et al.*, 2008; Van Schmus *et al.*, 2008). This boundary is recorded both in the ages of the terranes surrounding this structure and by geophysical anomalies, juxtaposing terranes with distinct geophysical signatures (Cavalcante *et al.*, 1998; Cavalcante, 1999; Campelo, 1999; Oliveira, 2008; Fuck *et al.*, 2013). The PSZ developed during the late Neoproterozoic, causing widespread displacement of tectonic blocks (e.g., Araujo *et al.*, 2013; Fossen *et al.*, 2022) and was reactivated in the Phanerozoic during rifting processes and formation of the Potiguar Basin (Hackspacher & Legrand, 1989; Nóbrega *et al.*, 2005).

To the southwest, the PSZ connects with the E-W-trending Patos Shear Zone (PaSZ), constituting part of an interconnected shear zone system that bounds voluminous Neoproterozoic intrusive magmatism in the Borborema Province (Archanjo *et al.*, 1998). This shear zone system is interpreted as synchronous or late-tectonic relative to the collision of the São Francisco and Congo cratons, probably controlling the emplacement of Ediacaran granitic plutons (Galindo *et al.*, 1995; Vauchez *et al.*, 1995; Archanjo *et al.*, 1998; Trindade *et al.*, 1999). Along its trace, the PSZ displays subvertical mylonitic foliation and subhorizontal stretching lineation, a pattern typical of a transcurrent regime (Archanjo *et al.*, 1998). Mineral assemblages and metamorphic textures indicate that the main mylonitization along the PSZ evolved under upper greenschist facies conditions (Hackspacher & Legrand, 1989; Archanjo *et al.*, 1998). McReath *et al.* (2002), however, observed that the porphyritic granites emplaced within the PSZ exhibit mineral parageneses compatible with amphibolite facies, indicating that the greenschist facies record would be linked to a later retrometamorphic event, unrelated to Ediacaran plutonism.

The PSZ, together with the NW-trending Frutuoso Gomes Shear Zone (FGSZ), played a fundamental role in the structural control of the emplacement of the Umarizal Pluton and other Ediacaran granitic bodies in the region (Archanjo *et al.*, 1998). Structural and kinematic data suggest that these shear zones penetrate deeply into the crust, as suggested by the presence of abundant low-angle reflections obtained in seismic profiles across the continental portion of the Potiguar Basin, interpreted as inherited Brasiliano structures following the fragmentation of the Pangaea continent in the Mesozoic (Matos, 1992; Archanjo *et al.*, 1998).

The Potiguar Basin, which hydrocarbon reservoirs of the Pendência Formation, is part of the Cretaceous rift system of northern Brazil. Its origin is linked to a Mesozoic rift event, related to the crustal stretching process that resulted in the breakup of Pangaea and culminated in the separation of the South American and African continents (Bertani *et al.*, 1990; Matos, 1992). The geometry and architecture of this basin were controlled and compartmentalized by the reactivation of pre-existing structures and crustal discontinuities in the Borborema Province, such as Neoproterozoic shear zones. This led to the development of a set of asymmetric half-grabens and internal highs with a dominant NE-SW trend (Neto *et al.*, 2007). The Pendência Formation is composed of alluvial, fluvio-deltaic, and lacustrine conglomerates, sandstones, and shales. Sedimentary infilling occurred synchronously with graben development, where a series of deep lakes of saline and fresh waters formed, accumulating thick siliciclastic wedges (Bertani *et al.*, 1990; Araripe & Feijó, 1994).

In recent years, deep geophysical investigation of the Borborema Province and its adjacent regions has increasingly employed the Magnetotelluric (MT) method. The focus of these studies has been to decipher the geometry and articulation of amalgamated crustal blocks, as well as to investigate the role of these major transcurrent lineaments in the lithospheric structure (e.g., Padilha *et al.*, 2014, 2017; Benevides *et al.*, 2026; Silva *et al.*, 2026). The contributions of these authors provide a fundamental foundation for understanding the regional lithospheric architecture and have dominantly adopted transects as acquisition strategy. However, previous MT surveys have concentrated mainly on portions to the east, west, and south of the area of interest of this study.

The central objective of this work is to characterize the three-dimensional geoelectrical structure of the Campo Grande Block and adjacent terrains, contributing to the understanding of the crustal architecture and tectonic evolution of the central portion of the Rio Grande do Norte Domain. Specifically, it seeks to: (i) define the geometry and depth extent of the main resistive domains, correlating them with the geological units mapped at the surface; (ii) characterize the conductive zones that bound these domains, investigating their association with regional tectonic structures, particularly the Portalegre Shear Zone; (iii) evaluate the capability of the broadband MT method, in a densified array configuration, to discriminate preserved Archean nuclei in polydeformed terranes; and (iv) establish comparisons with geoelectrical signatures documented in Archean terranes

from other localities, contributing to the understanding of the factors that control the magnetotelluric response of Precambrian gneiss domes.

Despite its relevance for understanding the crustal evolution of the province, the deep geometry of the Campo Grande Block remained unknown. Fundamental questions awaited investigation: what is the vertical extent of the Archean core? How do the different units composing the block articulate at depth? What is the geoelectrical expression of the Portalegre Shear Zone and to what depth does this structure penetrate the crust? Is it possible to distinguish the Archean core from its Paleoproterozoic envelope through the magnetotelluric signature? These questions could not be answered by the pre-existing regional MT surveys, whose station spacing did not allow adequate resolution for structures of this scale.

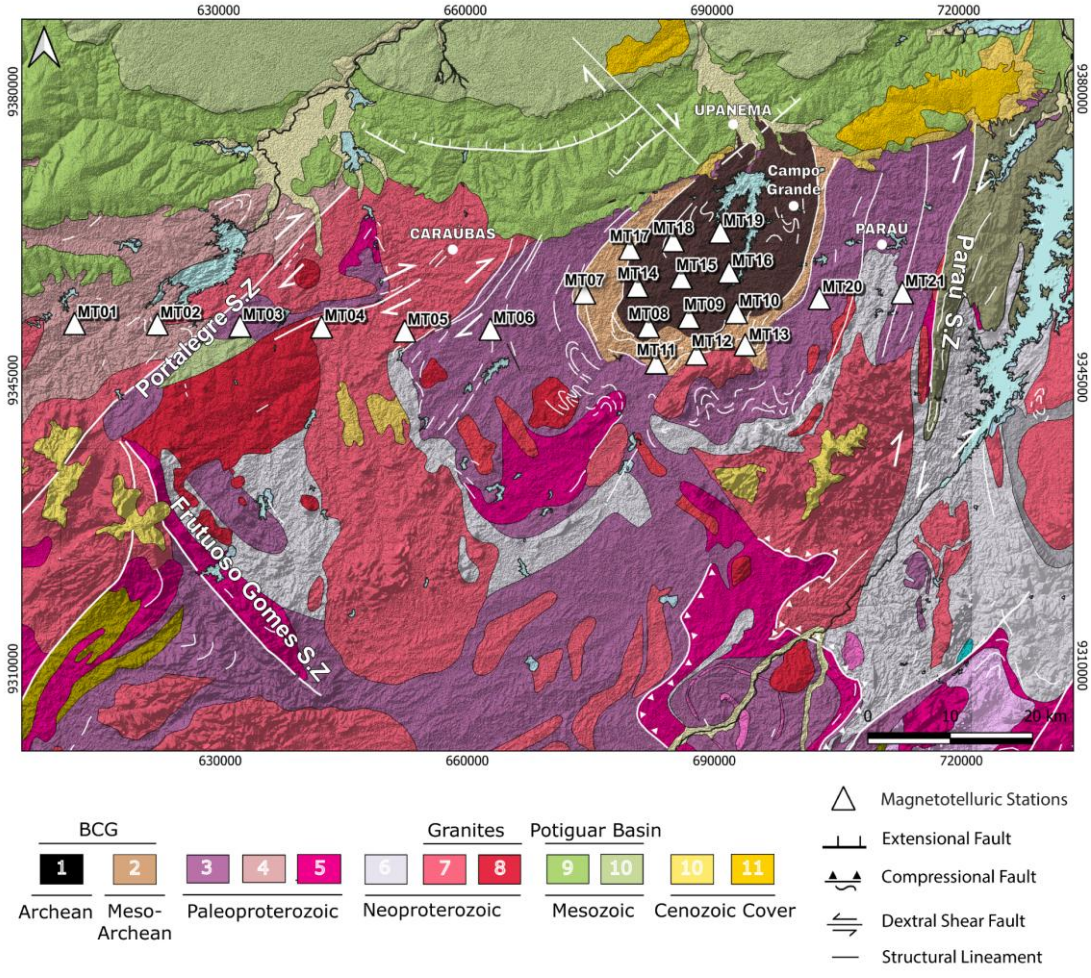

Figure 6 - Simplified geological map of the study area. The numbered legend corresponds to: 1 – Archean CGB Block; 2 – Mesoarchean rocks of the CGB; 3 – Caicó Complex; 4 – Jaguaretama Domain; 5 – Paleoproterozoic granites; 6 – Jucurutu Formation; 7 – Umarizal Granite; 8 – Tourão-Caraúbas Granite; 9, 10 – Potiguar Basin; 11 – Cenozoic cover.

3.5. Methodology

3.5.1. Data Acquisition

The broadband magnetotelluric (BBMT) survey was carried out within the framework of the INCT-Estudos Tectônicos, program, in partnership with the Federal University of Ceará (UFC). The study area covers the central portion of the Rio Grande do Norte Domain, between the municipalities of Itaú and Paraú, in the state of Rio Grande do Norte (fig. 6), a region in which the Campo Grande Block — one of the recognized Archean remnants in the Borborema Province — is embedded within the Paleoproterozoic basement of the Caicó Complex and bounded by the Portalegre and Paraú shear zones (Ferreira et al., 2020a,b).

Twenty-one stations were deployed in two complementary configurations (Fig. 6): (i) a regional E-W transect (profile A-A'), with 100 km of extension and an average spacing of 10 km between stations, oriented perpendicular to the main structures and geological units of the domain; and (ii) a 3×4 grid array positioned over the Campo Grande Block, with a spacing of approximately 5 km.

The instrumentation consisted of an ADU-07e central unit (Metronix) operating in autonomous mode, without a remote reference station. The sensor layout comprised two induction coils for recording the horizontal components of the magnetic field (Hx and Hy) and four $PbCl_2$ non-polarizable electrodes arranged in an orthogonal configuration for acquisition of the electric field components (Ex and Ey), following the procedure described by Simpson & Bahr (2005). The system was powered by 60 Ah stationary batteries.

Data were recorded across sampling bands covering periods from $\sim 10^{-5}$ s to $\sim 10^{-2}$ s, totaling approximately 20 hours of continuous acquisition per station. However, the high computational demand associated with 3D inversion and the low signal-to-noise ratio characteristic of the shortest periods motivated the selection of a subset in the range of $\sim 2.5 \times 10^{-4}$ s to $\sim 7.8 \times 10^{-3}$ s for the subsequent processing and modeling stages. After processing, the obtained transfer functions exhibit an average period coverage of approximately 10^{-3} s to 10^{2} s, although individual stations reach periods of up to 10^{4} s, thereby extending the investigation depth to lower crustal and upper mantle levels. The variability in usable bandwidth among stations reflects differences in signal quality, effective recording time, and cultural noise intensity at each acquisition site.

3.5.2. Theoretical Foundation

The magnetotelluric (MT) method is based on the simultaneous measurement of temporal variations of the electric (E) and magnetic (H) fields at the Earth's surface, induced by natural external sources. The relationship between these fields, in the frequency domain, is expressed by the impedance tensor Z, a complex transfer function defined by (Tikhonov, 1950; Cagniard, 1953; Vozoff, 1991):

$$E = Z \cdot H \tag{1}$$

where E and H represent the horizontal components of the electric and magnetic fields, respectively. The tensor Z contains information on the subsurface electrical conductivity distribution. From the tensor elements, the apparent resistivity (ρ_a) is calculated for each pair of components:

$$\rho_{ij} = \frac{1}{\omega \mu_0} |Z_{ij}|^2 \tag{2}$$

where ω is the angular frequency and μ_0 is the magnetic permeability of free space.

The penetration depth of the electromagnetic signal (skin depth, δ) depends on the period (T) and the resistivity of the medium (ρ), and is approximated by (Telford *et al.*, 1990; McNeill, 1990):

$$\delta \approx 500\sqrt{\rho_\alpha T} \tag{3}$$

This relationship implies that long periods (low frequencies) sample deeper structures, while short periods investigate shallow levels. For the period range used in this study and considering resistivities between 100 and 10,000 Ω·m, the investigation depth ranges from a few hundred meters to approximately 80 km.

3.5.3. Data Processing

The processing aimed to obtain robust transfer functions and to minimize noise influence on impedance estimates. The raw time series were converted to the frequency domain through windowed Fourier transform, and the removal of anthropogenic, cultural, and meteorological noise was conducted using the TSMP (Time Series Manipulation Process) algorithm, which enables the identification and filtering of interferences in specific segments of the time series (Borah *et al.*, 2015).

The main cultural noise source identified corresponds to the 60 Hz power grid and its even and odd harmonics, recognized in the spectral analysis performed in the TSPlotter software. For suppression of these signals, FIR (Finite Impulse Response) filters were manually generated for each acquisition channel (Ex, Ey, Hx, Hy) at the respective sampling frequencies. The MT dead band, characterized by low natural signal amplitude in the 1 s to 10 s range, represents an inherent limitation of the method and was addressed through careful selection of time windows with the best signal-to-noise ratio (Simpson & Bahr, 2005).

The calculation of transfer functions were calculated with the ProcMT software, which implements robust estimators based on weighted least-squares statistics. Data quality was evaluated through apparent resistivity and phase curves as a function of period, verifying the smoothness and consistency between the Zxy, Zyx, Zyy, and Zxx components (**Figure 7**). Stations with low-quality data in certain frequency bands were identified and the respective periods were excluded from the inversion. The absence of a remote reference station may have compromised impedance estimates at long periods, where coherent magnetospheric noise is more significant (Chave & Jones, 2012). The construction of the input model for the 3D inversion was carried out with the 3D Grid Academic software.

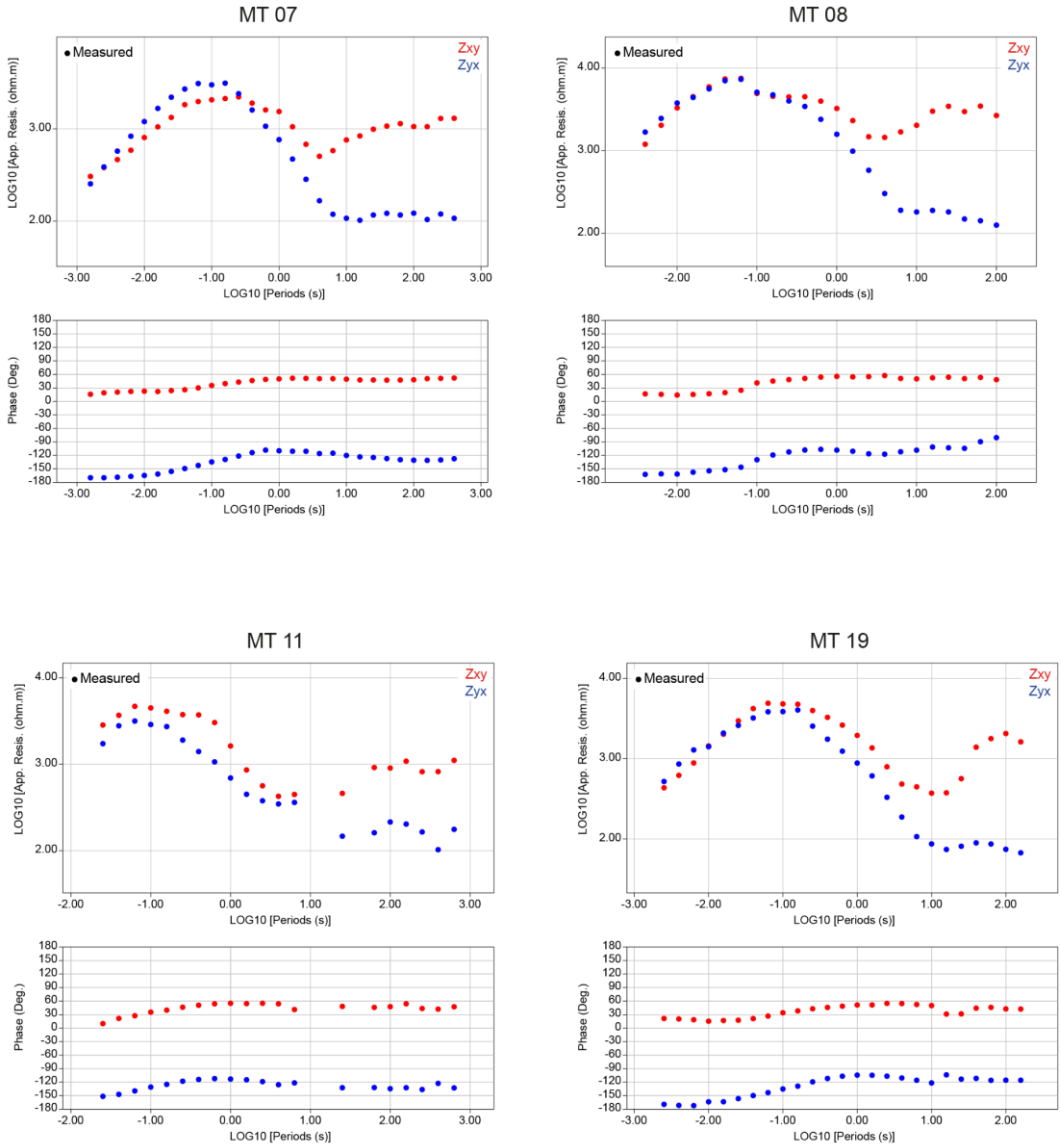

Figure 7 - Measured apparent resistivity (top panels) and phase (bottom panels) curves for representative stations MT-07, MT-08, MT-11, and MT-19. The off-diagonal impedance tensor components Zxy (red) and Zyx (blue) are plotted as a function of period in logarithmic scale.

3.5.4. Dimensionality Analysis

The determination of geoelectrical dimensionality serves as an indispensable preliminary step to magnetotelluric modeling, as it guides the choice of inversion strategy and allows assessment of the extent to which two-dimensional approximations are adequate or whether the structural complexity requires three-dimensional treatment (Groom & Bailey, 1989; Smith, 1995; McNeice & Jones, 2001). In this work, the analysis was conducted using the Phase Tensor, as proposed by Caldwell *et al.* (2004). The phase tensor (Φ)

possesses the fundamental property of being invariant under galvanic distortions caused by near-surface heterogeneities. This characteristic renders the analysis independent of superficial artifacts that compromise conventional decomposition methods, such as those of Bahr (1988) and Groom & Bailey (1989), which assume a 1D or 2D regional structure. The calculation was performed with the open-source package MTpy (Krieger & Peacock, 2014; Kirkby *et al.*, 2019).

The diagnostic parameter used to discriminate dimensionality is the normalized skew angle (β), which quantifies the asymmetry of the regional magnetotelluric response (Caldwell *et al.*, 2004). When the regional conductivity distribution is three-dimensional, β assumes values different from zero (±3°), reflecting asymmetry in the flow of induced currents. Graphically, the phase tensor is represented by an ellipse whose major and minor axes correspond to the principal axes Φmax and Φmin; in 1D structures, the ellipse degenerates into a circle, whereas increasing ellipticity and angular variation of the axes indicate the influence of laterally heterogeneous structures (Caldwell *et al.*, 2004).

The integrated analysis of the phase tensor ellipses for both station sets reveals that the crustal conductivity distribution in the study area is inherently three-dimensional at all sampled depth scales (**Figure 8**). The ellipse orientations and skew angle (β) values vary drastically among stations, indicating the absence of a consistent regional strike and reflecting a complex geology, satisfying the criterion of Caldwell *et al.* (2004) for identification of 3D structures. As emphasized by those authors, rapid spatial variation in the direction of the principal axes corresponds to a reliable indicator of three-dimensionality.

The results of the phase tensor analysis leave no margin for two-dimensional approximations. A 2D inversion would introduce artifacts in segments of greater lateral conductivity contrast, distorting the geological interpretation. The 3D inversion, in addition to honoring the complexity indicated by the β values, is the approach compatible with the grid geometry of the stations over the CGB. Furthermore, the station distribution positioned on the CGB is uniform in the form of a 4×3 grid, consistent with a 3D inversion.

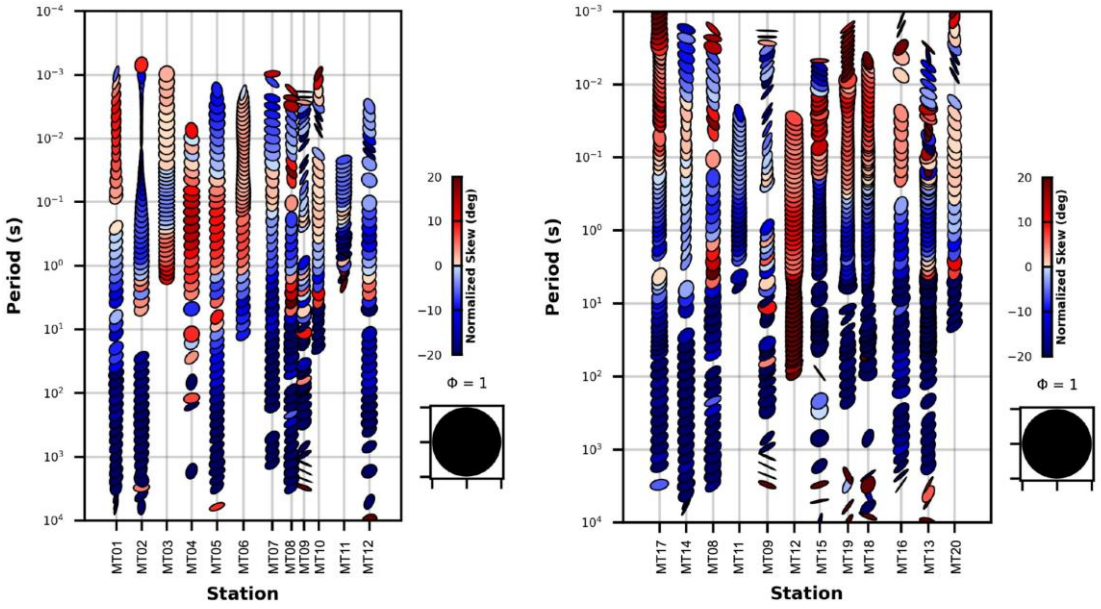

Figure 8 - Phase tensor ellipse plots as a function of period for stations along the E–W profile (left) and the CGB cluster (right). Ellipses are color-coded by the normalized skew angle (β): values near zero (light tones) indicate one- or two-dimensional electrical structure, whereas higher absolute values (dark blue and dark red) reflect significant three-dimensional character. A reference circle with Φ = 1 is shown for scale. Elongated ellipses denote lateral resistivity contrasts, and the orientation of the major axis indicates the geoelectric strike direction at each period.

3.6. Data Inversion

3.6.1. Inversion Configuration

The three-dimensional inversion was conducted with the ModEM (Modular Electromagnetic Inversion) code, developed by Egbert & Kelbert (2012) and detailed by Kelbert *et al.* (2014). The algorithm employs the Non-Linear Conjugate Gradient (NLCG) method to iteratively minimize the objective function, which combines the misfit between observed and calculated data (Φd) with a regularization term (Φm) that penalizes abrupt resistivity variations, weighted by the regularization parameter τ. The processing was performed on a parallel computing architecture (MPI) at the cluster of the University of Lisbon.

The four unrotated components of the impedance tensor (Zxx, Zxy, Zyx, Zyy) were inverted (**Figure 9**). The inclusion of the diagonal components (Zxx and Zyy), although theoretically null for one-dimensional and two-dimensional structures, incorporates information on three-dimensional heterogeneities and galvanic distortion effects (Kelbert *et al.*, 2014). The dimensionality analysis by phase tensor, previously performed, justifies

the adopted 3D approach, since several stations exhibited skew values $|\beta| > \pm 3°$ at intermediate periods, indicative of three-dimensional structure (Caldwell *et al.*, 2004).

The E-W transect model used 12 stations with an error floor of 5% for all components, a value that prevents high-quality data from excessively dominating the inversion without compromising sensitivity to the structures of interest (Miensopust, 2017). The computational mesh was built with 30 cells in the N-S direction, 78 cells in the E-W direction, and 52 vertical layers, with 10 padding cells in each horizontal direction. The horizontal spacing between stations was discretized into 2 km cells, ensuring at least four cells of separation between adjacent stations — a condition recommended to avoid numerical artifacts in the forward problem solution (Miensopust, 2017). The vertical layer thickness starts at 50 m and expands successively by a factor of 1.2, while the horizontal padding cells expand by a factor of 1.3. The starting model consists of a homogeneous half-space of 100 Ω·m.

The Campo Grande Block (CGB) model employed a more refined mesh, with 124 cells in the N-S direction, 124 cells in the E-W direction, and 157 vertical layers, with a horizontal spacing of 1 km and at least five cells between adjacent stations. The initial vertical layer thickness was reduced to 25 m, with a depth expansion factor of 1.2 and a horizontal expansion factor in the padding cells of 1.3. The error floor was set at 10%. The initial half-space adopted corresponds to 500 Ω·m. Topography was incorporated into the model through the 3D Grid Academic software, a procedure that enables adequate representation of altitude variations across the study area and minimizes distortions associated with the air-earth interface (Kelbert *et al.*, 2014). Bathymetric correction was not incorporated into the model, as the lateral extent of the inversion mesh is restricted to the continental portion and does not encompass oceanic regions.

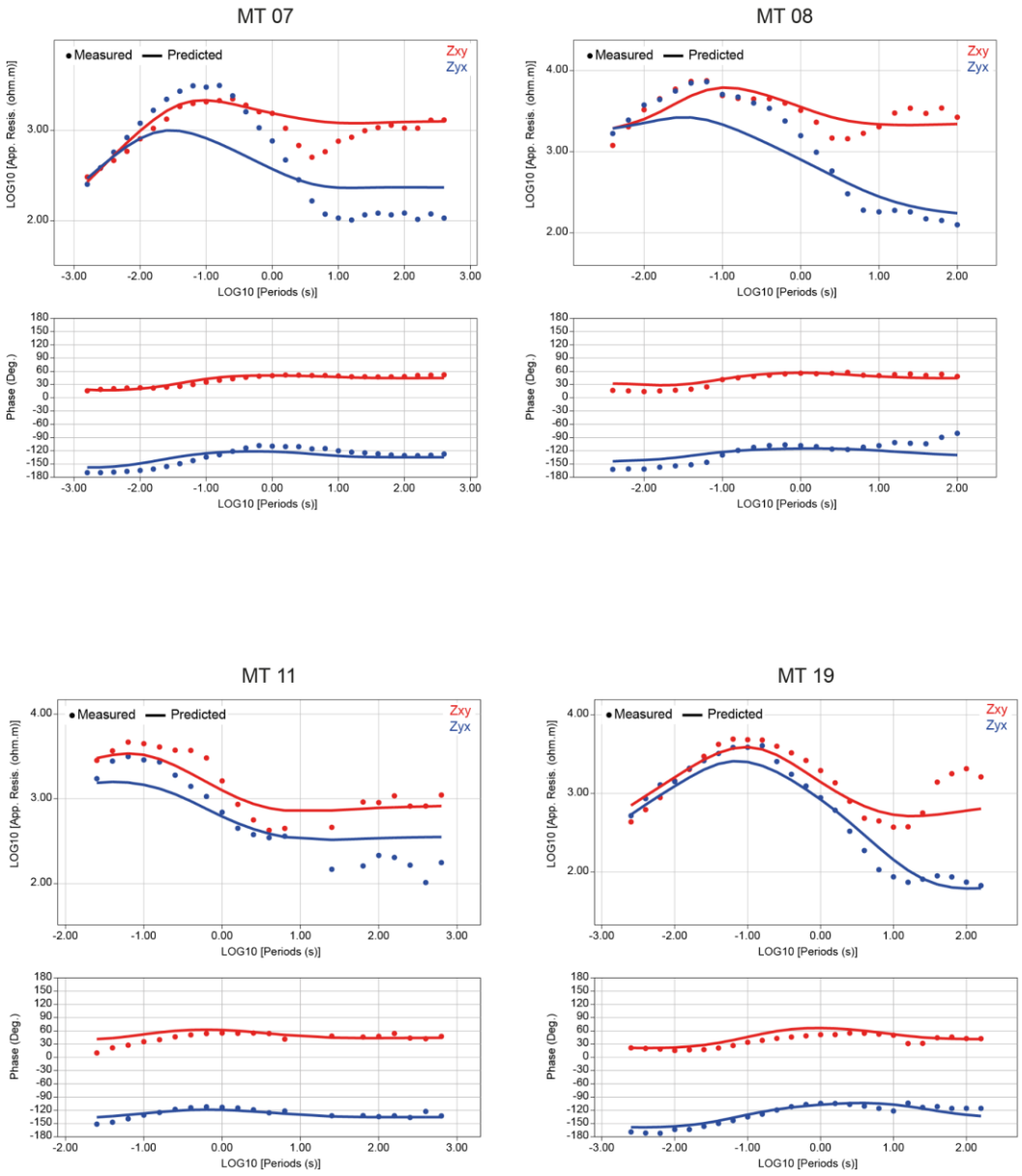

Figure 9 - Comparison between measured (dots) and predicted (solid lines) apparent resistivity (top panels) and phase (bottom panels) curves for representative stations MT-07, MT-08, MT-11, and MT-19. The off-diagonal impedance tensor components Zxy (red) and Zyx (blue) are shown as a function of period in logarithmic scale. Predicted responses were computed from the final three-dimensional resistivity model obtained by ModEM inversion.

3.7. Resolution

A widely adopted strategy for evaluating model resolution consists of running multiple inversions varying regularization and smoothing parameters, data subsets — in terms of included stations, impedance tensor components, and period bands — and starting

models, ranging from homogeneous half-spaces and 1D layered models to models incorporating *a priori* information (Yang *et al.*, 2015; Miensopust, 2017).

Additionally, skin depth estimates at the shortest period provide an indication of the vertical resolution limit at shallow depths, while the skin depth at the longest period signals the maximum depth to which resistivity information can be considered reliable (Niblett & Sayn-Wittgenstein, 1960; Miensopust, 2017) (**Figure 10**). It should be noted, however, that one-dimensional approximations of investigation depth, such as the skin depth (Niblett & Sayn-Wittgenstein, 1960; Bostick, 1977), are not necessarily representative in three-dimensional contexts, since induced currents can deflect around resistive bodies, significantly altering circulation paths and, consequently, the effective sampling depth (Miensopust, 2017). These are, therefore, rudimentary estimates that may indicate different investigation depths for each component of the impedance tensor. Nevertheless, some form of depth approximation must be considered to evaluate the spatial coverage of the data and guide the interpretation of the reliability limits of the inverted model (Miensopust, 2017). Based on this premise, a skin depth diagram was constructed in this work, calculated for the longest periods recorded at each station, in order to provide a theoretical estimate of the maximum investigation depth along the profile and, thus, constrain the interpretation of the conductive and resistive features imaged in the deepest portions of the model.

Therefore, prior to defining the final models, various configurations were systematically evaluated. Homogeneous half-spaces of 5,000, 3,000, 1,000, 500, and 100 Ω·m associated with different mesh geometries were tested, as well as error floor values of 10%, 15%, and 20%. The mean apparent resistivity value of the sites at high frequency is approximately 5,000 Ω·m for the E-W transect and 3,000 Ω·m for the CGB cluster, suggesting *a priori* that high-resistivity half-spaces would be the most appropriate. This is consistent with what was documented by Miensopust (2017), in considering "average" impedances to constrain the range of suitable starting models. However, these configurations presented convergence difficulties, imprinting high RMS values in the final models. The best fits were obtained with a 100 Ω·m half-space for the E-W transect and 500 Ω·m for the CGB (**Figure 11** and **Figure 12**).

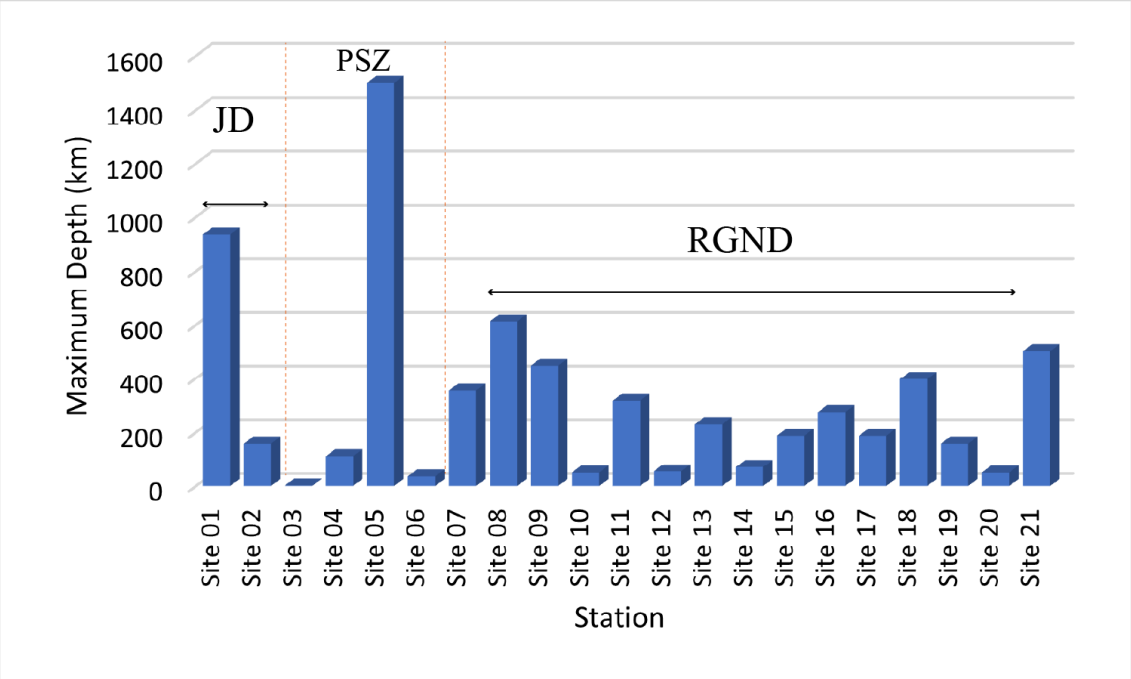

Figure 10 - Maximum penetration depth (skin-depth) chart for each MT station, subdivided according to geological domains. Variations in bar height reveal distinct electrical domains, ranging from resistive zones (high bars) to areas of signal attenuation over conductive structures (low bars). Legend: JD- Jaguaribe Domain; PSZ-Portalegre Shear Zone; RGND- Rio Grande do Norte Domain.

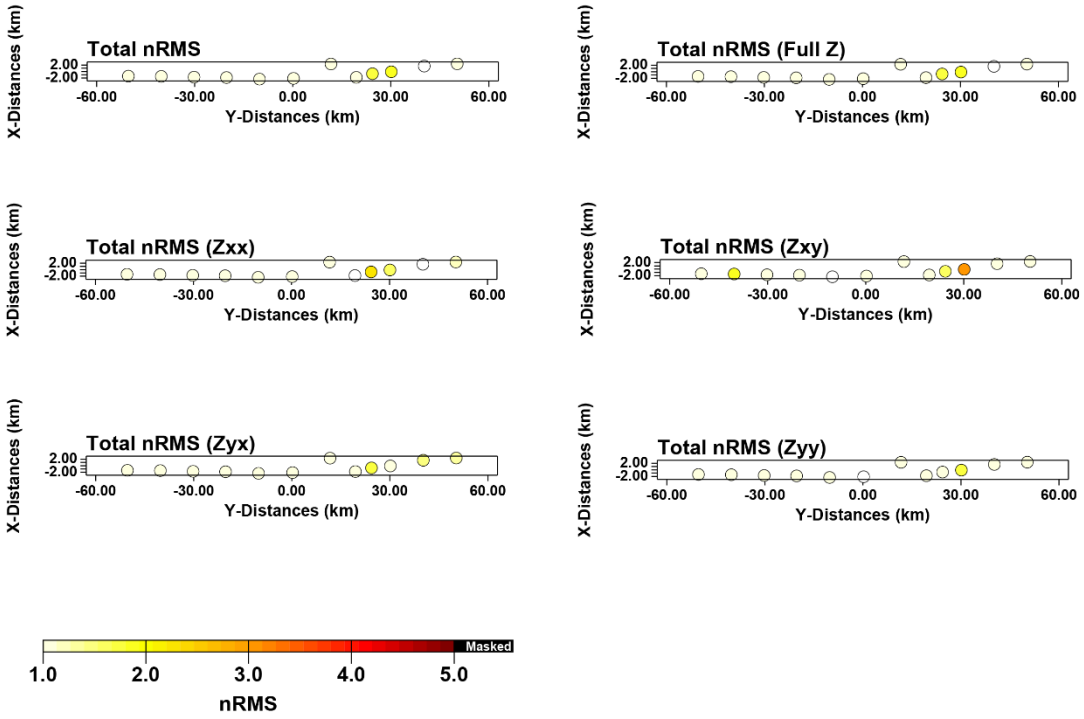

Figure 11 - Spatial distribution of the normalized root-mean-square (nRMS) misfit for the 3D MT inversion along the E–W profile stations. Maps show the total nRMS (top left), the full impedance tensor Z (top right), and the individual tensor components Zxx, Zxy, Zyx, and Zyy. Each circle represents one MT station,

color-coded according to its nRMS value. The 12 stations selected for the inversion along this transect are highlighted.

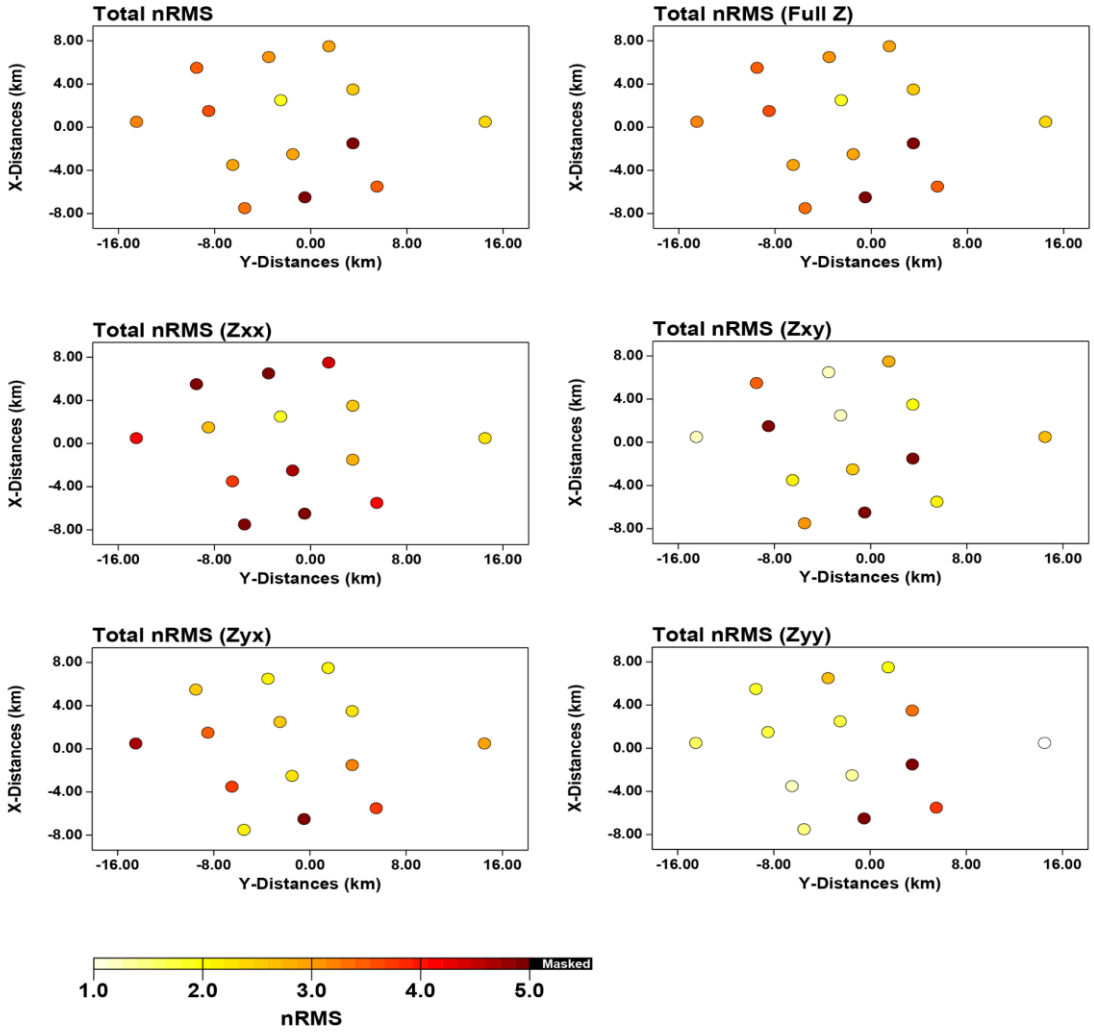

Figure 12 - Spatial distribution of the normalized root-mean-square (nRMS) misfit for the 3D MT inversion across the CGB cluster stations. Maps show the total nRMS (top left), the full impedance tensor Z (top right), and the individual tensor components Zxx, Zxy, Zyx, and Zyy. Each circle represents one MT station, color-coded according to its nRMS value.

The higher nRMS obtained for the Campo Grande Block model relative to the E-W transect reflects the greater three-dimensional complexity of the structures imaged in the grid configuration, where the resistive Archean core surrounded by conductors with irregular geometries in all directions imposes a significantly broader parameter space on the inversion algorithm, with greater trade-off between data fit and regularization (Miensopust, 2017). Additionally, the heterogeneity in bandwidth coverage among the grid stations — with some stations exhibiting maximum periods limited to 1–10 s —

restricts the model's ability to simultaneously reproduce the responses of all stations across the full period range, thereby contributing to the increase in global misfit. nRMS values between 3 and 5 are commonly reported in 3D inversions of dense arrays over geologically complex structures (e.g., Khoza *et al.*, 2013; Burd *et al.*, 2014) and are considered acceptable when the main anomalous bodies maintain positional consistency across the different tests performed.

3.8. Sensitivity Tests

The robustness of the conductive anomalies identified in the final models was evaluated through sensitivity tests, a procedure widely employed in 3D magnetotelluric studies to verify whether a given feature is required by the observed data or corresponds to an artifact of the inversion process. The test consists of replacing the conductive anomalies with resistive values in the final converged model and using the perturbed model as a starting point for a new inversion, keeping all other parameters unchanged. If the algorithm recovers the conductive features at the same positions, it is demonstrated that these are required by the data; otherwise, the anomaly is considered an artifact (Egbert & Kelbert, 2012; Miensopust, 2017; Schwalenberg *et al.*, 2002).

In the tests performed, all identified conductive bodies were simultaneously replaced by a resistive value of 1,000 Ω·m, while the resistive domains, computational mesh, and observed data set were kept unchanged. The error floor employed was 5% for the E-W transect and 10% for the CGB, values identical to those of the original inversions. The perturbed models were submitted to new inversion cycles with the ModEM code (Kelbert *et al.*, 2014).

In the E-W profile, the five conductors (C1, C2, C3, C4, and C5) were forced to 1,000 Ω·m. After 35 iterations, the algorithm recovered the five conductive anomalies at the same depths and lateral positions as the original model, including conductors C4 and C5, whose positions lie in the marginal portions of the investigation coverage. The recovery of these conductors, even in regions with lower station density reinforces that the observed data require the presence of these anomalies to be satisfactorily fitted.

In the three-dimensional model of the Campo Grande Block, the spatial domain does not encompass the Portalegre Shear Zone, so that conductor C1 does not form part of the set of tested features. Conductors C2, C3, C4, and C5, which surround the resistive Archean core at the western, eastern, southern, and northern margins respectively, were replaced

by 1,000 Ω·m and the perturbed model re-inverted under conditions identical to those of the original modeling.

After 72 iterations, the four conductors appear in the re-inverted model, with geometry and positions close to those of the original model, although they exhibit partially distinct geometric configurations. The observed variations reflect the non-uniqueness inherent to the magnetotelluric inverse problem, in which distinct resistivity models can satisfactorily reproduce the same data set (Chave & Jones, 2012). However, the positional consistency of the anomalies indicates that the existence of these conductive bodies is a requirement of the data, while the geometric details possess a greater degree of freedom.

3.9. Results

The three-dimensional electrical resistivity model obtained from the inversion of the MT data set reveals a markedly heterogeneous crustal architecture in the Rio Grande do Norte Domain. It should be noted that the interpretation of MT models, regardless of their dimensionality, requires analytical rigor: discontinuities in spatial sampling, insufficient fits between observed and calculated data, or records with low signal-to-noise ratio can generate artifacts that lead to geologically inconsistent interpretations. Miensopust (2017) demonstrates that such effects are frequently amplified in three-dimensional inversion approaches. Therefore, several mesh and half-space tests were performed, as well as sensitivity tests on the conductors found in the final models to ensure model robustness. The mean apparent resistivity value calculated for the sites at high-frequency sampling corresponds to 5,000 Ω·m, a value initially adopted as the homogeneous half-space for inversion tests. However, models constructed as half-spaces of 5,000 Ω·m, 3,000 Ω·m, 1,000 Ω·m, 500 Ω·m, and 100 Ω·m, associated with various mesh configurations, did not achieve satisfactory convergence of the inversion components, resulting in high RMS values in the final models. The best fits were obtained with a 100 Ω·m half-space for the E-W transect and 500 Ω·m for the CGB station cluster, which yielded significantly lower RMS values. It should be noted that, regardless of the RMS variations among the different tests, the main anomalous bodies characterized by contrasts between high and low resistivity maintained consistent spatial positions across all generated models, although they exhibited variations in depth estimates and edge effects. This behavior was observed in both the E-W transect inversions and those of the Campo Grande Block (CGB). The persistence of features under different parameterizations represents a robustness criterion

widely used in the MT literature (e.g., Burd *et al.*, 2014; Moorkamp *et al.*, 2022; Padilha *et al.*, 2016).

The final resistivity model of the E-W profile, obtained after 69 iterations with RMS error reduction from 3.50 to 1.07, presents values spanning a broad dynamic range, varying between 8 Ω·m and 10^4 Ω·m. The vertical section A-A' (**Fig.13**) allows the identification of three main resistive domains (R1, R2, R3) compartmentalized by three conductive bodies (C1, C2, C3).

The resistive body R1, positioned in the western portion of the profile beneath stations MT-01 and MT-02, presents resistivity values on the order of 10^4 Ω·m, gradually decreasing to approximately 10^3 Ω·m at the margins. The geometry is characterized by a domal aspect, with a well-defined resistivity contrast at approximately 8 km depth.

The R2 domain occupies the central portion of profile A-A'. This body exhibits a geometry reminiscent of plutonic structures, recording resistivities ranging between 10^4 and 400 Ω·m with decreasing resistivity at depth. The root of the body presents a funnel-shaped aspect, reaching a depth of approximately 16 km.

The R3 domain represents the most prominent geoelectrical feature of the model, positioned in the eastern portion of the profile. Resistivity values in the core of this body record values of 10^4 Ω·m with a decreasing gradient toward the margins, where values close to 10^3 to 400 Ω·m are recorded. The observed domal geometry extends from shallow crustal levels to approximately 17 km depth. The most resistive portion displays a domal aspect, while the lower-resistivity envelope surrounding it exhibits a southwestward dip.

Conductor C1 spatially coincides with the Portalegre Shear Zone (PSZ). This conductive structure dips westward and extends from approximately 2 km to 14 km depth, with resistivity values between 8 and 40 Ω·m, with the lowest resistivities concentrated in the core of the body and gradual increase toward the margins. The conductor establishes the boundary between the Jaguaribe Domain and the Rio Grande do Norte Domain, separating resistive bodies R1 and R2. The PSZ constitutes a structure hundreds of kilometers long with NNE–SSW trend, recognized as an important marker in the division of geological terranes (Cavalcante *et al.*, 1998; Cavalcante, 1999; Campelo, 1999; Oliveira, 2008; Fuck *et al.*, 2013). The structure developed mainly during the late Neoproterozoic, with reactivations in the Phanerozoic during the rifting processes and formation of the Potiguar Basin (Hackspacher & Legrand, 1989; Nóbrega *et al.*, 2005).

Conductor C2 is distinguished by its dominantly horizontal to slightly domal geometry. Resistivity contrasts along the E–W transect range between 20 and 40 Ω·m, with the anomaly occupying a depth interval between 4 and 10 km, restricted to the upper crust. In the CGB model, C2 yielded resistivity values of 100–200 Ω·m with resistivity contrasts reaching depths between 4 and 6 km. The higher resistivity values obtained for C2 in the CGB model relative to the E–W transect are attributed to differences in inversion parameterization between the two models, including the starting half-space (500 Ω·m vs. 100 Ω·m), error floor (10% vs. 5%), and mesh resolution (1 km vs. 2 km cell spacing), which influence the amplitude of recovered anomalies in regions of limited station coverage at the margins of the grid (Miensopust, 2017). The position of conductor C2 coincides with the surface expression and the full width of the Portalegre fault zone. The lateral connection with conductor C4 establishes continuity between the conductive anomalies on the western and southern margins of the block, configuring an arcuate conductive zone that partially envelops the resistive domains.

Conductor C3, the most prominent in terms of dimension, is situated in the eastern portion at the Paraú Shear Zone. This structure exhibits subcircular geometry with a slight westward dip, presenting resistivities between 20 and 40 Ω·m (E–W transect) and between 20 and 100 Ω·m (CGB model). The anomaly originates at approximately 4 km depth and extends to approximately 17 km, surpassing the estimated upper crust boundary. The westward dip, toward the interior of the block, implies that this structure may represent a shear zone with geometry that accommodates the regional tectonic vergence.

3.9.1. CGB 3D Model

The 3D inversion of magnetotelluric data allowed characterization of the crustal architecture of the Campo Grande Block **(Fig.14**). The resistivity model reveals a complex geoelectrical configuration, marked by well-defined resistive domains surrounded by conductive zones that delineate the main lithological and structural contacts.

The Campo Grande Block (CGB) inversion model started with an RMS of 6.82, finalizing at 3.14 after 106 iterations. Resistivity values in this model range between 2 Ω·m and 10^4 Ω·m. The CGB corresponds, in terms of geoelectrical signature, to domain R3 identified in the E–W transect. In three-dimensional visualization, a highly resistive core R3 (> 10^4

Ω·m) with domal geometry is distinguished, extending from the surface to approximately 5 km depth with a slight southwestward dip (**fig.16**). The core is enveloped by rocks of moderate resistivity (< 10^3 Ω·m), whose geometry indicates southwestward dipping, reaching depths of approximately 10 km. This envelope is notably more deformed compared to the central core, a feature evidenced by the irregularity of resistivity contours and the continuity of structures at depth. A distinctive characteristic of this domain is the resistivity zonation, which exhibits progressive decrease of values toward the block margins. In this 3D model, four main conductive bodies (C2, C3, C4, and C5) were identified, configuring a geometry that surrounds the resistive domains to the west, east, south, and north, respectively.

The main observed feature is the dip direction of the anomalies of the identified bodies. Conductor C5, positioned to the north of the main resistive block R3, presents E–W orientation, resistivity varying between 2 and 100 Ω·m, eastward dip, and is located in the vicinity of the Potiguar Basin limits. Conductor C3 displays a N–S strike and westward dip. This anomaly is clearly imaged in both the 3D model and the E–W profile, evidencing its lateral continuity and persistence at depth. At deeper crustal levels, conductor C3 interconnects with conductor C5 and is situated east of block R3. In turn, to the west of the resistive block, a new conductor C2 presents distinctive dome-shaped geometry, clearly observed in the E–W profile. This body connects laterally to conductor C4 in the southern portion of the model. Finally, conductor C4 is positioned to the south of resistive block R3 with resistivity contrast varying between 40 and 100 Ω·m, E–W orientation, dominantly horizontal geometry between depths of 5 to 11 km, reaching 17 km to the west. The connection with conductor C2 configures an arcuate conductive zone that partially envelops the resistive domains in their western and southern portions.

3.9.2. Limitations in the Interpretation of Conductors C4 and C5

Although confirmed by the sensitivity test, conductors C4 and C5 have dimensions that extend beyond the limits of the magnetotelluric survey coverage. This condition compromises the reliability of the geometry and magnitude of these anomalies, since features situated at the edges of the acquisition grid are particularly susceptible to edge effects and numerical artifacts inherent to the inversion process (Siripunvaraporn *et al.*, 2005).

Conductor C5 presents additional interpretive complexity due to its proximity to the Potiguar Basin. The resistivity contrast between the sedimentary fill of the basin and the crystalline basement can induce significant distortions in magnetotelluric responses, producing conductive artifacts that do not necessarily correspond to the basement structure (Jones, 1983; Groom & Bailey, 1989). The combination of positioning outside the effective acquisition coverage and influence of the Potiguar Basin renders C5 inappropriate for conclusive geological interpretations within the scope of this work.

Adequate characterization of C4 and C5 would require expansion of station coverage to the south and north, respectively. Future surveys including stations across the basement–basin transition and along the southern portions of the Campo Grande Block may clarify whether C4 and C5 represent extensions of the conductive zone system surrounding the block or constitute independent features with their own tectonic significance.

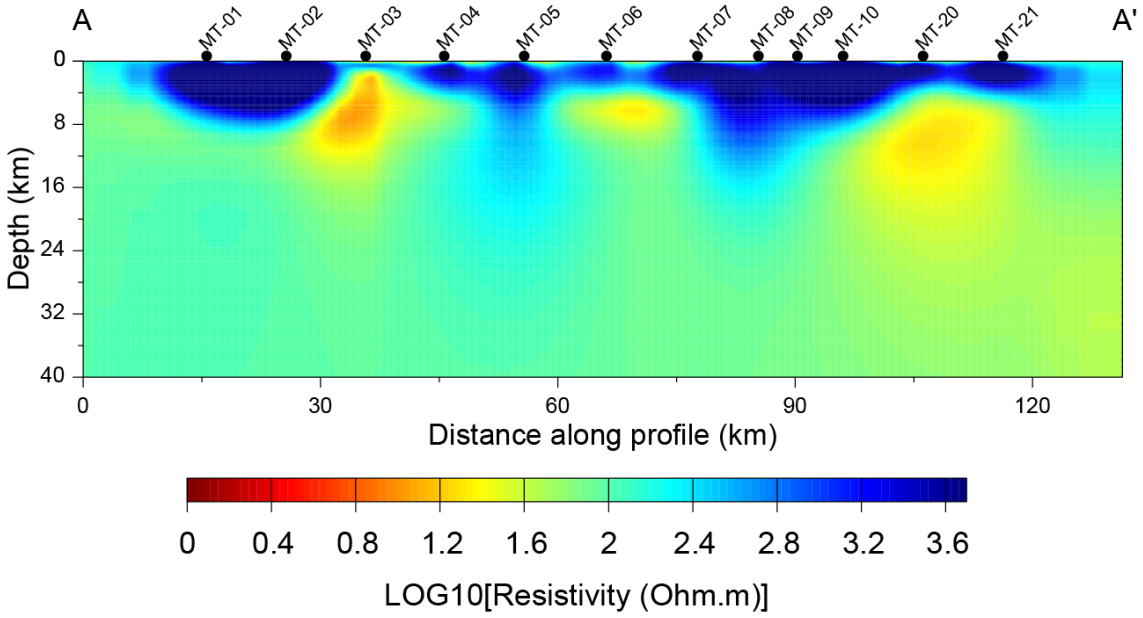

Figure 13 - East–west vertical cross-section (A–A′) extracted from the three-dimensional electrical resistivity model obtained by 3D inversion of broadband magnetotelluric data. The section extends the main E–W profile from station MT-01 (Itaú) to station MT-21 (Paraú), crossing the Campo Grande Block. Black dots indicate MT station locations. The resistivity color scale is given in $\log_{10}(\Omega \cdot m)$.

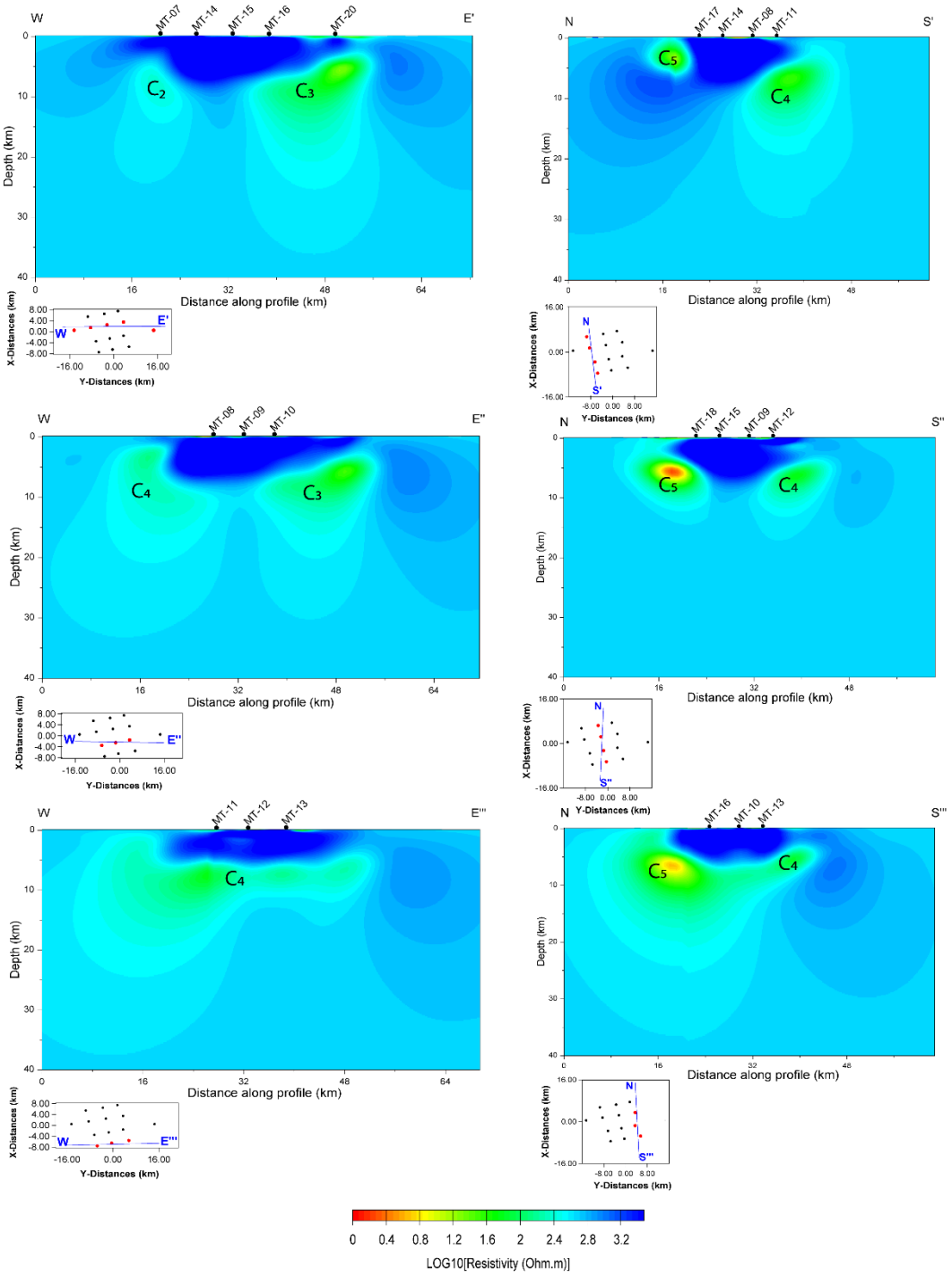

Figure 14 - East–west (left) and north–south (right) vertical cross-sections extracted from the three-dimensional electrical resistivity model obtained by 3D inversion of broadband magnetotelluric data from the Campo Grande Block cluster (CGB). Conductive anomalies C_2, C_3, C_4, and C_5 are indicated. Black dots indicate MT station locations.The resistivity color scale is given in $\log_{10}(\Omega \cdot m)$. Inset maps below each section show the position and orientation of the corresponding transect relative to the MT station array.

3.10. Discussion

The broadband magnetotelluric (BBMT) survey conducted in this work adopted 10 km spacing along the E–W profile and an infilled grid of 5 km over the Campo Grande Block. This array differs from previous regional surveys in the Borborema Province, which employed dominantly long-period data with average spacing of 60–70 km (Padilha *et al.*, 2017; Garcia *et al.*, 2019; Benevides *et al.*, 2026). The station infilling allowed superior resolution in characterizing shallow and intermediate crustal structures, enabling the discrimination of accretionary lithological domains that would remain indistinguishable in surveys with greater spacing. Station spacings of 5 km demonstrated that even infilled arrays present limitations in segregating gneisses and mafic rocks when both exhibit pronounced reflectivity (Ma *et al.*, 2021). In the present study, the distinction between the Archean migmatitic core and the surrounding Paleoproterozoic orthogneisses was possible through the resistivity contrast, where the core presents values exceeding 10,000 Ω·m while the envelope exhibits values on the order of 1,000 Ω·m. The broadband data processed in this work reach adequate depth to image from the upper crust to the middle–lower crust, although the resolution of mantle features requires complementation with long-period data, as demonstrated by studies in the Himalayan region (Sheng *et al.*, 2023) and in the Borborema Province (Padilha *et al.*, 2014; 2017; Garcia *et al.*, 2019; Benevides *et al.*, 2026).

3.10.1. Resistive domains in the understanding of tectonic partitioning of crustal blocks

The 3D electrical resistivity model obtained in this work reveals that the crust in the studied region is segmented into multiple dominantly resistive domains, with values between 1,000 and 10,000 Ω·m.

The highly resistive upper crustal blocks observed in the MT models are consistent with ancient and stable regions, which typically range between 1,000 and 10,000 Ω·m (Chave & Jones, 2012) and are associated with two lithological categories: (i) thermally stabilized ancient cratonic terrains and (ii) felsic granitic intrusions. Archean nuclei and basement highs share high-resistivity geoelectrical signatures (10^3–10^5 Ω·m) with domal or tabular geometries (Ma *et al.*, 2021; Benevides *et al.*, 2026; Padilha *et al.*, 2021; Sheng *et al.*, 2023). Magmatic arcs and intrusive granitic plutons act as resistive barriers capable of truncating ascending conductors (Yi *et al.*, 2022; Benevides *et al.*, 2026).

Resistive body R_1, positioned in the western portion of the profile beneath stations MT-01 and MT-02, presents core resistivity values on the order of 10^4 Ω·m and domal geometry with well-defined resistivity contrast at approximately 8 km depth. It correlates spatially with the orthogneisses and paragneisses of the Jaguaretama Complex, the Paleoproterozoic basement of the Jaguaribe Domain (Arthaud *et al.*, 2008), preserved west of the Portalegre Shear Zone. The elevated resistive signature is compatible with gneissic rocks of low porosity and absence of significant conductive phases.

Domain R_2 occupies the central portion of profile A–A' and exhibits funneled geometry reaching approximately 12 km depth, with resistivities between 10^4 and 400 Ω·m varying with depth. This body correlates spatially with Neoproterozoic granites. These high-K intrusions, crystallized during the Ediacaran (ca. 580 Ma), are classified as stocks or dikes belonging to the High-K Porphyritic Alkaline Suite (Nascimento *et al.*, 2000, 2008, 2015; Trindade *et al.*, 1999; Galindo, 1993). The progressive decrease in resistivity with depth may reflect vertical compositional differentiation within the plutonic body or fracture zones associated with plutonic emplacement along shear zones.

Domain R_3, in the eastern portion of the profile, records values of 10^4 Ω·m with a decreasing gradient toward the margins, where values between 10^3 and 400 Ω·m are observed. The domal geometry extends from shallow crustal levels to approximately 17 km depth, with a lower-resistivity envelope dipping southwestward. This domain correlates with the Campo Grande Block, where Archean migmatitic gneisses (2.98–2.66 Ga) crop out in the core, enveloped by Paleoproterozoic alkaline orthogneisses (Ferreira *et al.*, 2020a, 2020b, 2021). Thus, each resistive domain corresponds to a basement high of the same age but with different physical and electrical properties due to having undergone different tectonic and deformational events.

3.10.2. Fluid conduction mechanisms in conductive zones and conductive mineral phases: graphite, sulfides, and oxides

Anomalous ionic conductivity in crustal rocks can be attributed to three main mechanisms: (i) ionic conduction by saline aqueous fluids filling interconnected pore spaces and fractures, (ii) electronic conduction by interconnected opaque minerals such as graphite and sulfides, and (iii) partial melting, restricted to environments with elevated thermal regimes (Selway, 2014; Simpson & Bahr, 2005; Lin *et al.*, 2023). Above the brittle–ductile transition, the brittle crust sustains fracture networks through which

meteoric and hydrothermal fluids circulate freely (Connolly & Podladchikov, 2004); below this zone, plastic deformation progressively closes connected porosity and metamorphic reactions consume free fluids (Yardley & Valley, 1997). In the context of the Campo Grande Block, situated in thermally stabilized Precambrian terrain, the discussion therefore focuses on the relative contribution between ionic fluids and conductive mineral phases, and on the role of tectonic structures as controls on the geometry and persistence of anomalies at depth.

The 3D inversion delineated three main conductive bodies along the E–W transect: C1, C2, and C3, all confined to the upper crust (**Figure 15**). In the CGB model, conductors C2, C3, C4, and C5 surround the resistive core to the west, east, south, and north, respectively. The confinement of anomalies above the brittle–ductile transition imposes constraints on the mechanisms responsible for resistivity reduction, since the position of the anomalies within the brittle regime enables fluid circulation in interconnected fracture systems and damage zones associated with regional tectonic structures.

Conductor C1, imaged in the E–W profile, extends from approximately 2 km to 14 km depth with a westward dip, coinciding with the PSZ. This geometry agrees with the oblique transcurrent kinematics with an eastward thrust component documented by Archanjo *et al.* (2002). The hypothesis of conduction by saline aqueous fluids infiltrated along fracture systems is supported by Padilha *et al.* (2016) for analogous structures in the Borborema Province. The continuity of the anomaly at progressively greater depths, yet still within the brittle regime, indicates that the Portalegre fault zone maintains sufficient hydraulic connectivity to sustain fluid circulation to the base of the brittle crust (Hackspacher *et al.*, 1990). Penetrative fabrics that were partially reactivated during Mesozoic rifting may preserve sufficient residual permeability to maintain fluid circulation, as demonstrated regionally by Santos *et al.* (2014) and Padilha *et al.* (2016, 2017). This interpretation finds direct support in the work of Padilha *et al.* (2016), who identified an analogous conductor beneath the Patos Lineament, confined between 10 and 20 km depth, attributed to electrolytic conduction by brines percolating through the shear zone above the brittle–ductile transition. A similar pattern for crustal conductors beneath Mesozoic rift basins of the Borborema Province, such as Jatobá and Araripe, can be interpreted as resulting from ionic conduction in fracture zones reactivated during rifting (Santos *et al.*, 2014; Padilha *et al.*, 2016, 2017). The recurrence of this pattern in multiple structural contexts — both beneath Brasiliano shear zones and beneath Mesozoic rift

basins — indicates that electrolytic conduction by brines operates as a recurrent mechanism in the upper crust of the province, conditioned by the existence of fracture zones with sufficient connectivity to maintain fluid percolation networks.

Conductor C3, present in both models, corresponds to the largest anomaly in the studied area. The body extends from ~4 km to 17 km depth, with resistivities between 20 and 100 Ω·m, N–S strike, subcircular geometry with a slight westward dip, positioned east of the resistive block. In the CGB 3D model, C3 interconnects with conductor C5 at deeper crustal levels. Its position coincides with the Paraú Fault System, which delimits the Campo Grande Block from the Itajá Block. The vertical extent encompasses practically the entire thickness of the brittle crust, favoring the hypothesis of electrolytic conduction by saline aqueous fluids circulating along the fracture network generated by tectonic activity, although the documented presence of retroeclogite lenses with opaque phases and manganiferous protoliths in the eastern margin shear zones indicates that solid-state conduction mechanisms may operate complementarily.

The presence of outcropping retroeclogite lenses at the margin of the migmatitic dome, with dimensions up to 120 m (Ferreira *et al.*, 2023), raises the question regarding the existence of analogous bodies at depth and their potential contribution to the conductivity of C3. The P–T trajectory of the retroeclogites, with peak at ~60 km depth for a standard lithostatic gradient and exhumation to mid-crustal conditions (<6.0 kbar; Ferreira *et al.*, 2023), indicates that these rocks were exhumed from upper mantle depths to the crustal levels where they currently crop out. In collisional belts, high-pressure rock lenses are preserved as tectonic fragments incorporated into shear zones during ascent, distributed from the surface to intermediate crustal depths (Guillot *et al.*, 2009; Warren, 2013). The record of eclogite lenses at the surface is therefore evidence of a system that likely contains analogous bodies at levels not exposed by erosion.

The mineral assemblage of the retroeclogites is relevant to conductivity in two aspects. First, the symplectitic textures replacing the high-pressure assemblage create a mesh with high proportion of intergranular boundaries between distinct phases (Cpx, Pl, Amph), favoring surface conduction and fluid retention in intergranular porosity. Second, the presence of magnetite and ilmenite as exsolution phases within this mesh (Ferreira *et al.*, 2023) introduces volumes with intrinsically very low resistivity. Should retroeclogite lenses exist at depth in the eastern margin shear zone, their contribution to C3 may be twofold: rock volume more conductive than the host orthogneisses and a past source of

metamorphic fluids released during hydration of the eclogitic assemblage. Additionally, Ferreira *et al.* (2023) described lenses composed of banded spessartine garnet with exceptional MnO contents (6.4–6.6 wt%), whose supracrustal protoliths indicate sediments enriched by oceanic processes. Mn-oxide-rich sediments precipitated during oceanic subduction and incorporated into shear zones can act as agents of crustal conductivity (Raju *et al.*, 2022), and the documented existence of manganiferous protoliths in the CGB constitutes local evidence that materials with conductive potential were effectively incorporated into the crust during Neoproterozoic evolution.

The temporal convergence of two fluid-generating processes in the CGB is directly relevant to the conductivity of C3. The retrogression of the retroeclogites, dated between 623 and 590 Ma (Ferreira *et al.*, 2023), released metamorphic fluids through hydration of the high-pressure assemblage. Contemporaneously, fluid-assisted anatexis of the migmatitic orthogneisses at ca. 570 Ma (Ferreira *et al.*, 2021) mobilized additional volumes of H_2O through the shear zones. These two fluid pulses, channeled through the same structures, enriched the eastern margin shear zones with aqueous solutions that, upon cooling and reacting with the host rock, may have deposited solid conductive phases and maintained partially interconnected fluid networks.

The generation of metamorphic fluids during orogenic processes represents an additional mechanism for supplying conductive solutions to crustal shear zones. The migration of these fluids with magma through brittle zones of the crust can result in evolution toward CO_2-rich fluids (Frost & Frost, 1987), which may persist for intervals of 0.1 to 1 Ga at average mid-crustal temperatures of 400 °C (Jones, 1992). However, Bailey (1990) and Thompson & Connolly (1990) argued that free aqueous fluids in the deep crust are not preserved for periods exceeding ~100 Ma without a recharge mechanism, although Glover & Vine (1995) demonstrated that fluids can be continuously generated by granulite-facies metamorphism in the continental crust. In the CGB, where the migmatitic orthogneisses of the Caicó Complex record multiple metamorphic events including the Brasiliano orogeny (~600–570 Ma), the last metamorphic event is sufficiently ancient for free aqueous fluids to have been dissipated. This finding reinforces that solid-state conductivity mechanisms — graphite, sulfides, interconnected oxides, and intergranular conduction by grain-size reduction — constitute relevant complementary explanations for the crustal conductors preserved in the CGB since the Neoproterozoic. Graphite films deposited along grain boundaries by carbon-rich fluids during past tectonothermal events

remain stable up to temperatures of approximately 900 °C (Pineau & Mathez, 1990) and can persist in the upper crust under reducing conditions, although at shallow depths oxidation and microfractures tend to disrupt their interconnectivity (Mathez *et al.*, 1995). Interconnected sulfides represent an additional possibility. Ma *et al.* (2021), in the Canadian Superior Craton, attributed shallow crustal conductors (<15 km) to sulfides, and Saxena *et al.* (2021) demonstrated that a few volume percent can reproduce typical MT anomaly conductivities — however, in the CGB sulfides have not been described in reportable concentrations in the migmatites (Ferreira *et al.*, 2021), rendering this contribution speculative.

The eastern margin may contain a greater concentration of retroeclogite lenses at depth — a possibility consistent with the heterogeneous distribution of metamafic boudins documented in collisional belts (Jolivet *et al.*, 2003), or the shear zone controlling C3 may have experienced later or more intense reactivation than on the western margin, preserving greater fluid connectivity.

Conductor C2 is located at the western margin of the CGB, adjacent to a subsidiary fault with NE–SW trend parallel to the Portalegre Shear Zone, interpreted as an extension of this transcurrent system. The relatively attenuated resistivity (100–200 Ω·m) and the vertical extent restricted between 5 and 6 km depth suggest a conductor positioned entirely above the brittle–ductile transition, where fracture permeability allows the circulation and accumulation of electrolytic solutions in interconnected fracture systems (Unsworth *et al.*, 2000; Bedrosian *et al.*, 2002; Padilha *et al.*, 2016). Shear zones operate as structural traps that channel fluids of deep origin, maintaining anomalous conductivities even in stable cratonic terranes (Raju *et al.*, 2022; Becken & Ritter, 2012).

The domal geometry of C2, however, differs from the typically subvertical conductors associated with transcurrent fault zones (Becken & Ritter, 2012; Unsworth *et al.*, 2000). This geometry may indicate that the conductor does not exclusively reflect the fault zone but rather a fluid accumulation in a structural domain bounded by the permeability contrast between the rigid Archean core and the surrounding orthogneisses. In MT imaging of gneiss domes, conductive anomalies with sub horizontal or domal geometry in the first few kilometers of depth are frequently interpreted as fluid accumulation horizons controlled by rheological or lithological interfaces (Ritter *et al.*, 2003; Jones, 1992).

The moderate resistivity of C2 and its restricted depth are compatible with a shear zone that experienced partial healing over geological time, through progressive fracture closure and sealing by recrystallization in a structure not reactivated since its last thermal event (Abdul Azeez *et al.*, 2017). In the CGB, the last documented fluid influx event in the shear zones dates from ca. 570 Ma (Ferreira *et al.*, 2021). At this margin, Ferreira *et al.* (2023) documented retroeclogite boudin lenses with dimensions up to 120 m, hosted within the migmatitic orthogneisses and deformed together with the stromatic leucosomes. The retrogression involved intense hydration, with the formation of coarse amphibole attesting to aqueous fluid activity that interacted with the migmatitic host rocks during exhumation. Concurrently, Ferreira *et al.* (2021) documented that the migmatitic orthogneisses experienced anatexis assisted by influx of H_2O-rich fluids at ca. 570 Ma, generating leucosomes with ilmenite as an accessory phase.

The migmatitic orthogneisses of the CGB are products of an integrated process of deformation-controlled melt segregation, developed at deep levels of the continental crust during partial melting of plutonic protoliths (Sawyer, 2008; Sawyer *et al.*, 2011; Brown & Johnson, 2019). The formation of migmatites in orogenic belts and magmatic arcs exerts direct influence on the rheological behavior, chemical differentiation, architecture, and density of the continental crust (Vanderhaeghe, 2009; Brown *et al.*, 2011; Brown & Johnson, 2019; Reichardt & Weinberg, 2012). The migmatitic orthogneisses of the western margin contain abundant primary biotite (20–30% in residues; Ferreira *et al.*, 2021), a phyllosilicate with high cation exchange capacity which, associated with blastomylonitic fabrics, configures texturally favorable conditions for surface conduction.

The geochemical characteristics of these migmatites are governed by the composition and structure of the protolith, as well as by the partial melting reactions that generate chemical disequilibrium between melt and residue components (Sawyer, 2008; White & Powell, 2010). During partial melting, the CGB experienced pervasive ductile deformation and developed numerous high-strain zones, structures that may have facilitated the migration of aqueous fluids through the crust (Ferreira *et al.*, 2020a; Sawyer, 2010).

In this context, the residual resistivity of 100–200 Ω·m may reflect the superposition of three minority contributors. The first is intergranular conduction by grain-size reduction in tectonites, a mechanism demonstrated experimentally by ten Grotenhuis *et al.* (2004) and invoked by Abdul Azeez *et al.* (2017) to explain residual conductivities in healed fault zones. In mylonites, grain-size reduction and phase mixing promoted by progressive

deformation increase the proportion of conductive surfaces, generating a network that operates in parallel with electrolytic conduction in pores (Kluge *et al.*, 2022). Warren & Hirth (2006) documented that grain-size-sensitive deformation mechanisms operate effectively in deformed peridotites, and an analogous behavior in crustal silicates cannot be ruled out. The second contributor corresponds to the presence of magnetite and ilmenite as exsolution phases in the retroeclogites, whose intrinsic resistivities are orders of magnitude lower than those of the host silicates (Nover, 2005); these phases, documented petrographically by Ferreira *et al.* (2023), constitute the available mineral evidence to justify solid-state conductivity at the western margin of the CGB. The third is the primary biotite in migmatitic residues (20–30% modal; Ferreira *et al.*, 2021), whose charged intergranular surfaces generate conductivity along the electrical double layer (EDL), as demonstrated by Kluge *et al.* (2022) in phyllosilicate-rich mylonites of the Alpine Fault. The conductivity observed in C2 therefore results from the combined action between residual electrolytic fluids in the fractures of the healed shear zone and these three solid-state conduction mechanisms, whose simultaneous operation is favored by the shared history of hydration, deformation, and exhumation between the retroeclogites and the host migmatitic orthogneisses.

The hydric influx during exhumation of the CGB was sufficiently intense to promote pervasive hydration of mineral assemblages in mafic rocks interpreted as retroeclogites (Ferreira *et al.*, 2025; Gordilho-Barbosa *et al.*, 2025). This hydration, concentrated along the shear zones delimiting the block and at the contacts between metamafic rock lenses and the gneissic host, favored the generation of permeable fracture networks saturated by aqueous fluids. The presence of fluid-associated conductors in the Campo Grande Block may require recharge mechanisms — either meteoric infiltration along fractures outcropping at the surface, or episodic release of fluids stored in deeper reservoirs — or alternatively, that the Neoproterozoic reactivation of the shear zones rejuvenated permeability and permitted a new phase of fluid infiltration whose geoelectrical signature remains recorded in the current models.

In this manner, the integrated geoelectrical configuration of the CGB suggests that ionic conduction by fluids interconnected in fracture networks of the shear zones delimiting the CGB constitutes the first-order mechanism, supported by the position of conductors entirely above the brittle–ductile transition, by the compatibility of resistivity values with modest fractions of electrolytic fluid (Raju *et al.*, 2022; Padilha *et al.*, 2016), and by the

documented presence of crustal-scale shear zones — Portalegre, Paraú, and associated branches — that provide the necessary structural conduits. Solid-state conduction mechanisms — intergranular conduction by grain-size reduction in tectonites and electrical double layer conductivity in biotite-rich migmatitic residues — act as second-order contributors that collectively sustain the residual geoelectrical anomaly even in shear zones partially healed since the Neoproterozoic.

3.10.3. Identifying lithospheric boundaries and crustal growth using magnetotellurics, geochronology, and Nd isotopes

The accretionary orogenic collage of the CGB derives from a complex diversity of protolith sources, reflecting polyphase continental evolution with components of different scales, compositions, and ages (Ferreira *et al.*, 2020a,b). The Campo Grande Block (CGB), with an Archean core (2.98–2.66 Ga; Ferreira *et al.*, 2020a,b) surrounded by Paleoproterozoic orthogneisses of the Caicó Complex and bounded to the west by the Portalegre Shear Zone, records a polyphase history that includes high-pressure metamorphism in eclogite facies (Ferreira *et al.*, 2023, 2025) and intense Brasiliano deformation with formation of mylonites and anastomosing shear zones (Nóbrega, 2004; Castro *et al.*, 2012). The thermal and compositional contrasts between continental and oceanic lithosphere controlled subsidence processes governed by plate tectonics, allowing the mechanical coupling of microcontinents and magmatic arc remnants in the orogenic wedge. In this context, magmatic arc formation operates as the most efficient mechanism for maintaining the continental crust reservoir, making it unrealistic to invoke any model that calls upon fractionation of a single magmatic event to produce continental crust (Ferreira *et al.*, 2020a,b). The T_{DM} model age map based on Nd isotopes suggests that crustal growth of the Campo Grande Block shows an age progression from center to margin, typical of cherogenic models in orogenic systems (Ferreira *et al.*, 2020a,b).

The geoelectrical architecture of the CGB, revealed by the 3D model, is compatible with the center-to-margin crustal growth model proposed by Ferreira *et al.* (2020b)(**Figure 16**). The highly resistive core R3a (10^4 Ω·m) with domal geometry extending to ~5 km depth and a slight southwestward dip correlates with the Archean tonalitic to granitic migmatitic complex (2.98–2.66 Ga). The high resistivity geoelectrical signature down to deep crustal levels supports the interpretation that the CGB represents a thermally cooled Archean lithospheric fragment. The moderate-resistivity envelope R3b (10^3 Ω·m) with

progressive zonation toward the margins correlates with the Paleoproterozoic alkaline orthogneisses surrounding the migmatitic core, described as a 10 to 20 km ring of coarse-grained orthogneisses with biotite and K-feldspar (Ferreira *et al.*, 2020a,b). The intensification of deformation at the margins, in contrast to the preserved core, is consistent with the reworking processes documented by Ferreira *et al.* (2020a,b) at the outer margins of the Archean dome. The southwestward dip of the envelope may reflect kinematics associated with regional transcurrent shear zones with SSW–NNE trend. Terrane accretion and partial melting, particularly at the root of magmatic arcs from 2.2 Ga onward, promoted differentiation and growth of the continental crust (Ferreira *et al.*, 2020a,b).

The four conductors surrounding the CGB (C2, C3, C4, and C5) configure a system of anomalies that delineates the tectonic contacts between the CGB and adjacent terrains. The connectivity between C3 and C5 on the eastern and northern margins, and between C2 and C4 on the western and southern margins, indicates that these anomalies represent crustal-scale shear zones that accommodated deformation during the Brasiliano orogenic collage. Transcurrent shear zones did not act merely as accommodation but played an active role in fluid mobilization and transport of deep crustal material. The progressive decrease in resistivity from core to margins reflects the gradient of crustal reworking documented by Ferreira *et al.* (2020a,b). The recurrent association between Archean rocks and Paleoproterozoic complexes suggests accretionary collision processes that resulted in the formation of basement highs subsequently deformed during the Brasiliano/Pan-African Orogeny (Van Schmus *et al.*, 2003; Arthaud *et al.*, 2008; Brito Neves & Fuck, 2014). Regarding crustal thickness in the region, Lima *et al.* (2015) defined an upper crust of the RGND at 17 km and the Moho interface at approximately 31.5 km depth.

The convergence between the multiple proposed mechanisms and the observations from the three-dimensional MT model reinforces the interpretation of the conductors as geoelectrical expressions of preserved tectonic boundaries, which record the interaction between the Archean core of the Campo Grande Block and the reworked domains of the Rio Grande do Norte Domain throughout the polycyclic evolution of the Borborema Province. Collectively, the geoelectrical configuration of the CGB — a resistive core surrounded by conductors of variable magnitude — is consistent with the model of a rigid and depleted Archean crustal fragment surrounded by regional deformation

accommodation zones that concentrate fluids, opaque minerals, and high-conductivity structures. This architecture finds direct parallels with gneiss domes worldwide, where the core of resistive Archean granulitic mylonites (>5,000 Ω·m) is flanked by conductors associated with Paleoproterozoic thrust zones (Yin et al., 2014), as well as in resistive basement highs (>10,000 Ω·m) bounded by graphite-rich conductors (Khoza *et al.*, 2013). In this manner, ancient nuclei with already metasomatized lithosphere generate a thermal plume that may have facilitated the ascent of magma and associated fluids to middle to lower crustal levels, producing conductive anomalies analogous to those observed, in which conductivity results from both the conductive minerals inherent to the intrusive mafic–ultramafic rocks and the residual saline fluids from crystallization (Abdul Azeez *et al.*, 2017).

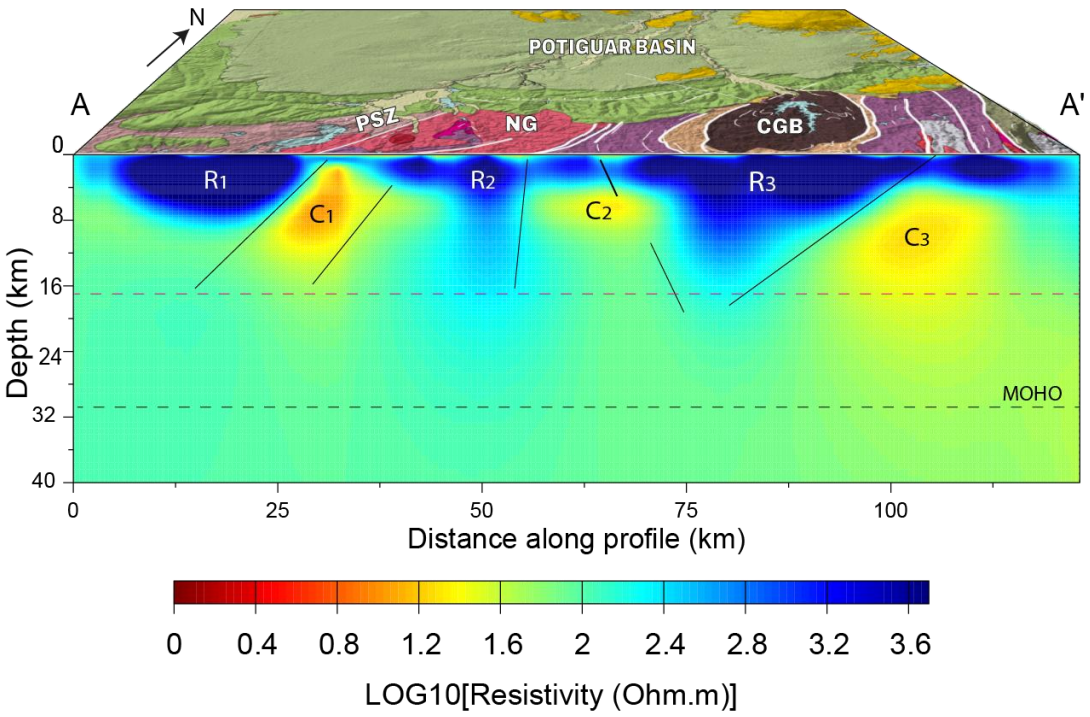

Figure 15 - Vertical section of the three-dimensional electrical resistivity model obtained from the 3D inversion of MT data. The interpreted resistive cores R1, R2 and R3 and conductive cores C1, C2 and C3 are indicated. Overlaid lines represent the main identified/inferred fault/shear zones (solid lines). The red and black dashed lines mark the upper-lower crustal boundary and the Moho discontinuity defined by Lima et al. (2015). Legend: PSZ - Portalegre Shear Zone, NG - Neoproterozoic Granite, CGB- Campo Grande Block.

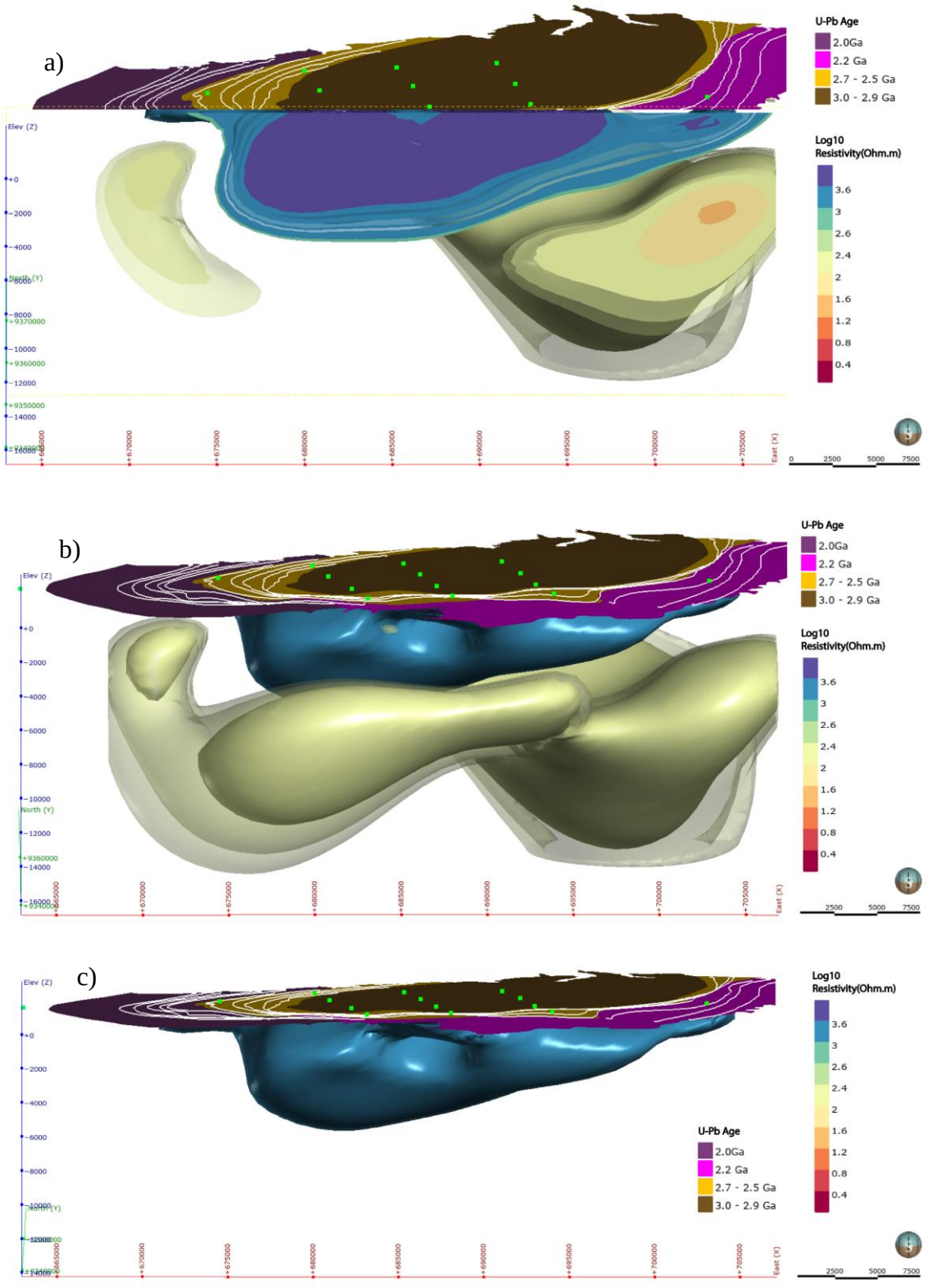

Figure 16 - Three-dimensional electrical resistivity model obtained from 3D MT inversion, integrated with the crustal block age framework proposed by Ferreira et al. (2020b) and visualized in Leapfrog. (**a**) Internal cross-sectional view highlighting subsurface resistivity variations within the model volume. (**b**) Overview of all conductive and resistive anomalies identified in the 3D model. (**c**) Resistive body showing a gentle dip toward the southwest. Surface polygons represent crustal domains classified by U–Pb ages Ferreira et al. (2020b). Green squares indicate MT station positions. The resistivity color scale is given in $\log_{10}(\Omega \cdot m)$.

3.11. Conclusions

1 – The 3D MT method with high resolution and station spacing between 5–10 km offers conditions for significantly better resolution compared to that achieved by regional surveys, enabling the discrimination of lithological domains and the characterization of the geometry of structures that remained indistinguishable in more widely spaced grids.

2 – The combination of 3D resistivity models with U-Pb/Sm-Nd geochronological data shows that infilled-grid MT inversion discriminates crustal domains of distinct ages and compositions, even in polydeformed terranes. The resulting model exposes a partitioned crust: resistive blocks of different generations are separated by conductive zones that mark the main tectonic boundaries. This configuration reinforces the interpretation that the Campo Grande Block records polycyclic crustal evolution from the Mesoarchean to the Neoproterozoic (Ferreira et al., 2020a, 2021), with each accretionary event adding material to the margins of the original nucleus, being compatible with the tectonic model established for the region, which recognizes the existence of Archean nuclei preserved as inliers in Paleoproterozoic basement, subsequently affected by transcurrent tectonics during the Brasiliano Orogeny (Brito Neves *et al.*, 2000; Ferreira *et al.*, 2020a,b).

3 – The concentric architecture observed in the CGB 3D model, with a highly resistive core enveloped by progressively lower-resistivity material, is compatible with a center-to-margin crustal growth model. The Archean core ($>10^4$ Ω·m) represents the primordial crustal fragment, crystallized between 2.98 and 2.66 Ga (Ferreira *et al.*, 2020a). The moderate-resistivity envelope (~10^3 Ω·m) correlates with the Paleoproterozoic orthogneisses of the Caicó Complex, accreted during Rhyacian collisional events (2.25–2.15 Ga).

4 – The three-dimensional geoelectrical architecture of the Campo Grande Block reveals a crustal architecture consistent with the polyphase tectonic evolution documented in the geological literature. The domal-geometry resistive core, with a slight southwestward dip, corresponds to the preserved Archean crustal fragment, while the moderate-resistivity envelope with zonation toward the margins reflects the ring of progressively reworked Paleoproterozoic orthogneisses. The progressive decrease in resistivity from the block core to its margins, passing through the orthogneiss envelope to the marginal conductive zones, reflects the gradient of crustal reworking documented by Ferreira et al. (2020a,b),

in which deformational and metamorphic processes intensify toward the margins of the Archean dome.

5 – Conductors C1, C2, and C3, confined entirely above the brittle–ductile transition, record the combined action of two conductivity mechanisms. The first-order mechanism corresponds to ionic conduction by saline aqueous fluids circulating in interconnected fracture networks along the Portalegre (C1), Paraú (C3), and associated branch (C2) shear zones, an interpretation supported by the compatibility of resistivity values (3–200 Ω·m) with modest fractions of electrolytic fluid and by the recurrence of this pattern in multiple structural contexts of the Borborema Province (Santos *et al.*, 2014; Padilha *et al.*, 2016, 2017). Solid-state conduction mechanisms — Fe-Ti oxides in retroeclogite lenses, intergranular conduction by grain-size reduction in tectonites, and electrical double layer conductivity in biotite-rich migmatitic residues — act as second-order contributors that sustain the residual anomaly in shear zones partially healed since the Neoproterozoic.

6 – The presence of outcropping retroeclogite lenses with dimensions up to 120 m (Ferreira *et al.*, 2023), whose mineral assemblage includes symplectitic textures with magnetite and ilmenite and manganiferous protoliths (spessartine garnet with 6.4–6.6% MnO), constitutes evidence that materials with conductive potential were incorporated into the shear zones at the CGB margin during Neoproterozoic evolution. The temporal convergence between eclogite retrogression (623–590 Ma) and fluid-assisted anatexis of migmatitic orthogneisses (~570 Ma) generated two pulses of metamorphic fluids channeled through the same structures, enriching the shear zones with aqueous solutions and depositing solid conductive phases that contribute to the conductivity observed in the models.

Acknowledgments

This study was financed in part by the Coordenação de Aperfeiçoamento de Pessoal de Nível Superior — Brasil (CAPES) — Finance Code 001. The first author is thankful to Proex/CAPES for the internship provided during the master's research. This study is also a contribution of the INCT-Estudos Tectônicos (CNPq 57.3713/2008-1).

REFERÊNCIAS BIBLIOGRÁFICAS

Adám, A. (2005). Graphite/graphitic rocks as cause of the electric conductivity anomaly and their relationship to the tectonics-a review. Acta Geodaetica et Geophysica Hungarica, 40(3-4), 391-411. *https://doi.org/10.1556/ageod.40.2005.3-4.11*

Almeida, F. D., Hasui, Y., Brito Neves, B. D., & Fuck, R. A. (1977). Províncias estruturais brasileiras. Simpósio de Geologia do Nordeste, 8(1977), 363-391.

Almeida, F. F. M., Hasui, Y., de Brito Neves, B. B., & Fuck, R. A. (1981). Brazilian structural provinces: an introduction. Earth-Science Reviews, 17(1-2), 1-29. *https://doi.org/10.1016/0012-8252(81)90003-9*

Alvim, P. F., Dantas, E. L., Fuck, R. A., & Ferreira, A. C. (2026). A lost fragment of Siderian oceanic and juvenile arc crust preserved in the Borborema province, northeast Brazil. *Precambrian Research*, *433*, 107979. https://doi.org/10.1016/j.precamres.2025.107979

Angelim, L. A. D. A. (2006). Geologia e recursos minerais do estado do Rio Grande do Norte. CPRM; FAPERN.

Araripe, P. D. T., & Feijó, F. J. (1994). Bacia potiguar. *Boletim de Geociências da PETROBRAS*, *8*(1), 127-141. Disponível em: https://bgp.petrobras.com.br/bgp/article/view/620

Araujo, C. E. G., R. F. Weinberg, and U. G. Cordani (2013), Extruding the Borborema Province (NE Brazil): A two-stage Neoproterozoic collision process, Terra Nova, 26, 157–168. *https://doi.org/10.1111/ter.12084*

Archanjo C.J., Macedo J.W.P., Galindo A.C., Araujo M.G.S. 1998. Brasiliano Crustal extension and emplacement fabrics of the magerite-charnockite pluton of Umarizal, Noth-east Brazil. Precambrian Research, 87(1-2):19-32. *https://doi.org/10.1016/S0301-9268(97)00050-8*

Archanjo, C. J., Trindade, R. I., Bouchez, J. L., & Ernesto, M. (2002). Granite fabrics and regional-scale strain partitioning in the Seridó belt (Borborema Province, NE Brazil). Tectonics, 21(1), 3-1. *https://doi.org/10.1029/2000TC001269*

Arthaud, M. H., Caby, R., Fuck, R. A., Dantas, E. L., & Parente, C. V. (2008). Geology of the northern Borborema Province, NE Brazil and its correlation with Nigeria, NW Africa. https://doi.org/10.1144/SP294.4

Azeez, K. A., Patro, P. K., Harinarayana, T., & Sarma, S. V. S. (2017). Magnetotelluric imaging across the tectonic structures in the eastern segment of the Central Indian Tectonic Zone: preserved imprints of polyphase tectonics and evidence for suture status of the Tan Shear. *Precambrian Research*, *298*, 325-340. https://doi.org/10.1016/j.precamres.2017.06.018

Bahr, K. (1988). Interpretation of the magnetotelluric impedance tensor: regional induction and local telluric distortion. Journal of geophysics, 62(1), 119-127. https://n2t.net/ark:/88439/y031103

Bailey, R. C. (1990). Trapping of aqueous fluids in the deep crust. Geophysical Research Letters, 17(8), 1129–1132. https://doi.org/10.1029/GL017i008p01129

Becken, M., & Ritter, O. (2012). Magnetotelluric studies at the San Andreas Fault Zone: implications for the role of fluids. Surveys in Geophysics, 33, 65–105. https://doi.org/10.1007/s10712-011-9144-0 *https://doi.org/10.1007/s10712-011-9144-0*

Bedrosian, P. A., Unsworth, M. J., & Egbert, G. D. (2002). Magnetotelluric imaging of the creeping segment of the San Andreas Fault near Hollister. Geophysical Research Letters, 29(11), 1506. https://doi.org/10.1029/2001GL014119

Benevides, A. S., Fontes, S. L., Meju, M. A., Maurya, V. P., Fuck, R. A., Padilha, A. L., ... & La Terra, E. F. (2026). Lithospheric structure and its relationship to rifting and magmatism in the Ceará Central domain of northwestern Borborema Province in Brazil revealed by 3D magnetotelluric inversion. Journal of the Geological Society, 183(2), jgs2025-025. https://doi.org/10.1144/jgs2025-025

Bertani, R. T., Costa, I. G., & Matos, R. M. D. (1990). Evolução tectono-sedimentar, estilo estrutural e habitat do petróleo na Bacia Potiguar. In: Raja Gabaglia, G. P. & Milani, E. J. (Orgs.), Origem e evolução de bacias sedimentares. Rio de Janeiro: Petrobras, p. 291–310.

Boerner, D. E., Kurtz, R. D., & Craven, J. A. (1996). Electrical conductivity and Paleo-Proterozoic foredeeps. Journal of Geophysical Research, 101(B6), 13775–13791. https://doi.org/10.1029/96JB00171

Bologna, M. S., Egbert, G. D., Padilha, A. L., Pádua, M. B., & Vitorello, Í. (2017). 3-D inversion of complex magnetotelluric data from an Archean-Proterozoic terrain in northeastern São Francisco Craton, Brazil. *Geophysical Journal International*, *210*(3), 1545-1559. https://doi.10.1093/gji/ggx261

Borah, U. K., Patro, P. K., & Suresh, V. (2015). Processing of noisy magnetotelluric time series from Koyna-Warna seismic region, India: a systematic approach. Annals of Geophysics, 58(2), G0222-G0222. https://doi.org/10.4401/ag-6690

Bostick, F. X. (1977). A simple almost exact method of MT analysis. In: Workshop on Electrical Methods in Geothermal Exploration, U.S. Geological Survey.

Brito Neves, B. B., Santos, E. J., & Van Schmus, W. R. (2000). Tectonic history of the Borborema Province, northeastern Brazil. In: Cordani, U. G., Milani, E. J., Thomaz Filho, A., & Campos, D. A. (Eds.), Tectonic Evolution of South America, p. 151–182.

Brito Neves, B. B. (2011). The Paleoproterozoic in the South-American continent: diversity in the geologic time. Journal of South American Earth Sciences, 32(4), 270-286. https://doi.org/10.1016/j.jsames.2011.02.004

Brito Neves, B. B., & Fuck, R. A. (2014). The basement of the South American platform: Half Laurentian (N-NW) + half Gondwanan (E-SE). Precambrian Research, 244, 32–74. https://doi.org/10.1016/j.precamres.2013.09.020

de Brito Neves, B. B., Fuck, R. A., & da Cruz Campanha, G. A. (2021). Basement inliers of the Brasiliano structural provinces of South America. *Journal of South American Earth Sciences*, *110*, 103392. https://doi.org/10.1016/j.jsames.2021.103392

Neves, B. B. D. B., Fuck, R. A., & Campanha, G. A. D. C. (2022). The statherian taphrogenesis of the South American Platform. *Brazilian Journal of Geology*, *52*, e2021053.https://doi.org/10.1590/2317-4889202220210053

Brito Neves, B. B. D., Van Schmus, W. R., Santos, E. J. D., Campos Neto, M. D. C., & Kozuch, M. (1995). O evento Cariris Velho na Província Borborema: integração de dados, implicações e perspectivas. Revista Brasileira de Geociências, 25(4), 279-296. https://doi.org/10.25249/0375-7536.1995279296

Brown, M., Korhonen, F. J., & Siddoway, C. S. (2011). Organizing melt flow through the crust. *Elements*, *7*(4), 261-266. https://doi.org/10.2113/gselements.7.4.261

Brown, M., & Johnson, T. (2019). Time's arrow, time's cycle: Granulite metamorphism and geodynamics. *Mineralogical Magazine*, *83*(3), 323-338. https://doi.10.1180/mgm.2019.19

Burd, A. I., Booker, J. R., Mackie, R., Favetto, A., & Pomposiello, M. C. (2014). Three-dimensional electrical conductivity in the mantle beneath the Payún Matrú Volcanic Field in the Andean backarc of Argentina near 36.5 S: Evidence for decapitation of a mantle plume by resurgent upper

mantle shear during slab steepening. *Geophysical Journal International*, *198*(2), 812-827. https://doi.org/10.1093/gji/ggu145

Caby, R., Sial, A. N., Arthaud, M., & Vauchez, A. (1991). Crustal evolution and the Brasiliano orogeny in Northeast Brazil. In The west African orogens and circum-Atlantic correlatives (pp. 373-397). Berlin, Heidelberg: Springer Berlin Heidelberg. https://doi.org/10.1007/978-3-642-84153-8_16

Cagniard, L. (1953). Basic theory of the magneto-telluric method of geophysical prospecting. Geophysics, 18(3), 605-635. https://doi.org/10.1190/1.1437915

Caldwell, T. G., Bibby, H. M., & Brown, C. (2004). The magnetotelluric phase tensor. Geophysical Journal International, 158(2), 457–469. https://doi.org/10.1111/j.1365-246X.2004.02281.x

Campelo, R.C., 1999. An´alise de terrenos na porç˜ao setentrional da Província Borborema, NE do Brasil: integraç˜ao de dados geol´ogicos e gravim´etricos. M.Sc. Thesis, Universidade Federal do Rio Grande do Norte. https://repositorio.ufrn.br/han dle/123456789/18769.

Castro, D.L., Bezerra, F.H.R., Sousa, M.O.L., Fuck, R.A., 2012. Influence of neoproterozoic tectonic fabric on the origin of the Potiguar Basin, northeastern Brazil and its links with west Africa based on gravity and magnetic data. J. Geodyn. 52, 29–42. https://doi.org/10.1016/j.jog.2011.09.002

Cavalcante, J. C. (1999). Limites e evolução geodinâmica do sistema Jaguaribeano, Província Borborema, Nordeste do Brasil.

Cavalcante, J. C., Sa, J. M., & Macedo, M. H. D. F. (1998). The Jaguaribeana Belt delimitation: Pb-Pb and Rb-Sr geochronological new data; A delimitacao da Faixa Jaguaribeana: novos dados geocronologicos Pb-Pb e Rb-Sr.

Chave, A. D., & Jones, A. G. (2012). The Magnetotelluric Method: Theory and Practice. Cambridge University Press.

Chen, L., Booker, J. R., Jones, A. G., Wu, N., Unsworth, M. J., Wei, W., & Tan, H. (1996). Electrically conductive crust in southern Tibet from INDEPTH magnetotelluric surveying. *Science*, *274*(5293), 1694-1696. https://doi.org/10.1126/science.274.5293.1694

Connolly, J. A. D., & Podladchikov, Y. Y. (2004). Fluid flow in compressive tectonic settings: Implications for midcrustal seismic reflectors and downward fluid migration. Journal of Geophysical Research: Solid Earth, 109(B4). https://doi.org/10.1029/2003JB002822

Correa, R. T., Vidotti, R. M., Fontes, S. L., Vasquez, M. L., & Scandolara, J. E. (2023). Tectonic and metallogenic implications of a metasomatized mantle inferred from magnetotellurics and gravity data: An example of Tapajós Mineral Province, Amazon Craton. *Tectonophysics*, *868*, 230099. https://doi.org/10.1016/j.tecto.2023.230099

Dantas, E. L., Van Schmus, W. R., Hackspacher, P. C., Fetter, A. H., Brito Neves, B. B., Cordani, U. G., Nutman, A. P., & Williams, S. (2004). The 3.4–3.5 Ga São José do Campestre Massif, NE Brazil: remnants of the oldest crust in South America. Precambrian Research, 130, 113–137. https://doi.org/10.1016/j.precamres.2003.11.002

Dantas, E.L., Souza, Z.S., Wernick, E., Hackspacher, P.C., Martin, H., Xiadong, D. and Li, J.W. (2013) Crustal growth in the 3.4-2.7 Ga São José do Campestre Massif, Borborema Province, NE Brazil. *Precambrian Research* 227: 120–156. https://doi.org/10.1016/j.precamres.2012.08.006

Egbert, G. D., & Kelbert, A. (2012). Computational recipes for electromagnetic inverse problems. Geophysical Journal International, 189(1), 251–267. https://doi.org/10.1111/j.1365-246X.2011.05347.x

Evans, R. L., Jones, A. G., Garcia, X., Muller, M., Hamilton, M., Evans, S., ... & Hutchins, D. (2011). Electrical lithosphere beneath the Kaapvaal craton, southern Africa. *Journal of Geophysical Research: Solid Earth*, *116*(B4). https://doi.org/10.1029/2010JB007883

Ferreira, A. C. D., Dantas, E. L., dos Santos, T. J. S., Fuck, R. A., & Tedeschi, M. (2020a). High-pressure metamorphic rocks in the Borborema Province, Northeast Brazil: Reworking of Archean oceanic crust during proterozoic orogenies. Geoscience Frontiers, 11(6), 2221–2242. https://doi.org/10.1016/j.gsf.2020.03.004

Ferreira, A. C., Dantas, E. L., Fuck, R. A., & Nedel, I. M. (2020b). Arc accretion and crustal reworking from late Archean to Neoproterozoic in Northeast Brazil. Scientific Reports, 10(1), 7855. https://doi.org/10.1038/s41598-020-64688-9

Ferreira, A. C., Dantas, E. L., Fuck, R. A., Nedel, I. M., & Reimold, W. U. (2021). Multiple stages of migmatite generation during the Archean to Proterozoic crustal evolution in the Borborema Province, Northeast Brazil. Gondwana Research, 90, 314–334. https://doi.org/10.1016/j.gr.2020.09.005

Ferreira, A., Stevens, G., Dantas, E. L., Fuck, R. A., dos Santos, T. J., & Leandro, M. V. (2023). Heterogeneous Archean oceanic protoliths in Neoproterozoic retrogressed eclogites from Northeast Brazil: petrological, geochemical and Sr–Nd–Pb–Hf isotopic constraints. *Lithos*, *460*, 107370. https://doi.org/10.1016/j.lithos.2023.107370

Ferreira, A., Stevens, G., Dantas, E. L., Fuck, R. A., & dos Santos, T. J. (2025). Crustal thickening, exhumation and metamorphic cooling of Neoproterozoic eclogites in NE Brazil: Timescale for the assembly of West Gondwana. *Gondwana Research*, *138*, 70-88.https://doi.org/10.1016/j.gr.2024.11.001

Fossen, H., Harris, L.B., Cavalcante, C., Archanjo, C.J., Ávila, C.F., 2022. The Patos-ernambuco shear system of NE Brazil: partitioned intracontinental transcurrent deformation revealed by enhanced aeromagnetic data. J. Struct. Geol. 158, 104573 https://doi.org/10.1016/j.jsg.2022.104573.

Frost, B. R., & Frost, C. D. (1987). CO_2, melts, and granulite metamorphism. Nature, 327, 503–506. https://doi.org/10.1038/327503a0

Fuck, R. A., Soares, J. E. O., & Lima, M. V. A. G. (2013). Seismic characteristics of the Borborema Province lithosphere. *XXV Simpósio de Geologia do Nordeste*, 495-496.

Galindo, A. C. (1993). Petrologia dos granitoides brasilianos da região de Caraúbas e Umarizal, oeste do Rio Grande do Norte. Tese de Doutorado, Centro de Geociências-UFPA, 370 p.

Galindo, A. C., Dall'Agnol, R., McReath, I., Lafon, J. M., & Teixeira, N. (1995). Evolution of Brasiliano-age granitoid types in a shear-zone environment, Umarizal-Caraubas region, Rio Grande do Norte, northeast Brazil. *Journal of South American Earth Sciences*, *8*(1), 79-95. https://doi.org/10.1016/0895-9811(94)00043-2

Galindo, A. C., Maia, H. N., Souza, L. C., Srivastava, N. K., Fillipi, R. R., Oliveira, M. T. D, & Araújo, A. G. D. S. (2012). Carta geológica: folha Apodi. Escala 1:100.000. CPRM- Serviço Geológico do Brasil.

Ganade, C. E., Cordani, U. G., Agbossoumounde, Y., Caby, R., Basei, M. A., Weinberg, R. F., & Sato, K. (2016). Tightening-up NE Brazil and NW Africa connections: New U–Pb/Lu–Hf zircon data of a complete plate tectonic cycle in the Dahomey belt of the West Gondwana Orogen in Togo and Benin. *Precambrian Research*, *276*, 24-42. https://doi.org/10.1016/j.precamres.2016.01.032

Garcia, X., Julià, J., Nemocón, A. M., & Neukirch, M. (2019). Lithospheric thinning under the Araripe Basin (NE Brazil) from a long-period magnetotelluric survey: Constraints for tectonic inversion. *Gondwana Research*, *68*, 174-184. https://doi.org/10.1016/j.gr.2018.11.013

Glover, P. W. J., & Vine, F. J. (1995). Beyond KTB—Electrical conductivity of the deep continental crust. Surveys in Geophysics, 16(1), 5–36. https://doi.org/10.1007/BF00682710

Gordilho-Barbosa, R., da Silva Aires, F., Ferreira, A., Dantas, E. L., Gilio, M., Pestilho, A. L. S., & Veloso, Â. S. R. (2025). QuiG elastic modeling reveals HT/LP metamorphic overprint in a garnet-clinopyroxene amphibolite: an example from Western Gondwana. Lithos, 108283. https://doi.org/10.1016/j.lithos.2025.108283

Groom, R. W., & Bailey, R. C. (1989). Decomposition of the magnetotelluric impedance tensor in the presence of local three-dimensional galvanic distortion. Journal of Geophysical Research, 94(B2), 1913–1925. https://doi.org/10.1029/JB094iB02p01913

Guillot, S., Hattori, K., Agard, P., Schwartz, S., & Vidal, O. (2009). Exhumation processes in oceanic and continental subduction contexts: a review. *Subduction zone geodynamics*, 175-205. https://doi.org/10.1007/978-3-540-87974-9_10

Hackspacher, P. C., & Legrand, J. M. (1989). Microstructural and metamorphic evolution of the Portalegre shear zone, northeastern Brazil.

Hackspacher, P. C., & Sá, J. M. (1984). Critério litoestrutural para diferenciação do embasamento Caicó do grupo Seridó. *RN-Brasil. In: SBG/Núcleo Nordeste, Simpósio de Geologia do Nordeste*, *11*, 263-277.

Hackspacher, P. C., Van Schmus, W. R., & Dantas, E. L. (1990). Um embasamento transamazônico na Província Borborema. In *Congresso Brasileiro de Geologia* (Vol. 36, pp. 2683-2696).

Halliday, D., Resnick, R., & Walker, J. (1996). Fundamentals of Physics. 4th ed. John Wiley & Sons.

Hill, G. J., Roots, E. A., Frieman, B. M., Haugaard, R., Craven, J. A., Smith, R. S., ... & Sherlock, R. (2021). On Archean craton growth and stabilisation: Insights from lithospheric resistivity structure of the Superior Province. *Earth and Planetary Science Letters*, *562*, 116853. https://doi.org/10.1016/j.epsl.2021.116853

Hollanda, M. H. B., Archanjo, C. J., Souza, L. C., Dunyi, L., & Armstrong, R. (2011). Long-lived paleoproterozoic granitic magmatism in the Seridó-Jaguaribe domain, Borborema Province–NE Brazil. *Journal of South American Earth Sciences*, *32*(4), 287-300. https://doi.org/10.1016/j.jsames.2011.02.008

Jolivet, L., Faccenna, C., Goffe, B., Burov, E., & Agard, P. (2003). Subduction tectonics and exhumation of high-pressure metamorphic rocks in the Mediterranean orogens. *American Journal of Science*, *303*(5), 353-409.

Jones, A. G. (1983). On the equivalence of the “Niblett” and “Bostick” transformations in the magnetotelluric method. Journal of Geophysics, 53, 72–73. https://n2t.net/ark:/88439/y020744

Jones, A. G. (1992). Electrical conductivity of the continental lower crust. In: Fountain, D. M., Arculus, R. J., & Kay, R. W. (Eds.), Continental Lower Crust. Elsevier, p. 81–143. https://ostrnrcan-dostrncan.canada.ca/handle/1845/191399

Jones, A. G. (1993). Electromagnetic images of modern and ancient subduction zones. Tectonophysics, 219(1–3), 29–45. https://doi.org/10.1016/0040-1951(93)90285-R

Jones, A. G., et al. (2009). Area selection for diamonds using magnetotellurics: Examples from southern Africa. Lithos, 112S, 83–92 https://doi.org/10.1016/j.lithos.2009.06.011

Käufl, J. S., Grayver, A. V., Comeau, M. J., Kuvshinov, A. V., Becken, M., Kamm, J., ... & Demberel, S. (2020). Magnetotelluric multiscale 3-D inversion reveals crustal and upper mantle

structure beneath the Hangai and Gobi-Altai region in Mongolia. *Geophysical Journal International*, *221*(2), 1002-1028. https://doi.org/10.1093/gji/ggaa039

Kawano, S., Yoshino, T., Katayama, I., 2012. Electrical conductivity of magnetitebearing serpentinite during shear deformation. Geophys. Res. Lett. 39, L20313.http://dx.doi.org/10.1029/2012GL053652.

Kelbert, A., Meqbel, N., Egbert, G. D., & Tandon, K. (2014). ModEM: A modular system for inversion of electromagnetic geophysical data. Computers & Geosciences, 66, 40–53. https://doi.org/10.1016/j.cageo.2014.01.010

Khoza, T. D., Jones, A. G., Muller, M. R., Evans, R. L., Miensopust, M. P., & Webb, S. J. (2013). Lithospheric structure of an Archean craton and adjacent mobile belt revealed from 2-D and 3-D inversion of magnetotelluric data: Example from southern Congo craton in northern Namibia. Journal of Geophysical Research: Solid Earth, 118, 4378–4397. https://doi.org/10.1002/jgrb.50258

Kirkby, A. L., Zhang, F., Peacock, J., Hassan, R., & Duan, J. (2019). The MTPy software package for magnetotelluric data analysis and visualisation. Journal of Open Source Software, 4(37), 1358. https://doi.org/10.21105/joss.01358

Kluge, E. K., Toy, V., & Lockner, D. (2022). Electrical properties and anisotropy of schists and fault rocks from New Zealand's Southern Alps under confining pressure. *Geosciences*, *12*(3), 121. https://doi.org/10.3390/geosciences12030121

Krieger, L., & Peacock, J. R. (2014). MTpy: a Python toolbox for magnetotellurics. Computers & Geosciences, 72, 167–175. https://doi.org/10.1016/j.cageo.2014.07.013

Lin, W., Yang, B., Han, B., & Hu, X. (2023). A review of subsurface electrical conductivity anomalies in magnetotelluric imaging. *Sensors*, *23*(4), 1803. https://doi.org/10.3390/s23041803

Lima, M. V. A. G., Berrocal, J., Soares, J. E. P., & Fuck, R. A. (2015). Deep seismic refraction experiment in northeast Brazil: New constraints for Borborema province evolution. Journal of South American Earth Sciences, 58, 335–349. https://doi.org/10.1016/j.jsames.2014.10.007

Ma, C., Naghizadeh, M., Adetunji, A., Lodge, R. W., Snyder, D., & Sherlock, R. (2021). Imaging Neoarchean crustal structures: An integrated geologic-seismic-magnetotelluric study in the western Wabigoon and Winnipeg River terranes, Superior craton. *Precambrian Research*, *364*, 106339. https://doi.org/10.1016/j.precamres.2021.106339

Magini, C., & Hackspacher, P. C. (2008). Geoquímica e ambiência tectônica do arco magmático de Pereiro, região NE da Província Borborema. *Brazilian Journal of Geology*, *38*(2), 336-355.

Mathez, E. A., Duba, A. G., Peach, C. L., Léger, A., Shankland, T. J., & Plafker, G. (1995). Electrical conductivity and carbon in metamorphic rocks of the Yukon-Tanana Terrane, Alaska. Journal of Geophysical Research, 100(B6), 10187–10196. https://doi.org/10.1029/95JB00615

Matos, R. M. D. (1992). The northeast Brazilian rift system. Tectonics, 11(4), 766–791. https://doi.org/10.1029/91TC03092

Matos, R.M.D., 1999. History of the Northeast Brazilian rift system: kinematics implications for the break-up between Brazil and West Africa. In: Cameron, N.R., Bate, R.H., Clure, V.S. (Eds.), The Oil and Gas Habitats of the South Atlantic. Geological Society, London, Special Publications, pp. 55–73. https://doi.org/10.1144/GSL.SP.1999.153.01.04

McNeice, G. W., & Jones, A. G. (2001). Multisite, multifrequency tensor decomposition of magnetotelluric data. Geophysics, 66(1), 158–173. https://doi.org/10.1190/1.1444891

McNeill, J. D. (1990). Use of electromagnetic methods for groundwater studies. *Geotechnical and environmental geophysics*, *1*(5), 191-218. https://doi.org/10.1190/1.9781560802785.ch7

McReath, I., Galindo, A. C., & Dall'Agnol, R. (2002). The Umarizal igneous association, Borborema Province, NE Brazil: implications for the genesis of A-type granites. *Gondwana Research*, *5*(2), 339-353. https://doi.org/10.1016/S1342-937X(05)70727-9

Medeiros, V. C. D., Medeiros, W. E. D., & Sá, E. F. J. D. (2011). Utilização de imagens aerogamaespectrométricas, Landsat 7 ETM+ e aeromagnéticas no estudo do arcabouço crustal da porção central do domínio da zona transversal, província Borborema, NE do Brasil. *Revista Brasileira de Geofísica*, *29*(1), 83-97. https://doi.org/10.1590/S0102-261X2011000100006

Meqbel, N. M., Egbert, G. D., Wannamaker, P. E., Kelbert, A., & Schultz, A. (2014). Deep electrical resistivity structure of the northwestern US derived from 3-D inversion of USArray magnetotelluric data. *Earth and Planetary Science Letters*, *402*, 290-304. https://doi.org/10.1016/j.epsl.2013.12.026

Miensopust, M. P. (2017). Application of 3-D electromagnetic inversion in practice: challenges, pitfalls and solution approaches. Surveys in Geophysics, 38, 869–933. https://doi.org/10.1007/s10712-017-9435-1

Moorkamp, M., Özaydın, S., Selway, K., & Jones, A. G. (2022). Probing the southern African lithosphere with magnetotellurics—Part I: Model construction. Journal of Geophysical Research: Solid Earth, 127(3), e2021JB023117. https://doi.org/10.1029/2021JB023117

Nascimento, M. A. L. D., Antunes, A. F., Galindo, A. C., Jardim de Sá, E. F., & Souza, Z. D. (2000). Geochemical signature of the Brasiliano-age plutonism in the Seridó belt, Northeastern Borborema Province (NE Brazil). *Revista Brasileira de Geociências*, *30*(1), 161-164.

Nascimento, M. D., Medeiros, V. D., & Galindo, A. C. (2008). Magmatismo ediacarano a cambriano no Domínio Rio grande do Norte, Província Borborema, NE do Brasil. *Estudos Geológicos*, *18*(1), 4-29.

Nascimento, M. A. L., Galindo, A. C., & de Medeiros, V. C. (2015). Ediacaran to Cambrian magmatic suites in the Rio Grande do Norte domain, extreme Northeastern Borborema Province (NE of Brazil): Current knowledge. *Journal of South American Earth Sciences*, *58*, 281-299. https://doi.org/10.1016/j.jsames.2014.09.008

Niblett, E. R., & Sayn-Wittgenstein, C. (1960). Variation of electrical conductivity with depth by the magneto-telluric method. Geophysics, 25(5), 998–1008. https://doi.org/10.1190/1.1438799

Nóbrega, M. A. D. (2004). Evolução estrutural e termocronológica meso-cenozóica da zona de cisalhamento Portalegre, Nordeste do Brasil.

Nóbrega, M. A., Sá, J. M., Bezerra, F. H. R., Neto, J. H., Iunes, P. J., Guedes, S., ... & Lima-Filho, F. P. (2005). The use of apatite fission track thermochronology to constrain fault movements and sedimentary basin evolution in northeastern Brazil. *Radiation Measurements*, *39*(6), 627-633. https://doi.org/10.1016/j.radmeas.2004.12.006

Nover, G. (2005). Electrical properties of crustal and mantle rocks—a review of laboratory measurements and their explanation. Surveys in Geophysics, 26, 593–651. https://doi.org/10.1007/s10712-005-1759-6

Oliveira, R. G. D. (2008). *Arcabouço geofísico, isostasia e causas do magmatismo cenozóico da Província Borborema e de sua margem continental (Nordeste do Brasil)* (Doctoral dissertation).

Padilha, A. L., Vitorello, I., Pádua, M. B., & Bologna, M. S. (2014). Electromagnetic constraints for subduction zones beneath the northwest Borborema province: Evidence for Neoproterozoic island arc–continent collision in northeast Brazil. Geology, 42(1), 91–94. https://doi.org/10.1130/G34747.1

Padilha, A. L., Vitorello, I., Pádua, M. B., & Fuck, R. A. (2016). Deep magnetotelluric signatures of the early Neoproterozoic Cariris Velhos tectonic event within the Transversal sub-province of the Borborema Province, NE Brazil. Precambrian Research, 275, 70–83. https://doi.org/10.1016/j.precamres.2015.12.012

Padilha, A. L., Vitorello, I., Pádua, M. B. D., Batista, J. C., & Fuck, R. A. (2017, December). 3D modeling of magnetotelluric data unraveling the tectonic setting and sources of magmatism in the northeastern corner of Borborema Province, NE Brazil. In AGU Fall Meeting Abstracts (Vol. 2017, pp. GP33A-0953).

Padilha, A. L., Vitorello, Í., de Pádua, M. B., & Fuck, R. A. (2019). Magnetotelluric images of Paleoproterozoic accretion and Mesoproterozoic to Neoproterozoic reworking processes in the northern São Francisco Craton, central-eastern Brazil. *Precambrian Research*, *333*, 105416. https://doi.org/10.1016/j.precamres.2019.105416

Padilha, A. L., Santos-Matos, A. C. L., Batista, J. C., Vitorello, I., Pádua, M. B., & Fuck, R. A. (2021). Magnetotelluric evidence for a Rhyacian suture zone hidden underneath the Seridó belt, Borborema Province, Northeastern Brazil. Precambrian Research, 365, 106413. https://doi.org/10.1016/j.precamres.2021.106413

Parente, C. V., & Arthaud, M. H. (1995). O Sistema orós-jaguaribe no Ceará, NE do brasil. *Revista Brasileira de Geociências*, *25*(4), 297-306.

Parkinson, W. D. (1959). Directions of rapid geomagnetic fluctuations. Geophysical Journal of the Royal Astronomical Society, 2, 1–14. https://doi.org/10.1111/j.1365-246X.1959.tb05776.x

Neto, O. P., Soares, U. M., Silva, J. G. F., Roesner, E. H., Florencio, C. P., Souza, C. A. V., & Neto, O. C. (2007). Bacia potiguar. *Bol. Geociências Petrobras*, *15*(2), 357-369.

Pineau, F., & Mathez, E. A. (1990). Carbon isotopes in xenoliths from the Hualalai Volcano, Hawaii, and the generation of isotopic variability. Geochimica et Cosmochimica Acta, 54(1), 217-227.https://doi.org/10.1016/0016-7037(90)90209-4

Raju, K., Patro, P. K., Borah, U. K., Srivastava, S., & Reddy, K. C. (2022). Evolution of eastern segment of the Central India Tectonic Zone: an insight from a magnetotelluric study. *Geophysical Journal International*, *230*(1), 272-287. https://doi.org/10.1093/gji/ggac073

Reichardt, H., & Weinberg, R. F. (2012). Hornblende chemistry in meta-and diatexites and its retention in the source of leucogranites: an example from the Karakoram Shear Zone, NW India. *Journal of Petrology*, *53*(6), 1287-1318. https://doi.org/10.1093/petrology/egs017

Ritter, O., Weckmann, U., Vietor, T., & Haak, V. (2003). A magnetotelluric study of the Damara Belt in Namibia: 1. Regional scale conductivity anomalies. *Physics of the Earth and Planetary Interiors*, *138*(2), 71-90. https://doi.org/10.1016/S0031-9201(03)00078-5

Roots, E. A., Hill, G. J., Frieman, B. M., Wannamaker, P. E., Maris, V., Calvert, A. J., ... & Snyder, D. B. (2022). Magmatic, hydrothermal and ore element transfer processes of the southeastern Archean Superior Province implied from electrical resistivity structure. *Gondwana Research*, *105*, 84-95. https://doi.org/10.1016/j.gr.2021.12.004

Sá, E. F. J. (1994). A faixa Seridó (Província Borborema, NE do Brasil) eo seu significado geodinâmico na cadeia Brasiliana/Pan-africana (Doctoral dissertation, Instituto de Geociências da Universidade de Brasília.).

Sá, J. M., McReath, I., & Leterrier, J. (1995). Petrology, geochemistry and geodynamic setting of Proterozoic igneous suites of the Orós fold belt (Borborema Province, Northeast Brazil). *Journal of South American Earth Sciences*, *8*(3-4), 299-314. https://doi.org/10.1016/0895-9811(95)00015-8

Santos, A. C. L. (2012). Imageamento Magnetotelúrico de Estruturas da Litosfera na Porção SE da Província Borborema. Tese de Doutorado, Universidade de Brasília.

Santos, A. C. L., et al. (2014). Deep structure of a stretched lithosphere: Magnetotelluric imaging of the southeastern Borborema Province, NE Brazil. Tectonophysics, 610, 39–50. https://doi.org/10.1016/j.tecto.2013.10.008

Santos, E. D. (1996, September). Ensaio preliminar sobre terrenos e tectônica acrescionária na Província Borborema. In *Congresso Brasileiro de Geologia* (Vol. 39, No. 1996, pp. 47-50). San Salvador, El Salvador: SBG Salvador.

Santos, E.J. and Medeiros, V.C. (1999) Constraints from granitic plutonism on Proterozoic crustal growth of the transverse zone, Borborema province, NE-Brazil. *Revista Brasileira de Geociências 29(1): 73–84. https://doi.org/10.25249/0375-7536.1999297384*

Santos, E. J. D., Brito Neves, B. B. D., Almeida, F. F. M. D., & Hasui, Y. (1984). Província Borborema. *O Pré-cambriano do Brasil*.

Santos-Matos, A., Padilha, A. L., Fuck, R. A., & Pádua, M. B. (2019). Preliminary Results of the 3-D Inversion of Magnetotelluric Data in the Southern Sub province of Borborema Province, Northeast Brazil.

Sawyer, E. W. (2008). Atlas of migmatites (Vol. 9). NRC Research press.

Sawyer, E. W. (2010). Migmatites formed by water-fluxed partial melting of a leucogranodiorite protolith: microstructures in the residual rocks and source of the fluid. *Lithos*, *116*(3-4), 273-286. https://doi.org/10.1016/j.lithos.2009.07.003

Sawyer, E. W., Cesare, B., & Brown, M. (2011). When the continental crust melts. *Elements*, *7*(4), 229-234. https://doi.org/10.2113/gselements.7.4.229

Saxena, S., Pommier, A., & Tauber, M. J. (2021). Iron sulfides and anomalous electrical resistivity in cratonic environments. *Journal of Geophysical Research: Solid Earth*, *126*(9), e2021JB022297. https://doi.org/10.1029/2021JB022297

Schwalenberg, K., Rath, V., & Haak, V. (2002). Sensitivity studies applied to a two-dimensional resistivity model from the Central Andes. Geophysical Journal International, 150, 673–686. https://doi.org/10.1046/j.1365-246X.2002.01734.x

Selway, K. (2014). On the causes of electrical conductivity anomalies in tectonically stable lithosphere. Surveys in Geophysics, 35, 219–257. https://doi.org/10.1007/s10712-013-9235-1

Sheng, Y., Jin, S., Comeau, M. J., Hou, Z., Zhang, L., Wei, W., & Ye, G. (2023). Relationship between the migration of crustal material, normal faulting, and gneiss domes in the vicinity of the dinggye region, Central part of the tethys–Himalaya terrane: Insights from the 3-D electrical structure. *Tectonophysics*, *869*, 230100. https://doi.org/10.1016/j.tecto.2023.230100

Silva, N. C. V., Magini, C., Dantas, E. L., da Silva, F. M., Branco, R. C., Fuck, R. A., ... & Moreira, V. S. (2026). 3D Magnetotelluric Architecture of Archean Nucleus São José do Campestre, Borborema Province, NE Brazil. *Journal of South American Earth Sciences*, 105995. https://doi.org/10.1016/j.jsames.2026.105995

Simpson, F., & Bahr, K. (2005). Practical Magnetotellurics. Cambridge University Press.

Siripunvaraporn, W., Egbert, G., & Uyeshima, M. (2005). Interpretation of two-dimensional magnetotelluric profile data with three-dimensional inversion: synthetic examples. Geophysical Journal International, 160(3), 804–814. https://doi.org/10.1111/j.1365-246X.2005.02527.x

Smith, J. T. (1995). Understanding telluric distortion matrices. Geophysical Journal International, 122(1), 219–226. https://doi.org/10.1111/j.1365-246X.1995.tb03549.x

Telford, W. M., Geldart, L. P., & Sheriff, R. E. (1990). Applied geophysics. Cambridge university press.

Ten Grotenhuis, S. M., Drury, M. R., Peach, C. J., & Spiers, C. J. (2004). Electrical properties of fine-grained olivine: Evidence for grain boundary transport. Journal of Geophysical Research: Solid Earth, 109(B6). https://doi.org/10.1029/2003JB002799

Thompson, A. B., & Connolly, J. A. D. (1990). Metamorphic fluids and anomalous porosities in the lower crust. Tectonophysics, 182, 47–55. https://doi.org/10.1016/0040-1951(90)90341-5

Tietze, K., & Ritter, O. (2013). Three-dimensional magnetotelluric inversion in practice—the electrical conductivity structure of the San Andreas Fault in Central California. *Geophysical Journal International*, *195*(1), 130-147. https://doi.org/10.1093/gji/ggt234

Tikhonov, A. N. (1950). On determining electrical characteristics of the deep layers of the Earth's crust. Doklady Akademii Nauk SSSR, 73(2), 295–297.

Trindade, R. I. F., Dantas, E. L., Babinski, M., & Van Schmus, W. R. (1999). Short lived granitic magmatism along shear zones: evidence from U-Pb zircon and sphene ages of Caraúbas and Tourão granites. In: Actas. Córdoba: SEGEMAR.

Unsworth, M. (2010). Magnetotelluric studies of active continent-continent collisions. Surveys in Geophysics, 31, 137–161. https://doi.org/10.1007/s10712-009-9086-y

Unsworth, M. J., Egbert, G. D., & Booker, J. R. (2000). High-resolution electromagnetic imaging of the San Andreas fault in central California. Journal of Geophysical Research, 104, 1131–1150. https://doi.org/10.1029/98JB01755

Valcácio, S. D. N., Souza, Z. S. D., & Oliveira, E. P. D. (2022). U-Pb zircon age of Ediacaran Umarizal Granite Suite and emplacement mechanism with high-T hornfels generation in Jucurutu Formation, Borborema Province, NE, Brazil. Brazilian Journal of Geology, 52, e20200129. https://doi.org/10.1590/2317-4889202220200129

Van Schmus, W. R., de Brito Neves, B. B., Hackspacher, P., & Babinski, M. (1995). UPb and SmNd geochronologic studies of the eastern Borborema Province, Northeastern Brazil: initial conclusions. *Journal of South American Earth Sciences*, *8*(3-4), 267-288. https://doi.org/10.1016/0895-9811(95)00013-6

Van Schmus, W. R., de Brito Neves, B. B., Williams, I. S., Hackspacher, P. C., Fetter, A. H., Dantas, E. L., & Babinski, M. (2003). The Seridó Group of NE Brazil, a late Neoproterozoic pre- to syn-collisional basin in West Gondwana: insights from SHRIMP U–Pb detrital zircon ages and Sm–Nd crustal residence (TDM) ages. *Precambrian Research*, *127*(4), 287-327. https://doi.org/10.1016/S0301-9268(03)00197-9

Van Schmus, W. R., Oliveira, E. P., Da Silva Filho, A. F., Toteu, S. F., Penaye, J., & Guimarães, I. P. (2008). Proterozoic links between the Borborema province, NE Brazil, and the central African fold belt. https://doi.org/10.1144/SP294.5

Vanderhaeghe, O. (2009). Migmatites, granites and orogeny: Flow modes of partially-molten rocks and magmas associated with melt/solid segregation in orogenic belts. *Tectonophysics*, *477*(3-4), 119-134. https://doi.org/10.1016/j.tecto.2009.06.021

Vauchez, A., Neves, S., Caby, R., Corsini, M., Egydio-Silva, M., Arthaud, M., & Amaro, V. (1995). The Borborema shear zone system, NE Brazil. *Journal of South American Earth Sciences*, *8*(3-4), 247-266. https://doi.org/10.1016/0895-9811(95)00012-5

Vozoff, K. (1991). The magnetotelluric method. https://doi.org/10.1190/1.9781560802686.ch8

Wannamaker, P. E., Jiracek, G. R., Stodt, J. A., Caldwell, T. G., Gonzalez, V. M., McKnight, J. D., & Porter, A. D. (2002). Fluid generation and pathways beneath an active compressional

orogen, the New Zealand Southern Alps, inferred from magnetotelluric data. Journal of Geophysical Research: Solid Earth, 107(B6), ETG-6. https://doi.org/10.1029/2001JB000186

Warren, C. J. (2013). Exhumation of (ultra-) high-pressure terranes: concepts and mechanisms. *Solid Earth*, *4*(1), 75-92. https://doi.org/10.5194/se-4-75-2013

Warren, J. M., & Hirth, G. (2006). Grain size sensitive deformation mechanisms in naturally deformed peridotites. Earth and Planetary Science Letters, 248, 438–450. https://doi.org/10.1016/j.epsl.2006.06.006

Weckmann, U. (2012). Making and breaking of a continent: following the scent of geodynamic imprints on the African continent using electromagnetics. Surveys in Geophysics, 33, 107–134. https://doi.org/10.1007/s10712-011-9147-x

White, R. W., & Powell, R. (2010). Retrograde melt–residue interaction and the formation of near-anhydrous leucosomes in migmatites. *Journal of Metamorphic Geology*, *28*(6), 579-597. https://doi.org/10.1111/j.1525-1314.2010.00881.x

Yang, B., Egbert, G. D., Kelbert, A., & Meqbel, N. M. (2015). Three-dimensional electrical resistivity of the north-central USA from EarthScope long period magnetotelluric data. *Earth and Planetary Science Letters*, *422*, 87-93. https://doi.org/10.1016/j.epsl.2015.04.006

Yardley, B. W. D., & Valley, J. W. (1997). The petrologic case for a dry lower crust. Journal of Gephysical Research, 102, 12173–12185. https://doi.org/10.1029/97JB00508

Yin, Y., Unsworth, M., Liddell, M., Pana, D., & Craven, J. A. (2014). Electrical resistivity structure of the Great Slave Lake shear zone, northwest Canada: implications for tectonic history. *Geophysical Journal International*, *199*(1), 178-199. https://doi.org/10.1093/gji/ggu251

Yi, X., Ye, G., Jin, S., & Wei, W. (2022). Constraints on the process and mode of the Paleo-Asian Ocean closure from the lithospheric conductivity structure of the south-eastern Central Asian Orogenic Belt. *Tectonophysics*, *838*, 229485. https://doi.org/10.1016/j.tecto.2022.229485

Young, H. D., Freedman, R. A., & Ford, A. L. (2009). Sears and Zemansk's University Physics with Modern Physics, (Çev. ed.: Hilmi Ünlü). *İstanbul: Pearson Education Yayıncılık Ltd. Şti*.